

Mastergradsoppgave i Kjemi

Marie Døvre Strømsheim

Understanding the
dispersion interaction in
density-functional theory
and prototyping
self-consistent orbital
dependent correlation
functionals

Omfang: 60 studiepoeng

KJEMISK INSTITUTT

Det matematisk-
naturvitenskapelige
fakultet

UNIVERSITETET I OSLO

05/2011



Contents

Contents	i
1 Introduction	2
2 Electronic Structure Theory	4
2.1 Wave function methods	4
2.1.1 The electronic Schrödinger equation	4
2.1.2 Hartree-Fock Theory	4
2.1.3 Beyond the Hartree-Fock approximation: electron correlation	6
2.2 Density Functional Theory	7
2.2.1 Hohenberg-Kohn Theory	7
2.2.2 Levy-Lieb constrained search	10
2.2.3 Lieb convex conjugate theory	11
2.2.4 Kohn-Sham theory	13
2.2.5 The local density approximation	15
2.2.6 The generalized gradient approximation	16
2.2.7 Hybrid Density Functional Approximations	17
2.2.8 The Optimized Effective Potential Method	17
3 Potential based methods	20
3.1 The Direct Optimization Approach	20
3.2 Optimization Techniques	21
3.2.1 Nelder-Mead Simplex algorithm	21
3.2.2 Quasi-Newton Methods	22
3.3 Applications of the Direct Optimization Approach	23
3.3.1 The Optimized Effective Potential Method	23
3.3.2 Determining Kohn-Sham quantities from accurate densities	24
3.3.3 The Lieb Functional Maximization	25
4 Intermolecular interactions in DFT	27
4.1 Empirical dispersion corrections in DFT	27
4.2 Dispersion within the Kohn-Sham framework	29
4.2.1 The Hellmann-Feynman electrostatic theorem	30
4.2.2 Ensuring the validity of the Hellmann-Feynman theorem	31
4.2.3 Computational details	32
4.2.4 Results and Discussion	33

4.2.5	Dispersion forces from electronic densities	35
5	A study of the helium dimer through the adiabatic connection	42
5.1	The Adiabatic Connection	42
5.2	An interaction adiabatic connection	44
5.3	The linear adiabatic connection	45
5.3.1	Comparison with BLYP	46
5.4	Range dependent contributions	50
5.5	The accuracy of the adiabatic connection for the interaction	51
6	Orbital dependent functionals	56
6.1	The B2PLYP double hybrid functional	56
6.2	Double-hybrid functionals based on DCPT2	58
6.3	A self-consistent DCPT2 double hybrid	60
6.4	Correlation functionals from the random-phase approximation	63
6.5	An adiabatic connection analysis of dRPA and SOSEX	67
7	Conclusions and Future Work	71
	Bibliography	74
A	Appendix: Draft Manuscript	79

Acknowledgements

I would like to thank and acknowledge everyone who helped during my master thesis. All the work presented here was done under the supervision and excellent guidance, not to mention endless patience, of Dr. Andrew Teale and Prof. Trygve Helgaker. I am grateful to Dr. Sonia Coriani, Dr. Thomas Bondo Pedersen, and Dr. Maria Francesca Iozzi for allowing me to use their RPA correlation energy code as part of this work. I am also thankful to Dr. Andreas Krapp for the DFT-D code, and helpful discussions with Prof. David Tozer from Durham University, and Prof. Mark Hoffmann from University of North Dakota. This project would also not have been possible without the help and support of everyone in the office: Vladimir Rybkin, Johannes Rekkedal, Kai Kaarvann Lange, and Patrick Merlot.

I am also grateful to Prof. Trygve Helgaker for allowing me to attend the 11th Sostrup summer school on quantum chemistry and molecular properties in summer 2010. In addition, I am grateful to the organizers of the annual meeting of the computational chemistry division of the Norwegian Chemical Society, which was held in Trondheim on November 22nd-23rd 2010, where I was able to present some of the preliminary results from this thesis.

Chapter 1

Introduction

With their famous paper in 1965, Kohn and Sham [1] provided the chemistry and physics communities with a practical manner of applying density functional theory (DFT), to medium and even large molecules and solids. The development of a large number of approximate exchange-correlation functionals, the central quantity of Kohn–Sham theory, has enabled the study of molecular systems, with a reasonable accuracy and at much lower computational cost compared to wave function methods. However, even though DFT describes covalent interactions well, it struggles to give a good description of non-covalent interaction. The description of long-range dispersion interaction has been a particular challenge to Kohn–Sham density functional methods. The failure of these methods to describe dispersion has been discussed widely in the literature [2–7].

This failure has meant that more computationally demanding wave function methods such as Møller–Plesset perturbation theory (MP2) or coupled cluster theory, are the preferred methods to apply to non-covalent interactions, despite their higher computational cost. In view of the high scaling of the computational cost of these wave function methods, which typically varies between $N^5 - N^8$, N being the number of basis functions, it is highly desirable to obtain an exchange-correlation functional which can accurately describe long-range interactions, the scaling of DFT being only $N^3 - N^4$. There have therefore been several attempts to include the dispersion energy within DFT.

The most fundamental of these attempts consist in determining an exchange–correlation functional such that a non-local dependence on the density is included in the correlation-functional. This approach has been taken by several authors through the use of the adiabatic connection [8–11]. Both Langreth et al. [12] and Dobson et al. [13–15] devised exchange–correlation functionals which incorporate dispersion, with the adiabatic connection fluctuation dissipation theorem as their starting point. In the case of range-separated hybrid exchange–correlation functionals, which will be discussed later in the thesis, this non-locality is included in the correlation functional through long-range contributions from wave function methods such as, MP2 [16] or coupled-cluster theory [17, 18]. These long-range contributions are applied in combination with short-range exchange-correlation functionals.

There have also been numerous empirical and semi-empirical attempts at the calculation of dispersion interactions in DFT. Becke and Johnson [19–21] derived a DFT model in terms of the exchange hole. This method, based upon the Becke–Roussel

functional [22], depends upon the occupied Hartree–Fock or Kohn–Sham orbitals, and the dipole–moment of the exact exchange hole. Completely empirical corrections to the Kohn–Sham energy such as the ones devised by Grimme et al. [23, 24] and Courminbeuf [25] have proven popular and effective over recent years in a variety of studies. These corrections are parametrized in terms of the approximate pairwise dispersion coefficients and are calibrated to suit each exchange–correlation functional individually. Their form resembles the term used in molecular mechanics for the van der Waals interaction. An example of such a van der Waals correction is demonstrated in Chapter 4 of this work.

The focus of this thesis is the investigation of stable self-consistent orbital dependent exchange–correlation functionals, which will be able to give a rigorous account of the dispersion interaction. Unfortunately, in DFT there is no systematic route towards the exact density functional. However, by providing a seamless connection between the non-interacting system used in Kohn–Sham DFT and the physical system described by wave function models, the adiabatic connection [8–11] provides a means to gain insight into the behaviour of the exchange–correlation functional, using the systematically improvable wave function theory. In this context, the formulation of Lieb is particularly convenient and is discussed in detail in Chapter 2. The numerical optimization methods used in this thesis are described in Chapter 3, as well as some of the key methods to which they are applied. In Chapter 4 follows a discussion of dispersion interactions in the Kohn–Sham framework with the Hellmann–Feynman electrostatic theorem [26] providing the link between the density and the dispersion force. We then proceed in Chapter 5 to consider the aforementioned evolution from the non-interacting system to the physical system, which allows us to obtain the dispersion interaction energy.

Having determined a method for recovering the dispersion energy and the corresponding Kohn–Sham components, the following two chapters focus on the investigation of self-consistent orbital-dependent density functionals, which may in the future be used to describe dispersion interactions. In this context we start by considering post-SCF corrections, including a novel application of degeneracy corrected perturbation theory (DCPT2) [27] in Chapter 6. We carry out this analysis using the newly implemented methods highlighted in Chapter 3. Then in Chapter 7, we investigate the use of the Random Phase Approximation (RPA), which has attracted a great deal of interest recently due to its low cost and ability to describe dispersion effectively [28]. Concluding remarks will be made in Chapter 8.

Chapter 2

Electronic Structure Theory

This chapter outlines the electronic structure methods used in this thesis, starting with the wave function methods, and continuing on to density functional theory (DFT). The reader is referred to the literature [29, 30] for a more detailed account.

2.1 Wave function methods

2.1.1 The electronic Schrödinger equation

Within the Born–Oppenheimer approximation, where the nuclei are viewed as stationary sources of Coulomb potentials, the time-independent Schrödinger equation for N particles is given by

$$\hat{H}\Psi = E\Psi. \quad (2.1.1)$$

where the spin-free non-relativistic Hamiltonian in atomic units (a.u.), \hat{H} for a system of N electrons takes the form

$$\hat{H} = -\frac{1}{2} \sum_i \nabla_i^2 - \sum_{iA} \frac{Z_A}{r_{iA}} + \sum_{i<j} \frac{1}{r_{ij}} + \sum_{A<B} \frac{Z_A Z_B}{R_{AB}} \quad (2.1.2)$$

where i and j denote the electrons of the system, and A and B denote the nuclei and Z_A is the charge of the nucleus A . The terms in Eq. (2.1.1) are as follows: the electronic kinetic, the nuclear-electronic attraction, the electron-electron repulsion and the nuclear nuclear repulsion energies respectively. The operator ∇_i^2 in the kinetic energy term is the Laplacian defined as

$$\nabla_i^2 = \frac{\partial^2}{\partial x_i^2} + \frac{\partial^2}{\partial y_i^2} + \frac{\partial^2}{\partial z_i^2} \quad (2.1.3)$$

The wave function Ψ , in Eq. (2.1.1) is an antisymmetric function of all the spatial and spin coordinates of the N electrons.

2.1.2 Hartree-Fock Theory

Within *ab initio* wave function theory one can systematically improve the wave function towards at the exact solution. At the simplest level of wave function theory, the Hartree-Fock approximation describes the wave function in terms of a single determinant,

known as a Slater determinant. A Slater determinant is an antisymmetric product of N orthonormal spin orbitals which in turn are products of the spatial orbital of the electron and its spin function

$$\Psi_{\text{HF}} = |\text{HF}\rangle = \frac{1}{\sqrt{N!}} \begin{vmatrix} \psi_1(x_1) & \psi_2(x_1) & \dots & \psi_N(x_1) \\ \psi_1(x_2) & \psi_2(x_2) & \dots & \psi_N(x_2) \\ \vdots & \vdots & & \vdots \\ \psi_1(x_N) & \psi_2(x_N) & \dots & \psi_N(x_N) \end{vmatrix}$$

One of the properties of a determinant is that when two columns are interchanged there is a change in sign which guarantees an antisymmetric wave function. Consequently, the determinant obeys the Pauli principle.

The spin orbitals which make up the best wave function are found by minimization of the Rayleigh ratio,

$$E_{\text{HF}}(R) = \min_{\Psi_{\text{HF}}} \frac{\int \Psi_{\text{HF}}^*(x; R) \hat{H} \Psi_{\text{HF}}(x; R) dx}{\int \Psi_{\text{HF}}^*(x; R) \Psi_{\text{HF}}(x; R) dx} \quad (2.1.4)$$

where the HF energy, $E_{\text{HF}}(R)$, depends upon the nuclear coordinates subject to the orthonormality constraints on the orbitals. When the lowest possible value of ε is found, the corresponding energy is identified as an upper bound to the ground state energy of the system.

The resulting minimization leads to a set of equations known as the Hartree-Fock equations. These are single-electron equations of the form:

$$\hat{F}_i \psi_i(1) = \varepsilon_i \psi_i(1) \quad (2.1.5)$$

where ε_i is the orbital energy and the Fock-operator is given by

$$\hat{F}_i = -\frac{1}{2} \nabla_i^2 - \sum_K \frac{Z_A}{r_{iA}} + \sum_{j=1}^N (\hat{J}_{ij} - \hat{K}_{ij}) \quad (2.1.6)$$

The integral J_{ij} is the representation of the Coulombic repulsion between the electrons. Antisymmetry gives rise to the exchange integral K_{ij} . This is evident from their integral forms:

$$J_{ij} = \int \int \psi_i^*(x_1) \psi_i(x_1) \frac{1}{r_{12}} \psi_j^*(x_2) \psi_j(x_2) dx_1 dx_2 \quad (2.1.7)$$

$$K_{ij} = \int \int \psi_i^*(x_1) \psi_j(x_1) \frac{1}{r_{12}} \psi_i(x_2) \psi_j^*(x_2) dx_1 dx_2 \quad (2.1.8)$$

There is an apparent dilemma in the Hartree-Fock scheme: in order to find the solutions to the Hartree-Fock equations one must already have the set of orbitals which give the lowest expectation value. Therefore the problem is solved self-consistently. A trial set of orbitals is chosen and the corresponding set of Hartree-Fock equations are set up. This gives a new set of orbitals which are used to calculate a new ratio. This procedure is repeated until a convergence criteria is met.

2.1.3 Beyond the Hartree–Fock approximation: electron correlation

The Hartree–Fock wave function $|\text{HF}\rangle$ provides us with an approximate description of the electronic system, where all the electronic interactions are described in an averaged manner, and all correlation and instantaneous interactions between the electrons are neglected. This description will be qualitatively correct for electronic systems where the exact wave function is dominated by one configuration, but it breaks down when there are more than one dominant configurations present in the exact wave function.

The best approximation for the exact wave function within a given orbital basis is provided by full configuration interaction (FCI) theory, where the wave function can be expressed as a linear combination of all Slater determinants that can be constructed from the orbitals in the orbital basis

$$|\text{FCI}\rangle = \left(1 + \sum_{ai} C_i^a \hat{\tau}_i^a + \sum_{a>b, i>j} C_{ij}^{ab} \hat{\tau}_{ij}^{ab} + \dots \right) |\text{HF}\rangle \quad (2.1.9)$$

where $\hat{\tau}_i^a$ and $\hat{\tau}_{ij}^{ab}$ are the operators which construct excited determinants through replacing the occupied spin orbitals i and j with the virtual spin orbitals a and b . The coefficients C_i^a and C_{ij}^{ab} are determined by minimizing the expectation value of the electronic Hamiltonian in the eigenvalue equation

$$\hat{H}_{\text{FCI}} |\text{FCI}\rangle = E_{\text{FCI}} |\text{FCI}\rangle. \quad (2.1.10)$$

The exact electronic Schrödinger equation can be approached systematically by increasing the number of virtual spin orbitals. However, this approach is problematic as it becomes increasingly difficult to include a sufficient number of virtual spin orbitals as the number of electrons in the system increases. If the excitations included are truncated at e.g. the doubles level, then the FCI model will not return an energy that scales correctly with the size of the system. Therefore, truncated configuration interaction (CI) for systems containing more than 10 electrons is not a valid approach.

The correlation energy being the difference between the FCI and Hartree–Fock energies, can be calculated using many body perturbation techniques such as Møller–Plesset perturbation theory, or coupled cluster theory. In second-order Møller–Plesset perturbation theory (MP2) the unperturbed system is described by the Hartree–Fock determinant and the zero-order Hamiltonian operator, $\hat{H}_0 = \sum_i \hat{F}_i$. The second order MP2 energy is

$$E_c^{\text{MP2}} = \frac{1}{4} \sum_{iajb} \frac{(ia|jb)[2(ai|bj) - (aj|bi)]}{\varepsilon_i + \varepsilon_j - \varepsilon_a - \varepsilon_b}. \quad (2.1.11)$$

The cost of evaluating this expression scales as N^5 where N is the number of basis functions. Whereas MP2 theory is able to recover a large amount of the correlation energy it does not provide a highly accurate representation of the electronic system. To obtain higher accuracy, coupled cluster theory is often a recommended method.

Coupled cluster theory calculates the correlation energy in a non-perturbative manner, but at a lower computational cost than the FCI method. The wave function is

parametrized in the following way

$$|\text{CC}\rangle = \left[\prod_{ai} (1 + t_i^a \hat{\tau}_i^a) \right] \left[\prod_{a \geq b, i \geq j} (1 + t_{ij}^{ab} \hat{\tau}_{ij}^{ab}) \right] \dots |\text{HF}\rangle \quad (2.1.12)$$

where t_I^A and t_{IJ}^{AB} are the singles and doubles excitation amplitudes. When all excitations are included in Eq. (2.1.12), this becomes equal to the FCI wave function of Eq. (2.1.9). Truncation yields a size-extensive approximation to the FCI wave function, where all determinants of the FCI wave function contribute but have approximate coefficients that are obtained as products of coupled cluster amplitudes. Whereas the FCI wave function is optimized variationally by the minimization of the expectation value of the Hamiltonian, the coupled-cluster wave function is optimized by a projection technique, which lowers the computational cost significantly.

In the coupled-cluster singles-and-doubles (CCSD) model, triple and higher excitation operators are omitted from the expansion in Eq. (2.1.12). The CCSD model, which scales as N^6 has a similar level of accuracy as the MP2 model, but is more robust since it is not based on perturbation theory. To obtain higher accuracy, triple excitations may be included, yielding the coupled-cluster singles-doubles-triples (CCSDT) model, which provides a highly accurate representation of the electronic systems, but a cost proportional to N^8 , which makes it unsuitable except for small systems. The coupled-cluster singles-doubles-perturbative-triples (CCSD(T)) model, where the effect of the triples excitations are included in a perturbative manner offers a good compromise between accuracy and cost, scaling as N^7 . The CCSD(T) model is often regarded to as the gold standard of *ab initio* theory since it represents the most accurate electronic structure model in widespread use.

2.2 Density Functional Theory

The purpose of this section is to give an overview of DFT. The Hohenberg–Kohn theorems [31] (HK) provide the backbone of the theory, providing the proof that the external potential is determined by the ground-state density. Following the discussion of Hohenberg–Kohn theory, we proceed to consider Levy–Lieb [32], which provides a more general DFT scheme. Lieb convex–conjugate theory [33] will be discussed as a way to get the ground–state energy when certain requirements are fulfilled. Finally, a practical scheme for obtaining the energy will be discussed.

2.2.1 Hohenberg–Kohn Theory

The first HK-theorem from 1964 [31] states that the external potential $v(\mathbf{r})$ is determined up to an additive constant, by the ground state electron density $\rho(\mathbf{r})$. The electronic Hamiltonian

$$H[v] = -\frac{1}{2} \sum_{i=1}^N \nabla_i^2 + \frac{1}{2} \sum_{i \neq j}^N \frac{1}{r_{ij}} + \sum_{i=1}^N v(\mathbf{r}_i) \quad (2.2.1)$$

is a functional of the external potential v . In Eq. (2.1.2) $v(\mathbf{r}) = -\sum_{iK} \frac{Z_K}{r_{iK}}$. Consider now two different external potentials v_1 and v_2 and assume that the wave functions

differ at the most by a phase factor

$$\Psi_0[v_1] = \gamma \Psi_0[v_2] = \Psi_0. \quad (2.2.2)$$

The Schrödinger equation for the two cases then gives:

$$H[v_1]\Psi_0 = E_0[v_1]\Psi_0 \quad (2.2.3)$$

$$H[v_2]\Psi_0 = E_0[v_2]\Psi_0 \quad (2.2.4)$$

when subtracted yields

$$(H[v_1] - H[v_2])\Psi_0 = \sum_i [v_1(\mathbf{r}_i) - v_2(\mathbf{r}_i)]\Psi_0 = E_0[v_1] - E_0[v_2]\Psi_0 \quad (2.2.5)$$

which, since the wave function Ψ_0 is multiplicative leads to the simplification

$$(H[v_1] - H[v_2]) = \sum_i [v_1(\mathbf{r}_i) - v_2(\mathbf{r}_i)] = E_0[v_1] - E_0[v_2] \quad (2.2.6)$$

This implies that the two potentials must be equal up to an additive constant

$$v_1 = v_2 + c, \quad (2.2.7)$$

Hence, if two potentials are chosen such that they differ by more than an additive constant, then the two wave functions must differ by more than a phase factor. Employing the Rayleigh–Ritz variation principle for such systems gives

$$\begin{aligned} E_0[v_1] &< \langle \Psi_0[v_2] | H[v_1] | \Psi_0[v_2] \rangle = \langle \Psi_0[v_2] | H[v_2] + \sum_i [v_1(\mathbf{r}_i) - v_2(\mathbf{r}_i)] | \Psi_0[v_2] \rangle \\ &= E_0[v_2] + (v_1 - v_2|\rho_2) \end{aligned} \quad (2.2.8)$$

$$\begin{aligned} E_0[v_2] &< \langle \Psi_0[v_1] | H[v_2] | \Psi_0[v_1] \rangle = \langle \Psi_0[v_1] | H[v_1] - \sum_i [v_1(\mathbf{r}_i) - v_2(\mathbf{r}_i)] | \Psi_0[v_1] \rangle \\ &= E_0[v_1] - (v_1 - v_2|\rho_1) \end{aligned} \quad (2.2.9)$$

Adding together the inequalities we obtain the following relationship

$$E_0[v_1] + E_0[v_2] < E_0[v_1] + E_0[v_2] + (v_1 - v_2|\rho_2 - \rho_1) \quad (2.2.10)$$

which is a contradiction unless $\rho_1 \neq \rho_2$. It then follows that two potentials differing by more than an additive constant must have different densities, which proves that the ground state density determines the external potential up to a constant. The implication of this result is that the electronic Hamiltonian and all possible wave functions are determined by the density [34]. The “strong form” of the Hohenberg–Kohn theorem obtained from Eq. (2.2.10),

$$(\Delta v | \Delta \rho) < 0 \quad (2.2.11)$$

demonstrates how two potentials cannot share the same density, as well as the relationship between the density and the potential. From Eq. (2.2.11) it follows that the density typically increases in the areas where the potential decreases.

Having outlined the Hohenberg–Kohn theorem, we will now assume ρ to be a ground state density with the associated wave function $\Psi[\rho]$. According to the Hohenberg–Kohn theorem there exists a universal density functional

$$F_{HK}[\rho] = \left\langle \Psi[\rho] \left| \hat{T} + \hat{V}_{ee} \right| \Psi[\rho] \right\rangle, \quad (2.2.12)$$

where \hat{T} and \hat{V}_{ee} are the kinetic energy and electron repulsion parts of the Hamiltonian in Eq. (2.1.2), which is uniquely defined (even in the case of degeneracies). We then continue by choosing a potential v which belongs to a ground state, but not necessarily $\Psi[\rho]$. It follows from the Rayleigh–Ritz variation principle that the energy of the ground state can be expressed as

$$E_0[v] \leq \left\langle \Psi[\rho] \left| \hat{T} + \hat{V}_{ee} \right| \Psi[\rho] \right\rangle = F_{HK}[\rho] + (v|\rho) \quad (2.2.13)$$

where the last term in (2.2.13) is defined as

$$(v|\rho) = \int v(\mathbf{r})\rho(\mathbf{r})d\mathbf{r} \quad (2.2.14)$$

It follows directly that we have the two inequalities:

$$E_0[v] \leq F_{HK}[\rho] + (v|\rho) \quad (2.2.15)$$

$$F_{HK}[\rho] \geq E_0[v] - (v|\rho) \quad (2.2.16)$$

which become equalities when ρ is the ground-state density of the external potential v , resulting in the Hohenberg–Kohn and Lieb variation principles respectively.

$$E_0[v] = \min_{\rho \in \mathcal{A}_N} (F_{HK}[\rho] + (v|\rho)), \quad v \in \mathcal{V}_N \quad (2.2.17)$$

$$F_{HK}[\rho] = \max_{v \in \mathcal{V}_N} (E_0[v] - (v|\rho)), \quad \rho \in \mathcal{A}_N \quad (2.2.18)$$

where we have introduced the sets \mathcal{A}_N and \mathcal{V}_N . The set \mathcal{A}_N consists of all pure state densities which belong to a ground state, and \mathcal{V}_N is the set containing all ground state potentials. The densities in \mathcal{A}_N are known as v -representable, whereas the potentials belonging to the set \mathcal{V}_N are referred to as ρ -representable.

The restriction of $F_{HK}[\rho]$ and $E_{HK}[v]$ to the domains $\rho \in \mathcal{A}_N$ and $v \in \mathcal{V}_N$ presents a serious limitation since these sets are unknown. The HK variation principle of Eq. (2.2.37) enables us to calculate the ground state energy of an N -electron system as long as the density functional $F_{HK}[\rho]$ in Eq. (2.2.18) is known. We note that $F_{HK}[\rho]$ can be obtained from the Lieb variation principle, but that this would require solving the many body problem in order to determine the ground state energy $E_{HK}[v]$. In light of these difficulties we instead proceed by modelling $F_{HK}[\rho]$ from the density. As a contrast, the wave function methods can be systematically improved to approach the exact solution, whereas no such systematic approach exists in DFT, due to the problems highlighted in this section. This provides the motivation for the work presented in Chapter 5 with the *adiabatic connection* [8–11].

2.2.2 Levy–Lieb constrained search

The HK–variation principle [31] provides a way to solve the many–body problem through a minimization with respect to the density rather than the wave function. However, the problem with this variation principle is that the sets \mathcal{A}_N and \mathcal{V}_N are unknown. To solve this problem Levy and Lieb [32] formulated a more general approach of minimizing with respect to the density.

From the previous section describing the HK–theorems the ground state energy was given as the minimum over all the v –representable densities. However, a minimum only exists when the potential belongs to \mathcal{V}_N . To lift this restriction, the ground state energy is instead reformulated as a greatest lower bound, the infimum, to the expectation value of the Hamiltonian

$$E_0[v] = \inf_{\Psi \in \mathcal{W}_N} \langle \Psi | H[v] | \Psi \rangle, \quad v \in \mathcal{U}_N \quad (2.2.19)$$

where the sets \mathcal{W}_N and \mathcal{U}_N are the sets of normalized N –electron wave functions of finite kinetic energy, and the potentials which provide a finite expectation value for the Hamiltonian, respectively.

We now proceed to introduce the N –representable densities, $\rho \in \mathcal{I}_N$, which belong to some antisymmetric N –electron wave function of finite kinetic energy $\Psi \in \mathcal{W}_N$. The densities that are N –representable fulfil the following requirements; all the densities are nonnegative, they integrate to N , and they have a finite von Weizsäcker kinetic energy.

$$\rho \geq 0, \quad \int \rho(\mathbf{r}) d\mathbf{r} = N, \quad T_W[\rho] < \infty, \quad \rho \in \mathcal{I}_N \quad (2.2.20)$$

The von Weizsäcker kinetic energy

$$T_W[\rho] = \frac{1}{2} \int |\nabla \rho^{\frac{1}{2}}(\mathbf{r})|^2 d\mathbf{r} = \frac{1}{8} \int |\nabla \rho(\mathbf{r})|^2 \rho^{-1} d\mathbf{r} \quad (2.2.21)$$

represents a lower bound to the true kinetic energy of an N –particle system, and is exact for the case of $N=1$. The above requirements in Eq. (2.2.20) make it possible to check whether a density belongs to \mathcal{I}_N or not, whereas in Hohenberg–Kohn theory, there is no way of determining whether a density belonged to \mathcal{A}_N .

We note that \mathcal{I}_N is not a vector space. However, it can be shown that the relationship

$$\mathcal{I}_N \subset X = L^3 \cap L^1 \quad (2.2.22)$$

holds where X is a proper vector space and L^p is the Lebesgue space of p –integrable functions with norm:

$$\|f\|_p = \left(\int_{\mathbb{R}} |f^p(\mathbf{r})| d\mathbf{r} \right)^{\frac{1}{p}}, \quad p \in [1, \infty). \quad (2.2.23)$$

The vector space of the potentials \mathcal{U}_N , is the dual, X^* of X , thereby ensuring a finite interaction, $(v|\rho)$, for all $\rho \in \mathcal{I}_N$.

$$(v|\rho) = \int v(\mathbf{r}) \rho(\mathbf{r}) d\mathbf{r} < \infty, \quad \rho \in \mathcal{I}_N \subset X = L^3 \cap L^1, \quad v \in \mathcal{U}_N = X^* = L^{3/2} + L^\infty, \quad (2.2.24)$$

Since \mathcal{U}_N is independent of the number of electrons in a given system it is henceforth denoted as \mathcal{U} .

Having identified the sets of densities and potentials, we return to the energy expression of Eq. (2.2.19). The minimization can be done by first minimizing with respect to a wave function in \mathcal{W}_N for a fixed ρ , and then finally, minimizing with respect to all allowed densities, $\rho \in \mathcal{I}_N$.

$$E_0[v] = \inf_{\rho \in \mathcal{I}_N} [\inf_{\Psi \rightarrow \rho} \langle \Psi | T + V_{ee} | \Psi \rangle + (v|\rho)], \quad v \in \mathcal{U} \quad (2.2.25)$$

$$E_0[v] = \inf_{\rho \in \mathcal{I}_N} (F_{LL} + (v|\rho)) \quad (2.2.26)$$

where we have introduced the *Levy–Lieb constrained search functional*, also referred to as the *Levy constrained search functional*

$$F_{LL}[\rho] = \min_{\Psi \rightarrow \rho} \langle \Psi | T + V_{ee} | \Psi \rangle \quad \rho \in \mathcal{I}_N, \quad (2.2.27)$$

where the infimum is replaced by a minimum since the a minimizing Ψ can be shown to exist for each $\rho \in \mathcal{I}_N$. It is important to note that in the case of $\rho \in \mathcal{A}_N$, the Levy–Lieb functional becomes equal to the Hohenberg–Kohn functional.

To summarize, Levy–Lieb theory removes the restriction of having to know whether a density is v -representable or a potential is ρ -representable. This is done by expanding the domain of the densities from \mathcal{A}_N to \mathcal{I}_N , and the potentials from \mathcal{V}_N to \mathcal{U} . Furthermore, whether a density is N -representable can be checked, as well as whether the potential belongs to \mathcal{U} .

2.2.3 Lieb convex conjugate theory

The representability problem of Hohenberg–Kohn theory is solved by Levy–Lieb theory, by the replacement of the unknown sets \mathcal{A}_N , \mathcal{V}_N with the known sets \mathcal{I}_N and \mathcal{U} respectively. However, a problem which remains is the existence of several minima, which may not be global in Eq. (2.2.26). This is effectively solved in Lieb theory by the introduction of Lieb’s convex universal density functional which guarantees the existence of a single global minimum.

To this end the Legendre–Fenchel transform is the central mathematical tool. This transform takes a function $f(x)$ and returns the conjugate of the function at y , where the conjugate function is the supremum over x of all the affine functions $\langle x|y \rangle - f(x)$:

$$f^*(y) = \sup_x (\langle x|y \rangle - f(x)) \quad (2.2.28)$$

It can be shown that the conjugate function $f^*(y)$ is convex, meaning that it is always overestimated by a linear interpolation:

$$f^*(cy_1 + (1 - c)y_2) \geq cf^*(y_1) + (1 - c)f^*(y_2), \quad 0 \leq c \leq 1 \quad (2.2.29)$$

If we perform a second Legendre–Fenchel transformation, we obtain the biconjugate of the original function $f(x)$

$$f^{**}(x) = \sup_y (\langle x|y \rangle - f^*(y)) \quad (2.2.30)$$

which by construction of the transformation is also convex. Furthermore, the relation between the function and its biconjugate can be shown to be

$$f^{**}(x) \leq f(x) \quad (2.2.31)$$

which is sharpened into an equality when $f(x)$ is a convex function:

$$f^{**}(x) = f(x) \quad (f \text{ convex}) \quad (2.2.32)$$

To summarize, if $f(x)$ is a convex function, it can be represented by its conjugate function $f^*(y)$ in the form

$$f^*(y) = \sup_x (\langle x|y \rangle - f(x)) \quad (2.2.33)$$

$$f(x) = \sup_y (\langle x|y \rangle - f^*(y)) \quad (2.2.34)$$

The convex functions $f(x)$ and $f^*(x)$ are then said to be mutually conjugate. We will now follow the work of Lieb and apply these relations to DFT.

Returning to the Rayleigh–Ritz variational principle in Eq. (2.2.19), we obtain for $0 \leq c \leq 1$

$$\begin{aligned} E_0[cv_1 + (1-c)v_2] &= \inf_{\Psi} (\langle \Psi | H[cv_1 + (1-c)v_2] | \Psi \rangle) \\ &= \inf_{\Psi} (c \langle \Psi | H[v_1] | \Psi \rangle + (1-c) \langle \Psi | H[v_2] | \Psi \rangle) \\ &\geq c \inf_{\Psi} \langle \Psi | H[v_1] | \Psi \rangle + (1-c) \inf_{\Psi} \langle \Psi | H[v_2] | \Psi \rangle \\ &= cE_0[v_1] + (1-c)E_0[v_2] \end{aligned} \quad (2.2.35)$$

This demonstrates the concavity of the ground state energy $E_0[v]$ with respect to the potential v . It follows directly that $-E_0[v]$ is convex in v and as Eq. (2.2.34) and Eq. (2.2.33), it may be represented exactly by its conjugate functional, here being the Lieb functional $F_L[\rho]$:

$$F_L[\rho] = \sup_{v \in X^*} (E_0[v] - (v|\rho)) \quad \rho \in X \quad (2.2.36)$$

$$E_0[v] = \inf_{\rho \in X} (F_L[\rho] + (v|\rho)) \quad v \in X^* \quad (2.2.37)$$

which are the Lieb and Hohenberg–Kohn variation principles respectively. The only difference to the general relationship between mutually conjugate functionals in Eq. (2.2.34) and Eq. (2.2.33) is in sign, and therefore the ground state energy $E_0[v]$ and the Lieb functional $F_L[\rho]$ are mutually conjugate functionals. Due to being mutually conjugate they both represent the same quantity, namely the electronic energy, in two different ways with respect to the dual variables v and ρ . A comparison can be made between this relationship to that between the total energy of a classical system represented by the Lagrangian, being a function of the velocity, and the Hamiltonian, which is a function of the momentum.

The convexity of the Lieb universal density functional, $F_L[\rho]$ means that the quantity $F_L[\rho] + (v|\rho)$ is convex, and as a consequence the minimization of the ground

state energy, $E_0[v]$ in Eq. (2.2.37) only having one, possibly degenerate, stationary point which is the global minimum. This circumvents the complications one might encounter with the Levy–Lieb universal functional, $F_{LL}[\rho]$, due to the possible the existence of several minima or saddle points. As a final note, the Lieb variation principle in Eq. (2.2.36) provides us with a way to calculate the Lieb universal density functional $F_L[\rho]$, using wave function techniques.

We will now consider the conditions which will result in the Hohenberg–Kohn and Lieb variation principles becoming equal. A rigorous treatment of these conditions would require an introduction of subdifferentials and subgradients from convex analysis. This is beyond the scope of this thesis, and we will therefore not discuss these concepts, but present the main result: The Lieb functional is differentiable on \mathcal{B}_N :

$$E[v] = F_L[\rho] + (v|\rho) \iff v(\mathbf{r}) = \frac{\delta F_L[\rho]}{\delta \rho(\mathbf{r})} \quad v \in \mathcal{V}_N, \quad \rho \in \mathcal{B}_N \quad (2.2.38)$$

where \mathcal{B}_N is the set of ensemble v -representable densities that can be written as a convex combination of degenerate v -representable densities belonging to \mathcal{A}_N . The relation between the subset \mathcal{B}_N and \mathcal{I}_N and \mathcal{A}_N is

$$\mathcal{A}_N \subset \mathcal{B}_N \subset \mathcal{I}_N \quad (2.2.39)$$

The Lieb functional is thus not differentiable everywhere, but only for the v -representable densities $\rho \in \mathcal{B}_N \subset \mathcal{I}_N$. It can be shown that the subset \mathcal{B}_N is dense in \mathcal{I}_N . Hence, any N -representable density can be approximated arbitrarily close by an ensemble v -representable density. This means that although not all N -representable densities are v -representable, any N -representable density can be approximated accurately by an v -representable density. We further note that the Hohenberg–Kohn functional is only defined for v -representable densities, but the Lieb functional is defined over all N -representable densities, but as pointed out, is only differentiable for $\rho \in \mathcal{B}_N$. As a final note, the Levy–Lieb functional is also defined for all N -representable densities, but little is known about its differentiability.

2.2.4 Kohn–Sham theory

Up to now the discussion has been the background for DFT. However, no practical way of obtaining the universal functional, F_L , has been brought up so far. The set of equations derived by Kohn and Sham [1] in 1965 became the foundation for the practical modelling of the density functional $F[\rho]$. These equations contained in principle the full exchange and correlation effects of a real, physical system and could in principle be solved self-consistently.

The ground state energy of a N -electron system, can be expressed as:

$$E_0[v] = (F[\rho] + (v|\rho)), \quad v \in \mathcal{V}_N, \quad \rho \in \mathcal{A}_N \quad (2.2.40)$$

The universal density functional may be further decomposed as:

$$F[\rho] = \frac{1}{2} \int \frac{\rho(\mathbf{r})\rho(\mathbf{r}')}{|\mathbf{r} - \mathbf{r}'|} d\mathbf{r}d\mathbf{r}' + G[\rho] \quad (2.2.41)$$

where the first term is the classical part of the Coulomb repulsion, denoted from here as $U[\rho]$, and the final term is a density functional containing the kinetic energy and the exchange-correlation effects. Kohn and Sham then went on to introduce a non-interacting system with the same density as a fully interacting system, i.e a real physical system.

Within this framework $G[\rho]$ can be expressed as [1]

$$G[\rho] \equiv T_s[\rho] + T_c[\rho] + V_{ee}[\rho] - U[\rho] \quad (2.2.42)$$

where $T_s[\rho]$ is the kinetic energy of the non-interacting system, $T_c[\rho]$ is the difference between the kinetic energy of the non-interacting and interacting system, V_{ee} is the electron-electron repulsion and $U[\rho]$ is the Coulomb repulsion. The known and unknown terms can be further separated into

$$G[\rho] \equiv T_s[\rho] + E_{xc}[\rho] \quad (2.2.43)$$

The last term is known as the exchange-correlation energy and contains the remaining unknown contributions to the total energy.

Due to the use of a non-interacting system with the density equal that of an interacting system, the Hamiltonian can be expressed as

$$\hat{H} = \hat{T} + \sum_i v_s(\mathbf{r}_i) \quad (2.2.44)$$

where $v_s(\mathbf{r})$ is the Kohn-Sham effective potential which is made up of the external potential due to the nuclei, the Coulomb potential and the unknown exchange-correlation potential

$$v_s(\mathbf{r}) = v_{\text{ext}}(\mathbf{r}) + \int \frac{\rho(\mathbf{r}')}{|\mathbf{r} - \mathbf{r}'|} d\mathbf{r}' + v_{xc}(\mathbf{r}) \quad (2.2.45)$$

The exchange-correlation potential is then further defined as [35]

$$v_{xc}(\mathbf{r}) = \frac{\delta E_{xc}[\rho]}{\delta \rho(\mathbf{r})} \quad (2.2.46)$$

The form of the Hamilton-operator and the fact that we are working with a non-interacting system leads to the Schrödinger equation being expressed as simple one electron equations [1]

$$\left[-\frac{1}{2} \nabla^2 + v_s(\mathbf{r}) \right] \varphi_p(\mathbf{r}) = \varepsilon_i \varphi_p(\mathbf{r}) \quad (2.2.47)$$

where the ground state energy of the non-interacting system is the sum of all the eigenvalues.

$$\sum_i^N \varepsilon_i = E_0 \quad (2.2.48)$$

It follows that the wave functions can be expressed as single determinants as was done for Hartree-Fock, the difference being that in Kohn-Sham DFT the wave function is

an antisymmetric product of all the Kohn-Sham orbitals. The density of the system is then a sum of all the densities of the occupied KS-orbitals

$$\rho(\mathbf{r}) = \sum_{i=1}^N |\varphi_i(\mathbf{r})|^2 \quad (2.2.49)$$

which is the same as the density of the physical system. However, so far only the energy of the non-interacting system has been accounted for. The goal of KS-DFT is to determine the energy of the real system. This is done by inserting $G[\rho]$ into the expression for the total energy in Eq. (2.2.40). The ground state energy of the Kohn-Sham system is expressed as

$$\begin{aligned} E_0 &= \sum_{i=1}^N \varepsilon_i = \sum_{i=1}^N \langle \varphi_i | \hat{T}_s + v_s | \varphi_i \rangle = \sum_{i=1}^N \langle \varphi_i | \hat{T}_s + v_{\text{ext}} + v_J + v_{\text{xc}} | \varphi_i \rangle \\ &= \hat{T}_s + \int \int \frac{\rho(\mathbf{r})\rho(\mathbf{r}')}{|\mathbf{r} - \mathbf{r}'|} d\mathbf{r}d\mathbf{r}' + \int \rho(\mathbf{r})v_{\text{ext}}(\mathbf{r})d\mathbf{r} + \int \rho(\mathbf{r})v_{\text{xc}}(\mathbf{r})d\mathbf{r} \end{aligned} \quad (2.2.50)$$

and the ground state energy for the physical system is from this recovered as

$$E_{\text{KS}}[\rho] = \sum_{i=1}^N \varepsilon_i + E_{\text{xc}}[\rho] - \frac{1}{2} \int \int \frac{\rho(\mathbf{r})\rho(\mathbf{r}')}{|\mathbf{r} - \mathbf{r}'|} d\mathbf{r}d\mathbf{r}' - \int v_{\text{xc}}(\mathbf{r})\rho(\mathbf{r})d\mathbf{r} \quad (2.2.51)$$

where the classical Coulomb repulsion has been halved in order to prevent double-counting. The interaction between the exchange-correlation potential and the density is also subtracted, and the exchange-correlation energy put in its place.

The Kohn-Sham formalism contains the exact energy of the ground state for any system. The challenge that remains is to find good approximations to the exchange-correlation energy. Examples of such approximations will be discussed in the following sections.

2.2.5 The local density approximation

The simplest approximation for the exchange-correlation functional is the *Local Density Approximation* (LDA). The LDA is based upon the model system of a uniform electron gas. Within this model the electrons are distributed in a uniform fashion in a cube of infinite volume and with a similarly distributed positive charge, such that the system is neutral. This system has by construction a fixed density, and as a result, the exchange-correlation is a functional of the local density. Hence the form is given as

$$E_{\text{xc}}^{\text{LDA}}[\rho] = \int \rho(\mathbf{r})\varepsilon_{\text{xc}}[\rho(\mathbf{r})]d\mathbf{r} \quad (2.2.52)$$

where $\varepsilon_{\text{xc}}[\rho(\mathbf{r})]$ is the exchange-correlation energy per electron. This can be divided up into exchange and correlation parts:

$$\varepsilon_{\text{xc}}[\rho(\mathbf{r})] = \varepsilon_{\text{x}}[\rho(\mathbf{r})] + \varepsilon_{\text{c}}[\rho(\mathbf{r})]. \quad (2.2.53)$$

It has been shown [36, 37] that the exchange part can be expressed as,

$$\varepsilon_x[\rho(\mathbf{r})] = -\frac{3}{4} \left(\frac{3}{\pi} \right)^{1/3} \rho^{1/3}(\mathbf{r}) \quad (2.2.54)$$

Hence the unknown part is $\varepsilon_c[\rho(\mathbf{r})]$, and is approximated in various ways by different LDA-approximation. The LDA-approach can be highly suitable when investigating metals, however, the electron density is strongly non-uniform in a molecule, leading to the need for a different approach.

2.2.6 The generalized gradient approximation

The generalized gradient approximation (GGA) attempts to take into account the changing density, by depending upon both the gradient of the density as well as local density.

$$E_{xc}^{GGA}[\rho_\alpha(\mathbf{r}), \rho_\beta(\mathbf{r})] = \int f[\rho_\alpha(\mathbf{r}), \rho_\beta(\mathbf{r}), \nabla\rho_\alpha(\mathbf{r}), \nabla\rho_\beta(\mathbf{r})] d\mathbf{r} \quad (2.2.55)$$

The exchange and correlation part of a GGA functional can be treated in a separate manner

$$E_{xc}^{GGA} = E_x^{GGA} + E_c^{GGA}. \quad (2.2.56)$$

The functional of Becke, Lee, Yang and Parr [38, 39] is an example of a GGA functional that will be used in this thesis. The exchange contribution used is the Becke functional, (B88X) [38], and the correlation is obtained by the LYP-functional [39]

$$\begin{aligned} E_c^{LYP}[\rho] = & -a \int \frac{4\rho_\alpha\rho_\beta}{\rho(1+d\rho^{-1/3})} d\mathbf{r} \\ & - ab \int \omega \left\{ \rho_\alpha\rho_\beta \left[2^{11/3} C_f(\rho_\alpha^{8/3} + \rho_\beta^{8/3}) + \left(\frac{47}{18} - \frac{7}{18}\delta \right) |\nabla\rho|^2 \right. \right. \\ & - \left. \left(\frac{5}{2} - \frac{1}{18}\delta \right) (|\nabla\rho_\alpha|^2 + |\nabla\rho_\beta|^2) - \frac{\delta - 11}{9} \left(\frac{\rho_\alpha}{\rho} |\nabla\rho_\alpha|^2 + \frac{\rho_\beta}{\rho} |\nabla\rho_\beta|^2 \right) \right] \\ & - \left. \frac{2}{3}\rho^2 |\nabla|^2 + \left(\frac{2}{3}\rho^2 - \rho_\alpha^2 \right) |\nabla\rho_\beta|^2 + \left(\frac{2}{3}\rho^2 - \rho_\beta^2 \right) |\nabla\rho_\alpha|^2 \right\} d\mathbf{r} \end{aligned} \quad (2.2.57)$$

$$\omega = \frac{\exp(-c\rho^{-1/3})}{1+d\rho^{-1/3}} \rho^{-11/3} \quad (2.2.58)$$

$$\delta = c\rho^{-1/3} + d \frac{\rho^{-1/3}}{1+d\rho^{-1/3}} \quad (2.2.59)$$

The different numerical parameters a, b, c and d are as follows: $a = 0.04918$, $b = 0.132$, $c = 0.2533$ and $d = 0.349$. This functional will be used later on in Chapter 5, for the adiabatic connection, and we will return to its explicit form then.

However, a problem which remains for both LDA and GGA functionals is the self-interaction error. Within Hartree-Fock theory, the exact exchange cancels the self-energy in the classical Coulomb contribution, avoiding an electron repelling itself.

However, LDA and GGAs contain approximations to the exchange contribution and these often do not adequately cancel the spurious self-interaction. One consequence of this is that exchange–correlation potential will not have a correct asymptotic behaviour, decaying exponentially instead of as $-\frac{1}{r}$ [38].

2.2.7 Hybrid Density Functional Approximations

The hybrid functionals were motivated by the adiabatic connection [8–11] as a manner to include fractional orbital exchange into the GGA exchange–correlation functional. These resulting functionals have the general form

$$E_{\text{xc}}^{\text{HYBRID}} = E_{\text{x}}^{\text{GGA}} + E_{\text{c}}^{\text{GGA}} + c_{\text{x}} E_{\text{x}}^0 \quad (2.2.60)$$

where the first two terms are the exchange and correlation from a GGA functional, and the last term is the orbital dependent exchange functional from Hartree–Fock

$$E_{\text{x}}^0 = - \sum_{ij} \int \int \frac{\varphi_i^*(\mathbf{r}) \varphi_j^*(\mathbf{r}') \varphi_j(\mathbf{r}) \varphi_i(\mathbf{r}')}{|\mathbf{r} - \mathbf{r}'|} d\mathbf{r} d\mathbf{r}' \quad (2.2.61)$$

which is evaluated with the Kohn–Sham orbitals φ_i . The original hybrid functional was the so called “Half and Half” of Becke [40], which contained 50% orbital dependent Hartree–Fock exchange. Several approximations have followed since this functional. However, in practical calculations having more than one parameter can be an advantage. The three-parameter B3LYP functional of Stevens et al. [41] has gained popularity over the years due to having a wide range of applicability [42],

$$E_{\text{xc}}^{\text{B3LYP}} = a E_{\text{x}}^{\text{LDA}} + (1 - a) E_{\text{x}}^0 + b E_{\text{x}}^{\text{B}} + c E_{\text{c}}^{\text{LYP}} + (1 - c) E_{\text{c}}^{\text{LDA}} \quad (2.2.62)$$

where the parameters are as follows: $a = 0.80$, $b = 0.72$, $c = 0.81$.

2.2.8 The Optimized Effective Potential Method

In 1953 Sharp and Horton [43] proposed replacing the non-multiplicative potential in Hartree–Fock by a local effective potential $v_{\text{eff}}(\mathbf{r})$ determined through a variational optimization of the orbital-dependent energy $E[\{\varphi_i\}]$

$$\frac{\delta E[\{\varphi_i\}]}{\delta v_{\text{eff}}(\mathbf{r})} = 0. \quad (2.2.63)$$

where $v_{\text{eff}}(\mathbf{r})$ is given by

$$v_{\text{eff}}(\mathbf{r}) = v_{\text{ext}}(\mathbf{r}) + v_{\text{J}}(\mathbf{r}) + v_{\text{x}}(\mathbf{r}) \quad (2.2.64)$$

where $v_{\text{ext}}(\mathbf{r})$ is the external potential, $v_{\text{J}}(\mathbf{r})$ is the Coulomb potential, and $v_{\text{x}}(\mathbf{r})$ is the *local* exchange potential, as opposed to the *non-local* Hartree–Fock potential. The effective potential enters the one-electron equations

$$\left[\hat{T} + v_{\text{eff}}(\mathbf{r}) \right] \varphi_i = \varepsilon_i \varphi_i \quad (2.2.65)$$

Talman and Shadwick [44] devised in 1979, the first practical application of this method to spherical atoms. The impact of their approach to Kohn–Sham theory was recognized by Sahni, Gruenebaum and Perdew [45], who recognised that the effective potential was equal to the Kohn–Sham potential, v_s ; the potential $v_x(\mathbf{r})$ being the functional derivative of the Hartree–Fock energy with respect to the density. A direct implication of this is that the method proposed by Sharp and Horton [43] can be regarded as an exchange-only density functional method. This method, became known as the optimized effective potential (OEP). This OEP-procedure can be applied to any energy expression providing a rigorous way to handle orbital-dependent functionals in the Kohn–Sham framework, although early approaches such as the one by Talman and Shadwick [44] focused on the Hartree–Fock expression for the energy.

Through the chain rule for functional differentiation, the OEP for an orbital-dependent energy functional may be written as [46]

$$v_{xc}(\mathbf{r}) = \frac{\delta E_{xc}[\varphi(\mathbf{r})]}{\delta \rho(\mathbf{r})} = \sum_i^N \int \frac{\delta E_{xc}[\varphi_i(\mathbf{r})]}{\delta \varphi_i(\mathbf{r}')} \frac{\delta \varphi_i(\mathbf{r}')}{\delta \rho(\mathbf{r})} + \frac{\delta E_{xc}[\varphi_i^*(\mathbf{r})]}{\delta \varphi_i^*(\mathbf{r}')} \frac{\delta \varphi_i^*(\mathbf{r}')}{\delta \rho(\mathbf{r})} d\mathbf{r}' \quad (2.2.66)$$

Further application of the chain rule gives the

$$\frac{\delta \varphi_i(\mathbf{r}')}{\delta \rho(\mathbf{r})} = \sum_i^N \int \frac{\delta \varphi_i(\mathbf{r}')}{\delta v_s(\mathbf{r}'')} \frac{\delta v_s(\mathbf{r}'')}{\delta \rho(\mathbf{r})} d\mathbf{r}'' \quad (2.2.67)$$

yielding for the exchange–correlation potential, $v_{xc}(\mathbf{r})$

$$v_{xc}(\mathbf{r}) = \sum_i^N \int \int \left[\frac{\delta E_{xc}[\varphi_i(\mathbf{r})]}{\delta \varphi_i(\mathbf{r}')} \frac{\delta \varphi_i(\mathbf{r}')}{\delta v_s(\mathbf{r}'')} + \frac{\delta E_{xc}[\varphi_i^*(\mathbf{r})]}{\delta \varphi_i^*(\mathbf{r}')} \frac{\delta \varphi_i^*(\mathbf{r}')}{\delta v_s(\mathbf{r}'')} \right] \frac{\delta v_s(\mathbf{r}'')}{\delta \rho(\mathbf{r})} d\mathbf{r}' d\mathbf{r}'' \quad (2.2.68)$$

The common factor in Eq. (2.2.68), being the inverse of the static density response function, which is a measure of the response of the density to an infinitesimal small change in the Kohn–Sham potential.

$$\chi_s(\mathbf{r}, \mathbf{r}') = \frac{\delta \rho(\mathbf{r})}{\delta v_s(\mathbf{r}')} \quad (2.2.69)$$

Acting on both sides of Eq. (2.2.68) with $\chi_s(\mathbf{r}, \mathbf{r}')$ and integrating, yields an integral equation for the exchange–correlation potential $v_{xc}(\mathbf{r})$,

$$\int v_{xc}(\mathbf{r}') \chi_s(\mathbf{r}, \mathbf{r}') d\mathbf{r}' = \sum_i^N \int \left[\frac{\delta E_{xc}[\varphi_i(\mathbf{r})]}{\delta \varphi_i(\mathbf{r}')} \frac{\delta \varphi_i(\mathbf{r}')}{\delta v_s(\mathbf{r})} + \frac{\delta E_{xc}[\varphi_i^*(\mathbf{r})]}{\delta \varphi_i^*(\mathbf{r}')} \frac{\delta \varphi_i^*(\mathbf{r}')}{\delta v_s(\mathbf{r})} \right] d\mathbf{r}' \quad (2.2.70)$$

First order perturbation theory gives

$$\frac{\delta \varphi_i^*(\mathbf{r}')}{\delta v_s(\mathbf{r})} = \sum_{i \neq j} \varphi_j(\mathbf{r}') \frac{\varphi_j^*(\mathbf{r}) \varphi_i(\mathbf{r})}{\varepsilon_i - \varepsilon_j}. \quad (2.2.71)$$

which can be inserted into Eq. (2.2.70), simplifying it further, and giving an expression which may be implemented computationally. The integral equation for $v_{xc}(\mathbf{r})$, can be

solved in each iteration of a Kohn–Sham equation. We note that it can be proven that this is equivalent to the minimization proposed by Sharp and Horton [43]. In Chapter 3 we will proceed to outline the scheme of Wu and Yang [47] to perform practical OEP calculations in finite Gaussian basis sets. This optimization method is directly related to the energy minimization proposed by Sharp and Horton [43].

Chapter 3

Potential based methods

Chapter 2 outlined the conjugate relationship between the energy functional $E_0[v]$ and the density functional $F_L[\rho]$. The Hohenberg–Kohn and the Lieb variation principles were introduced, where the first was a minimization over the densities to obtain $E_0[v]$, and the latter a maximization with respect to the potential to obtain $F_L[\rho]$. In this chapter we examine methods for performing these optimizations in a practical manner. The methods we will discuss are the Nelder–Mead and the quasi–Newton techniques for optimization of the functionals.

3.1 The Direct Optimization Approach

Up to this point there has been no mention of a practical manner to perform the Lieb maximization or the minimization of the energy through the OEP. Yang and Wu [47] introduced the idea of directly optimizing the external potential in a finite basis. This is carried out by expanding the potential in a finite set of Gaussian functions. As an example, the Kohn–Sham effective potential may be represented in the following way:

$$\begin{aligned} v_s(\mathbf{r}) &= v_{\text{ext}}(\mathbf{r}) + v_J(\mathbf{r}) + v_{\text{xc}}(\mathbf{r}) \\ &= v_{\text{ext}}(\mathbf{r}) + v_{\text{ref}}(\mathbf{r}) + \sum_t b_t g_t(\mathbf{r}) \end{aligned} \quad (3.1.1)$$

where $v_{\text{ext}}(\mathbf{r})$ denotes the external potential due to the nuclei, $v_J(\mathbf{r})$ denotes the Coulomb potential and $v_{\text{xc}}(\mathbf{r})$ is the exchange–correlation potential. The potential $v_{\text{ref}}(\mathbf{r})$ in the second line of Eq. (3.1.1) denotes a fixed reference potential, which represents the bulk of the rest of the effective potential, namely the exchange–correlation and the Coulomb potential. There are several possible choices for the reference potential. The reference here is given as the Fermi–Amaldi potential, and was chosen by Wu and Yang following work done by Zhao, Morrison and Parr [48]:

$$v_{\text{ref}}(\mathbf{r}) = \frac{N-1}{N} \int \frac{\rho_0(\mathbf{r}')}{|\mathbf{r} - \mathbf{r}'|} d\mathbf{r}'. \quad (3.1.2)$$

where $\rho_0(\mathbf{r}')$ is the fixed reference density. This potential is used for the reference to ensure that the exchange–correlation potentials has correct $-\frac{1}{r}$ asymptotic decay. The

last term on the same line is an expansion in Gaussian functions, g_t , with coefficients b_t , which must be determined. Herein lies the simplification of the direct optimization approach; the potential depends solely upon the expansion coefficients b_t in a linear manner. This simple technique can be applied to minimize an orbital dependent energy functional in the OEP-method discussed in Chapter 2, or to perform the Lieb maximization discussed in Section (2.2.3) as well as to determine the Kohn–Sham potential corresponding to a supplied density through the Wu–Yang approach, which will be discussed in Section (3.3.1).

3.2 Optimization Techniques

Once the effective potential is cast into a form similar to that of Eq. (3.1.1), standard optimization procedures may be applied to determine the optimal set of coefficients b_t . This set of coefficients may be obtained through standard optimization techniques such as the quasi-Newton method. However, these techniques require explicit expressions for the gradients and the Hessian associated with the given problem, which may prove cumbersome to implement in the case of complicated functionals. In the work presented in this thesis we investigate the application of a variety of functionals and for the purposes of prototyping we have implemented the Nelder–Mead simplex method and the quasi-Newton method with finite difference evaluation of the gradients, in the DALTON quantum chemistry program [49].

3.2.1 Nelder–Mead Simplex algorithm

The Nelder–Mead Simplex algorithm [50] was implemented in the DALTON quantum chemistry program [49] for prototyping purposes since it offers the advantage of circumventing the requirement of evaluating gradients or Hessians to perform an optimization. The search performed with this algorithm is based on the repeated evaluation of the function to be minimized. The method is therefore easy to implement and the possibly time consuming task of obtaining the derivatives is avoided, making the simplex algorithm highly useful for the investigation of new techniques and methods. The same method was employed in Refs. [51, 52] when studying two and four electron systems, where it was recognized that this method did not have a high degree of efficiency and required thousands of steps for a small system.

The simplex algorithm constructs an initial guess P_0 from the n variables to be optimized and constructs a simplex of $(n + 1)$ dimension from the vertices

$$P_i = P_0 + \lambda e_i \quad (3.2.1)$$

where each P_i is a vertex of the simplex, λ is a problem-dependent adjustable parameter and e_i are the unit vectors for the n variables. The search is performed by translating one vertex at a time along the surface of the function until an acceptable stationary point is located. The simplex first locates this stationary point through three operations; reflection, expansion and contraction. Considering the case of minimizations, the vertex with the highest value, P_h is reflected through the opposite side of the simplex to a point. This volume of the simplex is kept constant under the operation. The acceptance

of this point and the other operations of this method, namely contraction and expansion are performed in accordance to the heuristic rules of Nelder and Mead [50]. Through these operations the simplex eventually locates and zooms in on the minimum value of the function in question. The algorithm which was implemented in this work is the amoeba algorithm outlined in Numerical Recipes. [53]

3.2.2 Quasi-Newton Methods

The quasi-Newton family of methods represents robust and generally efficient approaches to optimize functions given their gradient and approximate Hessian. In the Newton method, the function to be optimized is expanded in a Taylor series around the current point \mathbf{b}_n . The function at the new point will then be

$$E(\mathbf{b}) = E_n + (\mathbf{b} - \mathbf{b}_n)^T \mathbf{g}_n + \frac{1}{2}(\mathbf{b} - \mathbf{b}_n)^T \mathbf{H}_n (\mathbf{b} - \mathbf{b}_n) + \dots \quad (3.2.2)$$

where E_n , \mathbf{g}_n and \mathbf{H} are the function, the gradient and the Hessian, respectively, evaluated at the current point. Truncating this expression at second order, and setting the gradient at this order to zero, we obtain the Newton step:

$$\mathbf{b}_{n+1} = \mathbf{b}_n - \mathbf{H}_n^{-1} \mathbf{g}_n. \quad (3.2.3)$$

The Newton step will yield the exact stationary point if the function to be evaluated is quadratic. However, in general an approximation to this stationary point is returned. To ensure that global convergence is achieved, constraints on the allowed step size in Eq. (3.2.3) can be imposed. These constraints lead to the level shifted step. Alternatively, a line search may be performed along the Newton step, also resulting in global convergence. When properly implemented, the full Newton step provides an efficient optimization for many functions, with convergence typically occurring in five to ten iterations, and exhibiting second-order convergence close to the minimum. However, an exact evaluation of the Hessian at each step is highly computationally demanding. Therefore, when this is the case, an approximate Hessian, which has a lower cost than the exact, can be applied. The application of such a Hessian leads to the step in Eq. (3.2.3) also becoming approximate, which can lead to slower convergence in the global and local regions. However, through choosing an appropriate approximation to the exact Hessian, the total computational cost can be reduced in comparison to the exact Newton method, these approaches are called quasi-Newton methods.

In this thesis, the choice of the Hessian is motivated by the following considerations; when studying the adiabatic connection a good approximation is to apply the Hessian for the non-interacting system to the interacting systems, due to this dramatically reducing the cost associated with the evaluation whilst not increasing the number of iterations significantly. A similar Hessian may also be applied in the OEP procedure.

The problem pertaining to both approaches is that the Hessian can become singular. In order to prevent this from causing optimization problems, regularization procedures are applied. Generally, these procedures involve determining the singular values of the Hessian and subsequently removing the smallest of these values. The approach applied in the present work is a singular value decomposition of the Hessian

$$\mathbf{H} = \mathbf{U} \mathbf{W} \mathbf{U}^T \quad (3.2.4)$$

where \mathbf{U} is an orthogonal matrix and \mathbf{W} a diagonal matrix which contains the singular values. The singular values are removed according to a filter, f_i , which is set either to 0 or 1 depending on whether the values are below or above a given threshold. This scheme is known as the truncated singular value decomposition (TSVD). An approximate Hessian may then be constructed as

$$\mathbf{H}^{-1} = \mathbf{U} \cdot [\text{diag}(f_i/w_i)] \cdot \mathbf{U}^T \quad (3.2.5)$$

where w_i are the singular values of \mathbf{H} , and the diagonal elements of \mathbf{W} . A typical choice for the threshold below which the filter is set to zero is $10^{-5} - 10^{-8}$.

The method of finite difference

The quasi-Newton methods requires the gradient to be calculated at each step. For prototyping it is important that this can be done easily, also for complicated functionals. Therefore we consider the method of finite difference [53]. Each element of the gradient \mathbf{g}_n in Eq. (3.2.3) is approximated by the central finite difference

$$g_i = \frac{E(b_i + h) - E(b_i - h)}{2h} \quad (3.2.6)$$

where $i=1$ up to the number of parameters in the set \mathbf{b} and h is the step length. Hence, each element of the gradient is determined by two function evaluations. In practice the use of this gradient together with an approximate Hessian results in a more rapid convergence than what is obtained with the Nelder–Mead method. The same gradient was also calculated at the end of the Nelder–Mead evaluations in order to verify that a stationary point had been located.

3.3 Applications of the Direct Optimization Approach

The direct optimization procedure discussed in Section 3.1 represents an efficient method for optimizing a variety of functionals. In the interest of prototyping and investigating a variety of energy functionals the numerical derivatives and the Nelder–Mead optimization scheme discussed in Sections (3.2.1) and (3.2.2) represents practical tools. In this context, each method represents a different objective functional and set of corresponding derivatives to be evaluated. In this section we proceed to discuss how the direct optimization method can be applied in the OEP method to minimize the energy. Then we will continue with outlining how the direct optimization can be applied to determine the Kohn–Sham potentials, and the densities which correspond to an accurate input wave function density. Finally, a practical manner of performing the Lieb maximization originally discussed in Section (2.2.3) will be outlined.

3.3.1 The Optimized Effective Potential Method

The first method to which Yang and Wu [47] applied their direct optimization scheme was the OEP–method discussed in Chapter 2. This approach is in line with the

original proposal of Sharp and Horton, to determine an effective potential, v_s under the stationary condition

$$\frac{\delta E[\{\varphi_i\}]}{\delta v_s} = 0 \quad (3.3.1)$$

Using the potential expansion discussed in Section 3.1 and applying the chain rule for functional derivation yields the following expression for the functional derivative of the energy with respect to the Kohn–Sham potential becomes

$$\frac{\partial E[\{\varphi_i\}]}{\partial b_t} = \sum_i \int \int \frac{\delta E[\{\varphi_i\}]}{\delta \varphi_i(\mathbf{r})} \frac{\delta \varphi_i(\mathbf{r})}{\delta v_s(\mathbf{r}')} \frac{\partial v_s(\mathbf{r}')}{\partial b_t} d\mathbf{r} d\mathbf{r}' + \text{c.c.} \quad (3.3.2)$$

where $\frac{\delta v_s(\mathbf{r}')}{\delta b_t} = g_t(\mathbf{r}')$ and first order perturbation theory provides an expression for $\frac{\delta \varphi_i(\mathbf{r})}{\delta v_s(\mathbf{r}')}$ which can be computed. The expression then becomes

$$\frac{\partial E[\{\varphi_i\}]}{\partial b_t} = \sum_i \int \int \frac{\delta E[\{\varphi_i\}]}{\delta \varphi_i(\mathbf{r})} \sum_{a \neq i} \varphi_a(\mathbf{r}) \frac{\varphi_a^*(\mathbf{r}') \varphi_i(\mathbf{r}')}{\varepsilon_i - \varepsilon_a} g_t(\mathbf{r}') d\mathbf{r} d\mathbf{r}' + \text{c.c.}$$

This expression is only valid for energy functionals of occupied orbitals. In the case of energy functionals dependent upon all eigenvalues and orbitals, extra terms must be included. The reader is referred to the discussion in Ref. [54] for additional information. Therefore expressions based on perturbation theory, or the random phase approximation, which will be discussed in Chapter 6 become more difficult to evaluate. However, for preliminary investigations and prototyping the implementation of these gradients may be circumvented by the application of the techniques presented in Sections (3.2.1) and (3.2.2). As a final note, the approximate Hessian proposed by Wu and Yang in Ref. [47] is of the form

$$\frac{\delta^2 E}{\delta b_u \delta b_t} \approx -2 \sum_i^{\text{occ.}} \sum_a^{\text{unocc.}} \frac{\langle \varphi_i | g_u(\mathbf{r}) | \varphi_a \rangle \langle \varphi_a | g_t(\mathbf{r}) | \varphi_i \rangle}{\varepsilon_i - \varepsilon_a} \quad (3.3.3)$$

which is simple to evaluate and demonstrates reasonable convergence rates.

3.3.2 Determining Kohn–Sham quantities from accurate densities

The ability to determine Kohn–Sham quantities corresponding to a prescribed density can often be a useful tool for analysis. For example in the case of such a prescribed density having been obtained through a highly accurate wave function method, the corresponding Kohn–Sham quantities such as the non-interacting kinetic energy, the Coulomb and exchange energies, and the exchange–correlation potentials represent accurate data which may be used to test new approximations. Wu and Yang [55] applied their direct optimization method to the determination of the aforementioned Kohn–Sham quantities. They based their approach on the Levy constrained search of Eq. (2.2.27) which was discussed in Section 2.2.2. To ensure the fulfilment of the constraint $\rho(\mathbf{r}) = \rho_{\text{inp}}(\mathbf{r})$, where $\rho(\mathbf{r})$ is the Kohn–Sham density determined from the occupied orbitals $\rho(\mathbf{r}) = 2 \sum_i^{N/2} |\varphi_i(\mathbf{r})|^2$, and $\rho_{\text{inp}}(\mathbf{r})$ is the prescribed density, Wu and Yang defined the following functional

$$W_s[\Psi_{\text{det}}, v(\mathbf{r})] = 2 \sum_i^{N/2} \langle \varphi_i | \hat{T} | \varphi_i \rangle + \int d\mathbf{r} v(\mathbf{r}) \{ \rho(\mathbf{r}) - \rho_{\text{inp}}(\mathbf{r}) \}. \quad (3.3.4)$$

where the first term is the non-interacting kinetic energy, and the second term contains the constraint on the density with the potential $v(\mathbf{r})$ acting as the Lagrange multiplier. Furthermore, it can be shown that $W_s[\Psi_{\text{det}}, v(\mathbf{r})]$ is a concave functional with respect to any variation in $v(\mathbf{r})$. We note from the discussion of Lieb–theory in Section (2.2.3), that a maximization of a concave functional with respect to the potential, $v(\mathbf{r})$ will lead to a single global stationary point. In this respect Wu and Yang developed a method to determine the Kohn–Sham non-interacting kinetic energy, which is an unconstrained maximization with respect to the potential:

$$T_s[\rho_{\text{inp}}(\mathbf{r})] = \max_{v(\mathbf{r})} W_s[\Psi_{\text{det}}[v(\mathbf{r})]]. \quad (3.3.5)$$

where T_s is the noninteracting kinetic energy and Ψ_{det} is a single determinant wave function and itself a function of the external potential. Their method is thus a special application of the Lieb maximization to $\lambda = 0$.

Inserting the potential expansion of Eq. (3.1.1) into Eq. (3.3.4) yields

$$\begin{aligned} W_s[\Psi_{\text{det}}[v(\mathbf{r})], v(\mathbf{r})] = & 2 \sum_i^{N/2} \langle \varphi_i | \hat{T} | \varphi_i \rangle + \int d\mathbf{r} \{ v_{\text{ext}}(\mathbf{r}) + v_0(\mathbf{r}) \} \{ \rho(\mathbf{r}) - \rho_{\text{inp}}(\mathbf{r}) \} \\ & + \int d\mathbf{r} \sum_t b_t g_t(\mathbf{r}) \{ \rho(\mathbf{r}) - \rho_{\text{inp}}(\mathbf{r}) \}. \end{aligned} \quad (3.3.6)$$

where the first and second derivatives can then be obtained with respect to the set of coefficients b_t as outlined by Wu and Yang [55]

$$\frac{\delta W_s[\Psi_{\text{det}}[v(\mathbf{r})], v(\mathbf{r})]}{\delta b_t} = \int d\mathbf{r} \frac{\delta W_s[\Psi_{\text{det}}[v(\mathbf{r})], v(\mathbf{r})]}{\delta v(\mathbf{r})} \frac{\delta v(\mathbf{r})}{\delta b_t} = \int (\rho(\mathbf{r}) - \rho_{\text{inp}}(\mathbf{r})) g_t(\mathbf{r}) d\mathbf{r} \quad (3.3.7)$$

$$\frac{\delta^2 W_s[\Psi_{\text{det}}, v(\mathbf{r})]}{\delta b_u \delta b_t} = 2 \sum_i^{\text{occ.}} \sum_a^{\text{unocc.}} \frac{\langle \varphi_i | g_u(\mathbf{r}) | \varphi_a \rangle \langle \varphi_a | g_t(\mathbf{r}) | \varphi_i \rangle}{\varepsilon_i - \varepsilon_a}. \quad (3.3.8)$$

This simple form for the Hessian allows for the application of the Newton method in a direct manner for all cases where the WY procedure is applied.

3.3.3 The Lieb Functional Maximization

The final application of the direct optimization method of Wu and Yang [55] we will consider is to the Lieb maximization previously discussed in Section 2.2.3. Wu and Yang made the realization that the procedure outlined in the previous section to obtain $T_s[\rho_{\text{inp}}(\mathbf{r})]$ could be generalized by scaling the two electron interaction by a coupling strength, λ , in the electronic Hamiltonian:

$$H_\lambda[v] = T + \lambda W_\lambda + \sum_i v(\mathbf{r}_i) \quad (3.3.9)$$

where T is the kinetic energy operator, W is the electron interaction operator and $v(\mathbf{r})$ is the external potential. We remember from Lieb convex conjugate theory that for full ($\lambda = 1$) interaction strength

$$F_L = \sup_{v \in X^*} (E[v] - (v|\rho)), \quad \rho \in X \quad (3.3.10)$$

From the Hamiltonian in Eq. (3.3.9) we note that the energy for each interaction strength is

$$E_\lambda[v] = \langle \Psi_\lambda[v] | H_\lambda[v] | \Psi_\lambda[v] \rangle \quad (3.3.11)$$

where Ψ_λ is the wave function optimized at a given coupling strength λ . Inserting this into Eq. (3.3.10) and denoting the supplied density as ρ_{inp} and the density associated with Ψ_λ as ρ , we obtain the Lieb functional at interaction strength λ

$$F_{L,\lambda}[\rho_{\text{inp}}] = \sup_{v \in X^*} [\langle \Psi[v] | T | \Psi[v] \rangle + \lambda \langle \Psi[v] | W | \Psi[v] \rangle + (v|\rho) - (v|\rho_{\text{inp}})] \quad (3.3.12)$$

We note that for the Kohn–Sham system, where $\lambda = 0$ the Lieb functional becomes

$$\begin{aligned} F_{0,\lambda}[\rho_{\text{inp}}] &= \sup_{v \in X^*} [\langle \Psi[v] | T | \Psi[v] \rangle + (v|\rho - \rho_{\text{inp}})] \\ &= \max_v [W_s] = T_s[\rho_{\text{inp}}] \end{aligned} \quad (3.3.13)$$

where the last two equalities hold if Ψ_0 is a single Slater determinant. The idea of turning the interaction on in a regular manner through a coupling strength between $\lambda = 0$ and $\lambda = 1$ will be further discussed in Chapter 5 for the adiabatic connection. For the time being we note that inserting the potential expansion of Eq. (3.1.1) into Eq. (3.3.12) and evaluating the gradient yields

$$\frac{\partial F_{L,\lambda}[\rho]}{\partial b_t} = \int [\rho_{\lambda,b_t}(\mathbf{r}) - \rho(\mathbf{r})] g_t(\mathbf{r}) d\mathbf{r} \quad (3.3.14)$$

which can be evaluated easily. The Hessian which is obtained

$$\frac{\partial^2 F_{L,\lambda}[\rho]}{\partial b_t \partial b_u} = \int \int g_t(\mathbf{r}) g_u(\mathbf{r}') \frac{\delta \rho(\mathbf{r})}{\delta v(\mathbf{r}')} d\mathbf{r} \quad (3.3.15)$$

is more complicated to evaluate, and therefore we apply in practice the gradient based in conjunction with the approximate quasi-Newton optimization techniques discussed in Section (3.2.2) with the Hessian for the non-interacting system of Eq. (3.3.8) at all λ . Convergence to a gradient norm less than 10^{-6} is typically reached in less than 10 iterations.

Chapter 4

Intermolecular interactions in DFT

Weak non-covalent intermolecular interactions such as dispersion play a central role in many areas of chemistry and biology, including protein folding, enzyme and catalytic reaction mechanisms, the way in which base pairs are stacked in the DNA molecule and in guest-host supramolecular chemistry. At the same time, DFT struggles to describe non-covalent interactions and in particular dispersion. In the present chapter we discuss dispersion within the framework of DFT. We first examine the DFT-D methods of Grimme et al. [23, 24] and then perform a more in-depth analysis of how dispersion could be treated in the Kohn–Sham framework by employing the Hellmann–Feynman electrostatic theorem [26] as a natural starting point.

4.1 Empirical dispersion corrections in DFT

As discussed in Chapter 2, one popular manner of introducing dispersion into DFT is by an empirical correction. The DFT-D corrections of Grimme [23, 24] have earlier been implemented in the linear scaling branch of DALTON by Andreas Krapp for a set of standard functionals. For the work presented here, they have also been added to the OEP branch of the DALTON-code and extended to include the B2PLYP-D and B97-D functionals. The B97-D functional is a GGA-type functional as discussed in Section 2.2.6. This functional has the form of Becke’s B97 approximation, which was optimized and fitted with respect to thermochemical data [56]. Grimme et al. [23] performed a re-optimization of the coefficients which define Becke’s B97 functional in order to account for the DFT-D corrections and avoid the possibility of double counting of the correlation effects. The B2PLYP functional of Ref. [57] includes in addition to Hartree–Fock and B88X exchange contributions [40], correlation contributions from the LYP functional [39] and MP2. This functional will be discussed in greater detail in Chapter 6. We note that this functional can also be corrected to account for dispersion in a similar manner to B97-D and this correction has been implemented as part of the work presented in this thesis.

The dispersion energies are long-ranged and the energy is given by

$$E_{\text{disp}} = - \sum_{n=3}^{\infty} \frac{C_{2n}}{R^{2n}} \quad (4.1.1)$$

where R is the internuclear separation, and C_n are the dispersion coefficients. The total energy in the DFT-D methods is the usual Kohn–Sham energy plus an extra term, which accounts for the dispersion energy in an approximate manner

$$E^{\text{DFT-D}} = E_{\text{KS}} + \tilde{E}_{\text{disp}} \quad (4.1.2)$$

where

$$\tilde{E}_{\text{disp}} = -s_6 \sum_{i=1}^{N-1} \sum_{j=i+1}^N \frac{C_6^{ij}}{R_{ij}^6} f_d(R_{ij}) \quad (4.1.3)$$

Here we note that s_6 is a scaling factor which is parametrized for each individual exchange–correlation functional, i and j are labels for the nuclei, N is the total number of nuclei and C_6^{ij} is the pairwise approximate dispersion coefficients defined in Ref. [23] and R_{ij} is the internuclear separation. The last term is a damping function, $f_d(R_{ij})$, which is applied in order to avoid any near singularities for separations R_{ij} much smaller than the van der Waals radii. The form chosen for this damping function is

$$f_d(R_{ij}) = \frac{1}{1 + e^{-d(R_{ij}/R_r - 1)}} \quad (4.1.4)$$

where R_r is the sum of the van der Waals radii of atom i and j and d is a parameter set equal to 20 in the case of B2PLYP. Looking at the expressions one notes that there is no dependence on the density. Therefore the functional of Eq. (4.1.2) will not explicitly take into account the charge–rearrangement induced by long-ranged interactions, effectively ignoring an important aspect of the dispersion interaction.

The interaction energy, E_{disp} is defined as the difference between the energy of the dimer and the two separate atoms. Throughout this work the entire interaction curve is referred to as the van der Waals interaction, whereas the long-ranged part of the interaction is called the dispersion region. The interaction energy curves for the helium dimer of Fig 4.1 demonstrate the performance of the B97-D and B3LYP-D functional, as well as the double hybrid B2PLYP with a dispersion correction, as the separation, R , is increased. The dispersion region for the dimer starts at approximately 7.5 a.u. The dashed line is the dispersion energy calculated using Eq. (4.1.1) applying the coefficients from Korona et al. [58] and hence represents an accurate reference value. The B2PLYP-D and B3LYP-D functionals do not bind in the van der Waals region, although they display significantly less repulsive behaviour than the uncorrected B2PLYP and B3LYP. The functional B97-D overbinds in the van der Waals region. However, although it is shown in Figure 4.1 that the B97-D functional does approach correct behaviour at very long-range it is also demonstrated in the same figure that the dispersion interaction energy is still too low in the region between 7.5 to 9.0 a.u. This simple example demonstrates the weakness of empirical corrections. Whilst they perform well for the large organic and biological systems they are parametrized for, they are not universally applicable. Furthermore, the correction term will not enter the Kohn–Sham equations since they are density-independent and therefore have no direct influence on the electronic structure. In the next section we consider how dispersion should affect the electronic density and how this occurs in a Kohn–Sham framework.

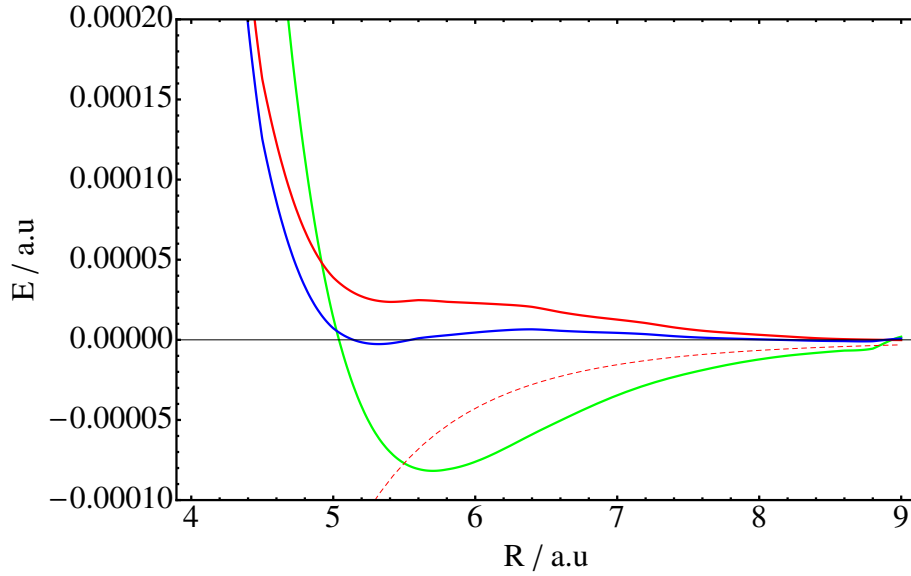


Figure 4.1: The interaction energy in a.u. between two helium atoms as a function of internuclear separation, R , calculated with uncontracted d-aug-cc-pVQZ basis set. The B97-D functional is the green line, B3LYP-D is red and B2PLYP-D is blue. The dashed line is the dispersion energy calculated using Eq. (4.1.1) with the coefficients of Korona et al. [58]

4.2 Dispersion within the Kohn–Sham framework

The Hellmann–Feynman electrostatic theorem presents a clear link between the density and the dispersion force, and is hence an ideal starting point for any investigation into dispersion within a Kohn–Sham framework. The work performed by Allen and Tozer [59] on the dispersion forces in the helium dimer within the Hartree–Fock–Kohn–Sham (HFKS) formalism represents the starting point of this discussion of dispersion treated in a Kohn–Sham framework. The difference between their work and the analysis presented here is that whereas they only treated a correlation potential $v_c(\mathbf{r})$, the full exchange–correlation potential is employed in this work, bringing the formulation within the Kohn–Sham framework. Throughout this chapter the Hellmann–Feynman force will be used as a measure of the quality of the Kohn–Sham density obtained through the application of the WY-procedure discussed in Section (3.3.2) to a CCSD(T) input density. Following the work of Allen and Tozer [59], the density distortions which arise for two helium atoms located a distance of 8.0–9.0 a.u. apart, will be presented. These density distortions are defined as

$$\Delta\rho(\mathbf{r}) = \rho^{\text{dimer}}(\mathbf{r}) - \rho^{\text{atom1}}(\mathbf{r}) - \rho^{\text{atom2}}(\mathbf{r}) \quad (4.2.1)$$

How these density distortions are obtained in a practical manner will be discussed in the section on computational details.

4.2.1 The Hellmann–Feynman electrostatic theorem

In 1939 Feynman proposed [26] a way to calculate intermolecular forces directly from the electronic density. It was shown that the force on the nucleus could be described with classical electrostatics provided that the correct quantum-mechanically determined electronic density is supplied. The total energy of the system is given by the expectation value of the electronic Hamiltonian in Eq. (2.1.2)

$$E = \left\langle \Psi \left| -\frac{1}{2} \sum_i \nabla_i^2 + \sum_{j>i} \frac{1}{r_{ij}} + \sum_i v(\mathbf{r}_i) + \sum_{A<B} \frac{Z_A Z_B}{R_{AB}} \right| \Psi \right\rangle \quad (4.2.2)$$

The force on a given nucleus can be calculated via differentiation. For example the x-component of the force on nucleus A is given by

$$F_{x,A} = -\frac{\partial E}{\partial X_A} \quad (4.2.3)$$

Substituting Eq. (4.2.2) into Eq. (4.2.3) gives

$$F_{x,A} = -\left\langle \psi \left| \frac{\partial \hat{H}}{\partial X_A} \right| \psi \right\rangle - \left\langle \frac{\partial \psi}{\partial X_A} \left| \hat{H} \right| \psi \right\rangle - \left\langle \psi \left| \hat{H} \right| \frac{\partial \psi}{\partial X_A} \right\rangle \quad (4.2.4)$$

$$= -\left\langle \psi \left| \frac{\partial \hat{H}}{\partial X_A} \right| \psi \right\rangle - E \left[\left\langle \frac{\partial \Psi}{\partial X_A} \left| \Psi \right\rangle + \left\langle \Psi \left| \frac{\partial \Psi}{\partial X_A} \right\rangle \right] \quad (4.2.5)$$

where the last term vanishes because of constant normalisation. Hence we are left with one term

$$F_{x,A} = -\left\langle \psi \left| \frac{\partial \hat{H}}{\partial X_A} \right| \psi \right\rangle \quad (4.2.6)$$

Due to the kinetic energy and the electron electron repulsion being independent of the nuclear coordinates, the only terms that will remain are the nuclear–nuclear repulsion and the external potential, giving the following force

$$F_{x,A} = -\sum_{A>B} Z_A Z_B \frac{X_{AB}}{R_{AB}^3} + Z_\alpha \sum_i \int \rho(\mathbf{r}) \frac{x_A}{r_{iA}^3} d\mathbf{r} \quad (4.2.7)$$

where X_A and X_{AB} are the x-coordinates of nucleus A relative to the origin and nucleus B respectively. Similarly x_A is the coordinate of the electron relative to nucleus A. Hence the force on a given nucleus is due to the charge of the electric field generated by the electrons times the charge of the nucleus, and the sum of all the other fields arising from the other nuclei present. The conjecture made by Feynman in his paper was that just as valence bonds are formed by a high concentration of charge between nuclei, van der Waals forces also arise when there is a higher level of charge concentrated between the nuclei. Two atoms separated by a large distance R , experience a distortion in their respective charge distributions towards each other, and hence a dipole moment of $\frac{1}{R^7}$ is induced. Feynman furthermore conjectured that a large part of the dispersion interaction force of magnitude $\frac{1}{R^7}$, arose from the attraction of each nucleus to its own

local distortion in the electronic charge distribution. This attraction being greater than the repulsion between the nuclei. Illustrations of this will be presented in the results section of the helium dimer at $R = 8.0, 8.5$ and 9.0 a.u. The conjecture was later verified by Hunt et al. [60] and discussed further by Allen and Tozer [59].

4.2.2 Ensuring the validity of the Hellmann–Feynman theorem

A.C. Hurley [61, 62] investigated the calculation of molecular energies through the electrostatic theorem of Hellmann and Feynman. He examined the necessary conditions for the theorem to hold. In this section we follow his argument to outline how we can ensure that the electrostatic theorem holds. Here, Ψ is a given normalized electronic wave function, such as those discussed in the chapter on electronic structure theory. This wave function may be represented in terms of a set of parameters, denoted by μ_r , which in theory constitutes an infinite set. The complication which occurs when the Hellmann–Feynman force is evaluated is that the set of parameters μ_r may themselves depend on the nuclear coordinates. An example where this is the case is for wave functions expressed in terms of molecular orbitals, which are described by nuclear centred atomic orbitals. The wave function and parameters

$$\Psi = \Psi(\mu_r; x_a) \quad (4.2.8)$$

$$\mu_r = \mu_r(X_A, Y_A, Z_A) \quad (4.2.9)$$

where X_A, Y_A, Z_A are the Cartesian nuclear coordinates, and x_a denote the spatial and spin coordinates of the electrons with respect to nucleus A . Taking the expectation value of the electronic Hamiltonian, where according to the BO–approximation the nuclei coordinates are stationary, $H(X_A, Y_A, Z_A)$ gives

$$E(X_A, Y_A, Z_A) \equiv \tilde{E}(X_A, Y_A, Z_A, \mu_r) = \langle \Psi(\mu_r; x_a) | H(X_A, Y_A, Z_A) | \Psi(\mu_r; x_a) \rangle \quad (4.2.10)$$

where $\tilde{E}(X_A, Y_A, Z_A, \mu_r)$ represents the energy for a wave function dependent upon the parameters μ_r . The force on a given nucleus is minus the derivative of the energy with respect to the nuclear coordinate X_A

$$\frac{\partial E}{\partial X_A} = \frac{\partial \tilde{E}}{\partial X_A} + \sum_{r=1}^{\infty} \frac{\partial \tilde{E}}{\partial \mu_r} \frac{\partial \mu_r}{\partial X_A}. \quad (4.2.11)$$

From the derivative it is evident that this reduces to the Hellmann–Feynman electrostatic theorem if the last term vanishes. By having the basis functions detached from the nuclei, and optimizing their positions to obtain their lowest energy, something which will be referred to as “floating functions” in this work, we make all the parameters independent of the nuclear coordinates and so,

$$\frac{\partial \mu_r}{\partial X_A} = 0 \quad (4.2.12)$$

Hurley formulated the *generalized electrostatic theorem*, stating that: in the case of all the parameters satisfying the Rayleigh Ritz variation principle, then there will be complete

agreement between the conventional method and the electrostatic theorem. The use of floating Gaussians [63] would ensure that the Hellmann–Feynman theorem held for a variational method. However, this thesis uses the CCSD(T) density, and coupled cluster is a non-variational method. The way to circumvent this remaining problem is through the use of the Lagrangian approach of Helgaker and Jørgensen [64–67]. The combined use of the Lagrangian method and floating Gaussian functions ensures the validity of the Hellmann–Feynman theorem for the non-variational CCSD(T) method.

4.2.3 Computational details

One physical motivation in support of using floating functions, is that when two atoms interact, there will be a deformation of the charge density surrounding each nucleus. When using basis functions that are situated on the nuclear centre, this deformation is not well accounted for without the aid of augmenting and higher angular momenta functions. By floating, a smaller basis set may be used to achieve the same effect. Floating functions had previously been used in the DALTON code [63], however this implementation had not been maintained, and therefore a new implementation had to be carried out. The necessary changes to allow for the optimization of the basis function positions were performed inside the geometry optimizer in the development OEP branch of the DALTON code, along with the construction of a more flexible molecular input, where any general system could in principle be used with floating basis functions.

The atom was defined to be a nuclear charge, with no basis functions and an additional centre with orbital basis functions, but zero charge. For the calculations which employed an auxiliary basis, such as the OEP or the WY methods described in Section 2.2.70 and 3.3.2, these basis functions were placed on the nuclear centre. Floating these sets had no observable effect on the calculated forces. The helium dimer studied here consists of two centres with nuclear charge Z , separated by a fixed distance R , and two centres with $Z = 0$ containing the orbital basis functions, whose positions are optimized to give the lowest energy. To correct for the basis set superposition error all calculations presented in this chapter are counterpoise corrected according to the scheme of Boys and Bernardi [68]. The procedure is as follows:

1. The redundant internal coordinates were determined and constraints introduced to ensure a rigid nuclear framework.
2. The positions of the floating functions were optimized at the CCSD(T)/uncontracted d-aug-cc-pVQZ level.
3. The energy of the atoms was then calculated with the use of the same optimized basis as the dimer, but with one nuclear centre removed.
4. The interaction energy was calculated by subtracting the energies of each atom calculated in the basis set of the dimer, from the dimer energy.

The BSSE-correction of Boys and Bernardi [68] is defined for the energy. A similar definition may be obtained for the forces by differentiation of the BSSE-correction of

the energy. The correction for the forces was obtained by calculating the Hellmann–Feynman force in the dimer, and in the same basis, calculating the molecular gradient on the individual atom in the same basis. The standard molecular gradient was applied for the atomic systems since removing one nuclear centre leads to the electrostatic theorem no longer being valid.

The Hellmann–Feynman theorem was used throughout this work to measure the accuracy of the Kohn–Sham densities. The forces calculated at CCSD(T) level were compared with the forces calculated from Kohn–Sham densities, providing a way of quantifying the accuracy of the density. The Kohn–Sham densities corresponding to the accurate densities calculated with the CCSD(T) method, were obtained by the scheme of Wu and Yang discussed in Section (3.3.2) of Chapter 3.

The Kohn–Sham potentials were also obtained utilizing the WY method. The Heaton–Burgess smoothing norm approach [69] with a regularization parameter of 10^{-5} was employed to ensure well behaved potentials. The correlation potentials for the dimer were obtained by applying the direct optimization method of Wu and Yang to a supplied Hartree–Fock density and then subtracting this approximate exchange potential from the full exchange–correlation potential.

Due to the small magnitude of the density distortions, capturing the charge–rearrangements proved a challenging task, and required careful thought with respect to the choice of basis sets used. Furthermore, due to the floating functions only being slightly displaced off the nuclear centres, as was noted by Hurley [61, 62], a high degree of accuracy was required in the initial optimization. Hence very tight convergence criteria on the nuclear gradient and energy were applied for all three geometries.

4.2.4 Results and Discussion

Choice of basis set

A range of correlation consistent basis sets developed by Dunning [70, 71] were considered in this work. Important factors considered when choosing the basis set, included the level of augmentation, the cardinal number, and whether the orbital and auxiliary potential expansion basis in the WY calculation should be kept equal. Figure 4.2, shows that the best agreement is found by having a large auxiliary basis set, in this case with cardinal number six. Figure 4.3 shows the counterpoise, and non–counterpoise corrected forces at an increasing level of augmentation, with the cardinal number being three and six for the orbital and auxiliary basis respectively. For the augmentation level, Figure 4.3 illustrates that the best agreement between the forces of the input density and the forces for the resulting Kohn–Sham density are found at the double augmentation level. Furthermore, the plot illustrates the significance of the BSSE–correction, particularly for basis sets with double or greater augmentation. The figure illustrates that the forces based on the CCSD(T) density and the Kohn–Sham density are closest at double augmentation. Dunning investigated the binding energy of the neon dimer [72] using CCSD(T), and concluded that the use of a d-aug-cc-pVQZ recovered 96 % of the binding energy.

The interaction energy for two helium atoms as a function of their internuclear separation R is displayed in Figure 4.4. An accurate reference for comparison is

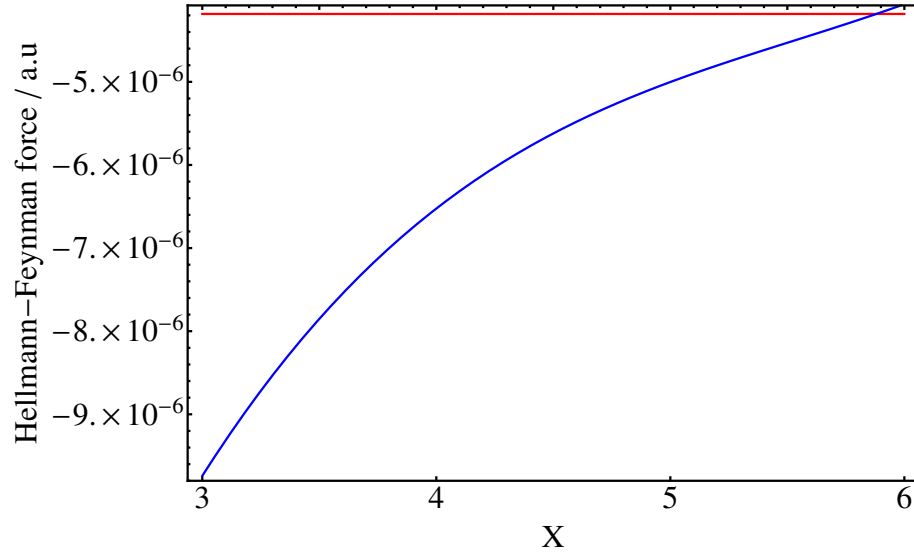


Figure 4.2: The Hellmann–Feynman forces calculated for a helium dimer at $R=9.0$ a.u., as a function of the cardinal number, X , for the auxiliary basis, where $X = 3, 4, 5$ and 6 . The orbital basis is un-contracted d-aug-cc-pVTZ, and the auxiliary un-contracted d-aug-cc-pVXZ. The red line are the forces calculated with the CCSD(T) densities, whereas the blue are the corresponding forces obtained with Kohn–Sham densities.

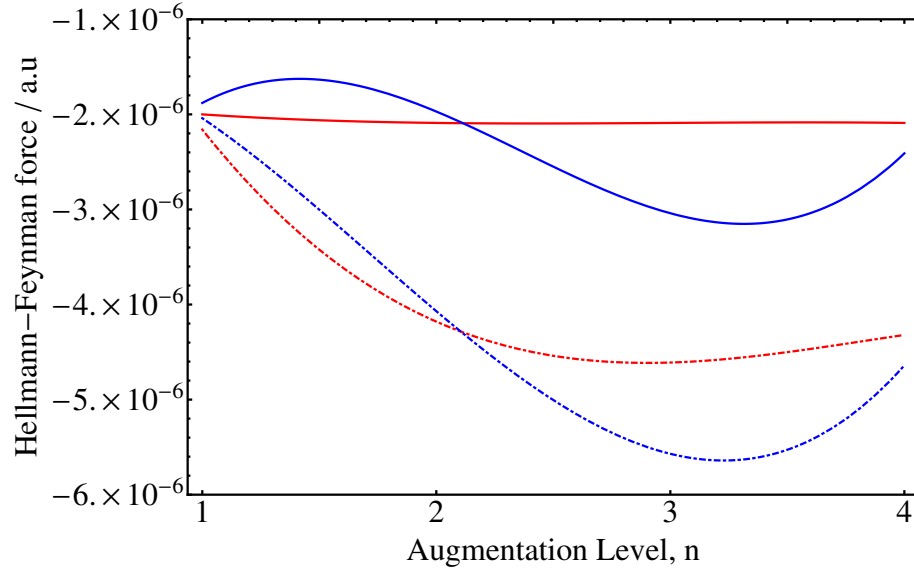


Figure 4.3: The Hellmann–Feynman forces calculated for the helium dimer at $R=9.0$ a.u., as a function of the level of augmentation, starting at single augmentation (labelled as 1 on the x -axis) and ending with quadruple augmentation (labelled by 4). The basis sets were un-contracted $naug$ -cc-pVTZ and $naug$ -cc-pV6Z for the orbital and auxiliary, respectively, where n is the level of augmentation. The BSSE-corrected forces are displayed with thick lines, and the un-corrected with dot-dashed lines. The red lines correspond to the forces obtained from the CCSD(T) densities, and the blue lines are the corresponding forces obtained with the Kohn–Sham densities.

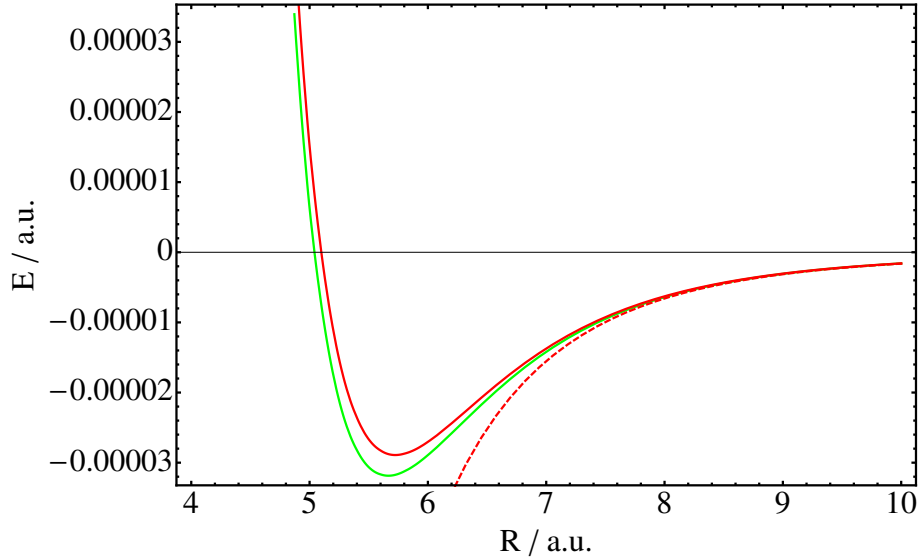


Figure 4.4: The interaction energy curve of two helium atoms where the red curve is calculated with d-aug-cc-pVTZ and the green is calculated with d-aug-cc-pVQZ, both uncontracted. The red dashed line is E_{disp} evaluated by the coefficients of Korona et al. [58] using Eq. (4.1.1). All quantities are in a.u.

provided by the dispersion energy calculated using Eq. (4.1.1) with accurate dispersion coefficients from Korona et al. [58]. It is clear from studying this figure that the onset of the dispersion region is approximately 8.0 a.u. Furthermore, a significant change is observed in the van der Waals minimum of the curve arising from the highest cardinal number in comparison with the lowest, the cardinal number of four providing a lower minimum.

4.2.5 Dispersion forces from electronic densities

In the rest of the work presented we will concentrate on the dispersion region, defined by internuclear separations beyond 8.0 a.u., and employ the d-aug-cc-pVQZ basis set to study the dimer at the three geometries $R=8.0$, 8.5 and 9.0 a.u. In order to provide an estimate of the accuracy of the WY method employed to investigate interactions of such a small magnitude we consider the forces acting on the nuclei. These forces are presented in Table 4.1. The forces are calculated at the CCSD(T) level through the standard geometrical derivative, and the Hellmann–Feynman theorem of Eq. (4.2.7). This provided an effective measure of whether the electrostatic theorem was satisfied by the use of floating functions. As can be observed in the table, the forces calculated at the CCSD(T) level agree to better than 10^{-7} , which surpasses the level of precision required in this work, and is a strong indication that the method is effective. For comparison the forces also were calculated using Eq. (4.2.13) with accurate dispersion coefficients of Korona et al. [58].

$$F_{\text{disp}} = -\frac{dE_{\text{disp}}}{dR} = -2n \sum_{n=3}^{\infty} \frac{C_{2n}}{R^{2n+1}} \quad (4.2.13)$$

Comparing these accurate forces with the ones obtained from relaxed CCSD(T) densities provides insight into the accuracy of the CCSD(T) results obtained at this level of theory. Through the WY procedure, the Kohn–Sham densities which should correspond to the relaxed CCSD(T) densities are obtained. The resulting Hellmann–Feynman forces obtained from these densities, show a discrepancy with the forces calculated with CCSD(T) densities. This discrepancy is of the order 5×10^{-7} and provides an estimate of the accuracy of reproduction of the CCSD(T) densities. However, the forces obtained with the Kohn–Sham densities preserve the trend displayed across the three geometries for the accurate forces. We now go on to discuss the electronic charge density distortions that arise with long-ranged interactions.

Table 4.1: The analytic, Hellmann–Feynman and accurate forces calculated using the dispersion coefficients of Korona et al. [58] which range from $n = 3$ to $n = 8$ in Eq. (4.2.13). calculated for the three geometries at uncontracted d-aug-cc-pVQZ/d-aug-cc-pV6Z level. Results are presented for the CCSD(T) method and the WY[CCSD(T)] approach. All the forces are of the magnitude 10^{-6} a.u.

R	$F_{\text{CCSD(T)}}^{\text{Ana}}$	$F_{\text{CCSD(T)}}^{\text{Hel.-Fey.}}$	$F_{\text{WY[CCSD(T)]}}^{\text{Hel.-Fey.}}$	F_{disp}
8.0	-4.9	-4.9	-4.4	-5.4
8.5	-3.8	-3.8	-3.3	-3.4
9.0	-2.8	-2.8	-2.4	-2.2

Density and potential differences

Figures 4.5, 4.6 and 4.7 are plots of the charge rearrangement as a result of the interaction between two helium atoms at $R=8.0$, 8.5 and 9.0 a.u. separation respectively. These are calculated by taking the difference between the density of dimer and that of each atom, calculated in the dimer basis set. The nuclei are then located at ± 4.0 , ± 4.25 and ± 4.5 a.u. The plots demonstrate that there is a significant buildup of charge density on the side of each nucleus that is closest to the other. This corresponds to the image portrayed by Feynman [26], and is consistent with the existence of an attractive force. The resulting forces which were calculated for the interaction at the aforementioned separations are all attractive, demonstrating that distortions at the 10^{-7} level induce an attractive force which outweighs the nuclear nuclear repulsion. Looking back at Eq. (4.2.7), the only attractive term is the one containing the interaction between the charge density $\rho(\mathbf{r})$ and the nuclear charge, Z . Comparing with the plots obtained by Allen and Tozer [59], there is a larger discrepancy between the CCSD(T) and Kohn–Sham density differences presented here, than the BD(T) and HFKS ones in Ref. [59]. This is reflected in the resulting forces calculated for the three geometries. However, it is important to keep in mind that the potential utilized in this work is $v_{\text{xc}}(\mathbf{r})$, rather than only the correlation potential. The explanation for the difference with the results of Allen and Tozer is that the expansion used in the effective potential of Wu and Yang [55] is not sufficiently flexible, whereas the approach employed in Ref. [59] did not require the auxiliary functions to be expanded.

The density difference plots show how the interaction decreases with an increasing distance R , the distortions close to the nucleus becoming smaller in magnitude. Through

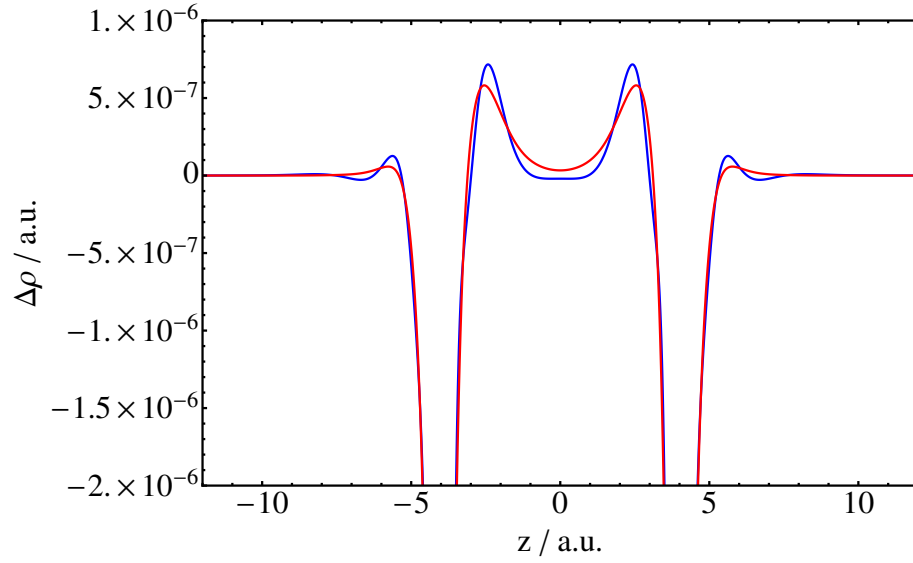


Figure 4.5: The CCSD(T) (in red) and the Kohn–Sham (in blue) density differences of two helium atoms at $R=8.0$ a.u., obtained by applying the WY scheme to the CCSD(T) relaxed density with uncontracted d-aug-cc-pVQZ/d-aug-cc-pV6Z basis sets for the orbital and potential expansion, respectively.

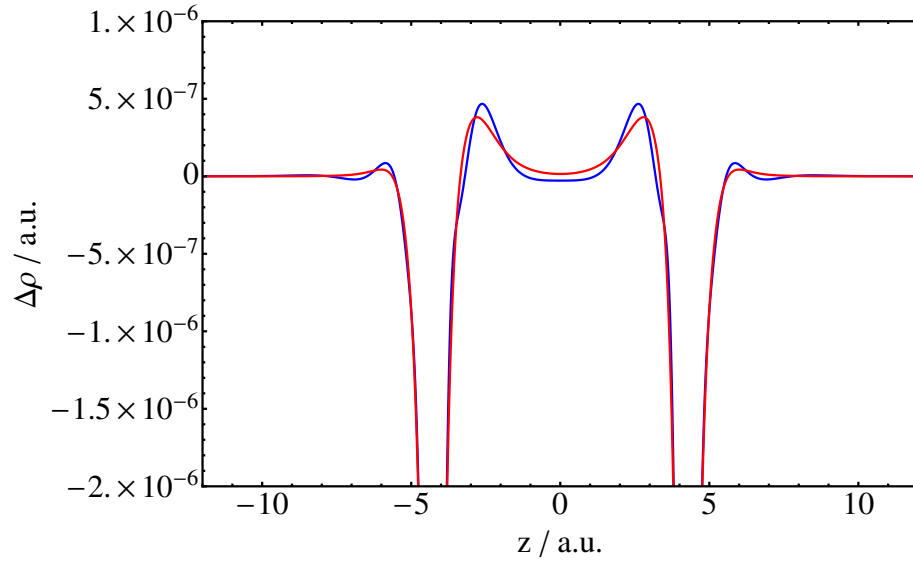


Figure 4.6: The density difference CCSD(T) (in red) and the Kohn–Sham (in blue) of two helium atoms at $R=8.5$ a.u., obtained by applying the WY scheme to the CCSD(T) relaxed density with uncontracted d-aug-cc-pVQZ/d-aug-cc-pV6Z basis sets for the orbital and potential expansion, respectively.

the application of the WY approach we are able to investigate the exchange–correlation part of the Kohn–Sham potential that reproduces the CCSD(T) densities. In the plots presented in this work, the spurious oscillations in the potential which are located at the nuclei have been removed through the smoothing norm procedure of Heaton Burgess [69].

The potentials displayed in Figure 4.8 and Figure 4.9 are the exchange–correlation

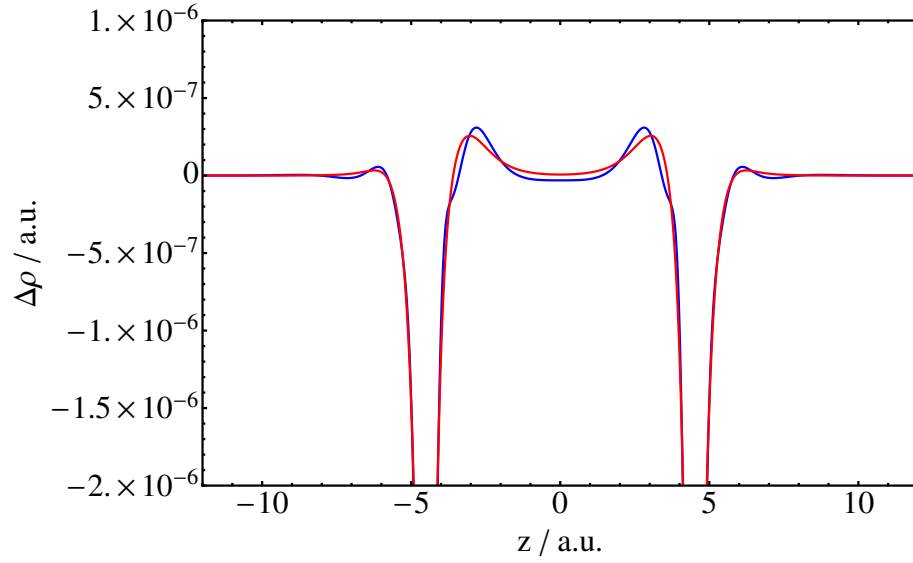


Figure 4.7: The density difference CCSD(T) (in red) and the Kohn–Sham (in blue) of two helium atoms at $R=9.0$ a.u., obtained by applying the WY scheme to the CCSD(T) relaxed density with uncontracted d-aug-cc-pVQZ/d-aug-cc-pV6Z basis sets for the orbital and potential expansion, respectively.

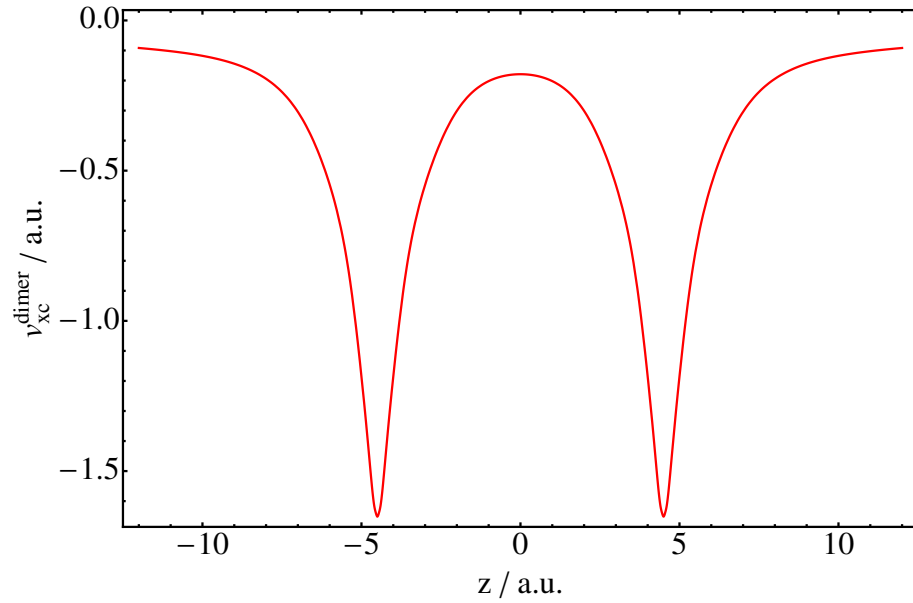


Figure 4.8: The exchange–correlation potential, $v_{xc}(\mathbf{r})$ for the helium dimer at $R=9.0$ a.u., obtained by applying the WY scheme to the CCSD(T) relaxed density with uncontracted d-aug-cc-pVQZ/d-aug-cc-pV6Z basis sets for the orbital and potential expansion, respectively.

and correlation potential respectively, of the dimer at $R=9.0$ a.u.

The correlation potential obtained by subtracting the approximate exchange potential determined in a WY(HF) calculation has a structure which closely resembles the accurate quantum Monte Carlo atomic potentials by Umrigar and Gonze in Ref. [73].

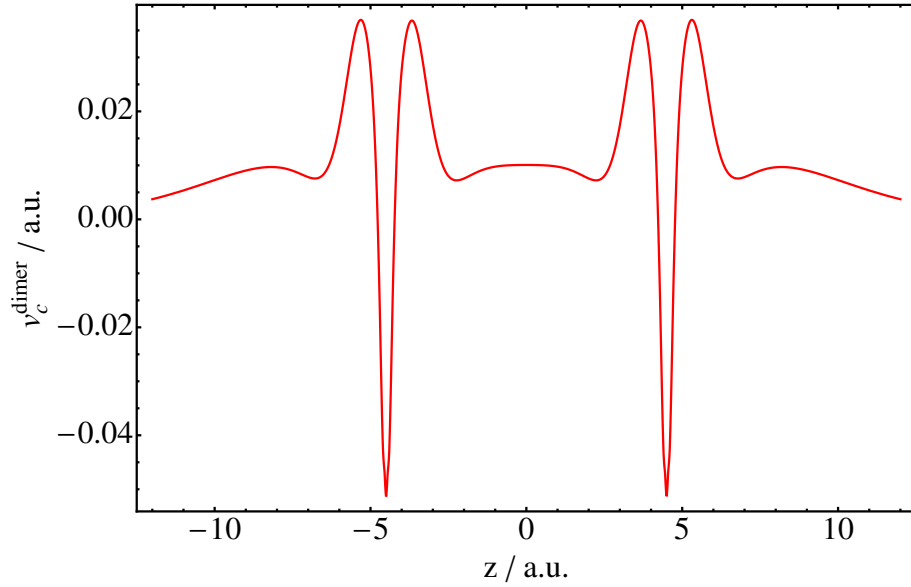


Figure 4.9: The correlation potential, $v_c(\mathbf{r})$ for the helium dimer at $R=9.0$ a.u., obtained by applying the WY scheme to the HF density with uncontracted d-aug-cc-pVQZ/d-aug-cc-pV6Z basis sets for the orbital and potential expansion and subtracting it from the exchange–correlation potential, $v_{xc}(\mathbf{r})$.

Energy components

The picture of the dispersion interaction given in this chapter is that subtle density distortions induced by the presence of a far away atom were the dominant contribution to the dispersion force. However, no information was retrieved concerning the resulting dispersion energy. Through studying the energy components one can form an understanding of how the total interaction energy is composed from the contributions to the Kohn–Sham energy, as well as gain insight into how the interaction arises. Table 4.2 displays the energy components for the dimer, and each atom and the subsequent BSSE corrections for the interactions. These Kohn–Sham quantities, T_s , E_{ne} , E_J and E_x , were obtained using the scheme of Wu and Yang, as described in the computational section of this chapter. The total kinetic energy, T , the electronic interaction, W , and the total energy of the system are determined by a CCSD(T) calculation. Finally the Kohn–Sham correlation energy is calculated via,

$$E_c = W - E_J - E_x + T_c \quad (4.2.14)$$

with T_c being the difference between the total and the non–interacting kinetic energy of the system and thus representing the correlation contribution to the kinetic energy. The total two–electron contribution then becomes by simple rearrangement, the sum of the Coulomb energy, the exchange energy and the difference $E_c - T_c$

$$W = E_J + E_x + E_c - T_c \quad (4.2.15)$$

By looking at the BSSE–corrected interaction energies of Table 4.2 it becomes clear that the dominant term in the above expression is the Coulomb energy, the exchange

and correlation terms being several orders of magnitude smaller. Looking again at the components for the interaction it is observed that the nuclear electron attraction energy E_{ne} is twice the magnitude of the Coulomb energy and the nuclear repulsion energy. The two latter quantities being similar to 10^{-5} a.u. for all three geometries. The picture that is forming is one where the large separation R leads to the dimer closely resembling two completely separated atoms. Hence the Coulomb interaction for the dimer will upon subtraction of two separate atoms, be the inter-atomic Coulomb repulsion. This repulsion, given by

$$J[\rho] = \frac{1}{2} \int \int \frac{\rho(\mathbf{r})\rho(\mathbf{r}')}{|\mathbf{r} - \mathbf{r}'|} d\mathbf{r}d\mathbf{r}'. \quad (4.2.16)$$

where \mathbf{r} denotes the position of electron 1 and \mathbf{r}' denotes the position of electron 2. We consider that electron 1 is localized to atom 1, and electron 2 is localized to atom 2. This allows us to approximate the denominator of Eq. (4.2.16) with the internuclear separation R . Assuming further that there is no density overlap between the atoms in the dimer, we may approximate the electron densities in Eq. (4.2.16) to be point charges, both of value -2. Taking the sum over the atoms for $R = 8.0$ a.u. returns a value of 0.5 a.u., which is exceedingly close to the Coulomb interaction energy in Table 4.2 and consequently, the two-electron interaction. This implies that the long-range Coulomb interactions dominate the two-electron interaction energy by inducing charge density distortions which are localized to each atom. As conjectured by Feynman [26], these local distortions give rise to the main part of the dispersion force on each nucleus. The small differences of each term from the idealized values in this discussion reflect the small density distortions discussed in Section 4.2.5.

Having understood the relative magnitudes of the interaction energy components by the simple analysis above, we note that the total interaction energy is close to the correlation energy recovered by DFT. Having differences of approximately 0.6, 0.3 and 0.1 μH for the geometries $R=8.0, 8.5$ and 9.0 a.u. This indicates that the other contributions essentially cancel, their sum reduces to approximately $-10^{-6}E_h$ for each of the geometries considered here. This emphasizes the delicate balance and cancellations between the various energy components.

To summarize, we have observed that the subtle density distortions which arise due to long-ranged dispersion interactions may be captured within a reasonable accuracy with the direct optimization procedure of Wu and Yang for determining the Kohn–Sham densities and potentials. The discrepancies between the CCSD(T) and Kohn–Sham density differences were larger than the ones reported by Allen and Tozer for the BD(T) and HFKS densities in Ref. [59]. This is due to considering the total exchange–correlation potential, v_{xc} instead of the correlation potential, v_c , and may be attributed to numerical difficulties associated with the expansion of the auxiliary basis. Further investigation of this effect is ongoing. In the present work, the level of accuracy is accepted, considering the small magnitudes of the dispersion interactions. The WY procedure has allowed us to investigate the Kohn–Sham energy components, and a comparison of the interaction energy components revealed subtle cancellations leading to a total interaction energy resembling the interaction correlation energy component in magnitude. We proceed in the following chapter to investigate the transition from a non-interacting Kohn–Sham system to the physical system.

Table 4.2: Total and interaction energies in a.u. calculated by applying the WY scheme of Wu and Yang [55] to an input CCSD(T) density using the uncontracted d-aug-cc-pVQZ/d-aug-cc-pV6Z basis set. CCSD(T) energy components are also included.

R	E_{tot}	T	W	E_{nn}	T_{s}	E_{ne}	E_{J}	E_{x}	E_{c}
<i>Dimer Total Energies</i>									
8.0	-5.805422392	5.802474344	2.393153977	0.500000000	5.729960999	-14.501050713	4.596356038	-2.048177379	-0.082511337
8.5	-5.805420069	5.802485101	2.363749593	0.470588235	5.729973638	-14.442242998	4.566950851	-2.048180899	-0.082508896
9.0	-5.805418269	5.802492615	2.337610272	0.444444444	5.729982357	-14.389965601	4.540810648	-2.048182817	-0.082507301
<i>Atomic Total Energies with Only the Near Atom Functions Included at the Dimer Optimized Positions</i>									
8.0	-2.902706854	2.901250419	0.946586071	0.000000000	2.864996812	-6.750543344	2.048182941	-1.024091471	-0.041251792
8.5	-2.902706854	2.901250419	0.946586071	0.000000000	2.864996812	-6.750543344	2.048182941	-1.024091471	-0.041251792
9.0	-2.902706854	2.901250419	0.946586071	0.000000000	2.864996812	-6.750543344	2.048182941	-1.024091471	-0.041251792
<i>BSSE Corrections</i>									
8.0	-0.000001144	0.000003302	0.000002472	0.000000000	0.000003120	-0.000006918	0.000006109	-0.000003055	-0.000000400
8.5	-0.000000986	0.000003723	0.000002527	0.000000000	0.000003555	-0.000007236	0.000006015	-0.000003007	-0.000000313
9.0	-0.000000745	0.000004015	0.000002382	0.000000000	0.000003866	-0.000007141	0.000005525	-0.000002762	-0.000000232
<i>BSSE Corrected Interaction Energies</i>									
8.0	-0.000006396	-0.000033099	0.499976892	0.500000000	-0.000038863	-0.999950189	0.499977938	0.000011672	-0.000006953
8.5	-0.000004389	-0.000023184	0.470572397	0.470588235	-0.000027096	-0.941141837	0.470572940	0.000008057	-0.000004688
9.0	-0.000003071	-0.000016253	0.444433367	0.444444444	-0.000018999	-0.888864630	0.444433717	0.000005648	-0.000003252

Chapter 5

A study of the helium dimer through the adiabatic connection

Chapter 4 examined the dispersion interaction for the helium dimer in the Kohn–Sham framework. We followed the work of Allen and Tozer [59], and studied the subtle density distortions which were the result of the presence of a distant atom, but carried out this analysis with respect to the full exchange–correlation potential, $v_{xc}(\mathbf{r})$ bringing the results into the full Kohn–Sham framework. Through these results we gained insight into the dispersion interaction, and how it arises. However, we are interested in attaining more information into the behaviour of the various Kohn–Sham components of the interaction energy. In order to achieve this we must go beyond the non-interacting Kohn–Sham system and approach the physical system. In order to connect the non-interacting system, and the physical system we employ the adiabatic connection [8–11], which will be introduced in the following section. Two manners of switching on the electronic interactions will be discussed, one applying a simple linear scaling of the interactions and another more complicated scaling based on the error function, which may be used to emphasize the range of the interactions.

5.1 The Adiabatic Connection

The Lieb theory discussed in Chapter 2 provides us with the necessary tools to study the evolution from the non-interacting Kohn–Sham system to the physical system with full interaction between the electrons. We begin by considering a system which can be described by the Hamiltonian:

$$H_\lambda[v] = -\frac{1}{2} \sum_{i=1}^N \nabla_i^2 + \frac{1}{2} \sum_{i \neq j}^N \omega_\lambda(r_{ij}) + \sum_{i=1}^N v(\mathbf{r}_i) \quad (5.1.1)$$

where the first term is the kinetic energy operator, the second is the electron–electron repulsion operator with a dependence on the parameter λ , and the last term contains the external potential $v(\mathbf{r})$. By introducing a dependence upon λ for the two-electron operator we may vary the electronic interactions, changing the system from non-interacting at $\lambda = 0$ to the fully interacting at $\lambda = 1$ with $\omega_0(r_{ij}) = 0$ and $\omega_1(r_{ij}) = \frac{1}{r_{ij}}$

respectively. We will consider two paths for connecting these two systems, the linear path and a range-dependent error-function path, which are defined by the choice of the two-electron interaction $\omega_\lambda(r_{ij})$ as

$$\omega_\lambda^{\text{lin}}(r_{ij}) = \frac{\lambda}{r_{ij}} \quad (\text{linear}) \quad (5.1.2)$$

$$\omega_\lambda^{\text{erf}}(r_{ij}) = \frac{\text{erf}\left(\frac{\lambda}{1-\lambda}r_{ij}\right)}{r_{ij}} \quad (\text{error function}) \quad (5.1.3)$$

where the linear dependence on λ represents the conventional choice, and the range of the electronic interactions can be investigated by the use of the error function.

The ground state energy as a functional of the external potential, v may be written as

$$E_\lambda[v] = \inf_{\hat{\gamma} \rightarrow N} \text{Tr} \hat{H}_\lambda[v] \hat{\gamma} \quad (5.1.4)$$

where the infimum is performed over all ensemble density matrices $\hat{\gamma}$ containing N electrons. Lieb [33] showed that the ground state energy, $E_\lambda[v]$ is continuous and concave with respect to v . Therefore it can be represented in an alternate way by its convex conjugate, the Lieb universal density functional, $F_\lambda[\rho]$. The latter being a functional of the electronic density ρ . The conjugate relationship of $E_\lambda[v]$ and $F_\lambda[\rho]$ may be generalized for all interaction strengths λ :

$$E_\lambda[v] = \inf_{\rho \in X} [F_\lambda[\rho] + (v|\rho)] \quad (5.1.5)$$

$$F_\lambda[\rho] = \sup_{v \in X^*} [E_\lambda[v] - (v|\rho)] \quad (5.1.6)$$

where X^* is dual to X . This quality ensures that the interaction $(v|\rho)$ is finite for all external potentials, $v \in X^*$ and densities $\rho \in X$. It was further shown by Lieb that the universal density functional in Eq. (5.1.6) may be expressed as a density-matrix constrained-search functional,

$$F_\lambda[\rho] = \inf_{\hat{\gamma} \rightarrow \rho} \text{Tr} \hat{H}_\lambda[0] \hat{\gamma} \quad (5.1.7)$$

It is important to note that the minimizations of the ground state energy functional in Eq. (5.1.4) and the density functional in Eq. (5.1.7) can be expressed in terms of the orbitals in an exact manner for $\lambda = 0$. For the cases of $\lambda > 0$ the equations become complicated many-body problems. The goal is to be able to study the link between the non-interacting system and the physical system and we therefore consider the relationship between $F_\lambda[\rho]$ for a general λ and its non-interacting limit $F_0[\rho]$,

$$F_\lambda[\rho] = F_0[\rho] + \int_0^\lambda \frac{dF_\lambda[\rho]}{d\lambda} d\lambda \quad (5.1.8)$$

Applying the Hellmann–Feynman theorem to Eq. (5.1.8)

$$\frac{dF_\lambda[\rho]}{d\lambda} = \text{Tr} \hat{W}'_\lambda \gamma_\lambda^\rho = \mathcal{W}_\lambda[\rho] \quad (5.1.9)$$

where \hat{W}_λ is the electron–electron repulsion operator in Eq. (5.1.1), with the prime denoting differentiation with respect to λ , and γ_λ^ρ is the minimizing density–matrix of Eq. (5.1.7) and noting that for the Kohn–Sham system the Lieb functional reduces to

$$F_0[\rho] = T_s[\rho] \quad (5.1.10)$$

where $T_s[\rho]$ is the non–interacting kinetic energy, the universal density functional can then be formulated as

$$F_\lambda[\rho] = T_s[\rho] + \int_0^\lambda \mathcal{W}_\nu[\rho] d\nu \quad (5.1.11)$$

where the integral gives the sum of the electronic interaction energies and a small correction to the non–interacting kinetic energy $T_c = T_\lambda - T_s$, where T_λ is the kinetic energy at interaction strength λ . This in turn can be decomposed into the following components

$$\int_0^\lambda \mathcal{W}_\nu[\rho] d\nu = J_\lambda[\rho] + E_{x,\lambda}[\rho] + E_{c,\lambda}[\rho] \quad (5.1.12)$$

where the first term is the classical Coulomb contribution given by

$$J_\lambda[\rho] = \frac{1}{2} \iint \omega_\lambda(r_{12}) \rho(\mathbf{r}_1) \rho(\mathbf{r}_2) d\mathbf{r}_1 d\mathbf{r}_2 \quad (5.1.13)$$

the second term is the exchange energy given by

$$E_{x,\lambda}[\rho] = \text{Tr} \hat{W}_\lambda \hat{\gamma}_0^\rho - J_\rho[\rho] \quad (5.1.14)$$

and the correlation energy is

$$E_{c,\lambda}[\rho] = \int_0^\lambda \mathcal{W}_{c,\nu}[\rho] d\nu \quad (5.1.15)$$

The exchange and correlation energies may be combined into the exchange–correlation energy given by

$$E_{xc,\lambda}[\rho] = \int_0^\lambda \mathcal{W}_{xc,\nu}[\rho] d\nu \quad (5.1.16)$$

We have now defined the three integrals, $\mathcal{W}_\lambda[\rho]$, $\mathcal{W}_{xc,\lambda}[\rho]$ and $\mathcal{W}_{c,\lambda}[\rho]$, which represent the Coulomb–exchange–correlation, exchange–correlation and correlation energies respectively. These integrands can be recovered by supplying a highly accurate approximation of the physical density at $\lambda = 1$ to the universal Lieb functional in Eq. (5.1.6) for all values of λ , and calculating $F_\lambda[\rho]$ from $\lambda = 0$ to $\lambda = 1$.

5.2 An interaction adiabatic connection

The last section of Chapter 3 concerned the practical calculation of the Lieb maximization which was performed by employing the direct optimization technique of Wu and Yang [55]. For the work carried out in this thesis we apply this technique as implemented in Refs. [74, 75], for both the conventional linear and the error function adiabatic

connection paths. In order to evaluate the dispersion interaction it is necessary to consider how this interaction energy may be represented in terms of the adiabatic connection integrands. We do this by defining the helium dimer as a supermolecule (SM) and its two constituent atoms as subsystems (SS). This allows us to write the interaction energy as

$$\begin{aligned} E_{\lambda}^{\text{int}} &= E_{\lambda}^{\text{SM}} - \sum E_{\lambda}^{\text{SS}} = E_{\text{nn}} + \left[T_s^{\text{SM}} - \sum T_s^{\text{SS}} \right] + \left[E_{\text{ne}}^{\text{SM}} - \sum E_{\text{ne}}^{\text{SS}} \right] \\ &+ \left[J_{\lambda}^{\text{SM}} - \sum J_{\lambda}^{\text{SS}} \right] + \int_0^{\lambda} \left[\mathcal{W}_{\text{xc},\nu}^{\text{SM}} - \sum \mathcal{W}_{\text{xc},\nu}^{\text{SS}} \right] d\nu \end{aligned} \quad (5.2.1)$$

which is in terms of the exchange–correlation integrands defined in the previous section. Analogous expressions may be derived for the other integrands $\mathcal{W}_{\nu}[\rho]$ and $\mathcal{W}_{\text{c},\nu}[\rho]$. The calculation of these integrands for the super and subsystems are carried out by applying the methodology of Refs. [74, 75], with the same d-aug-cc-pVQZ/d-aug-cc-pV6Z basis sets for the orbital and potential expansion as employed in Chapter 4. Uncontracted basis sets are used for all calculations. The expression of Eq. (5.2.1) allows us to write the interaction integrands as

$$\mathcal{W}_{\text{typ}}^{\text{int}}[\rho] = \mathcal{W}_{\text{typ}}^{\text{SM}}[\rho] - \sum \mathcal{W}_{\text{typ}}^{\text{SS}}[\rho] \quad (5.2.2)$$

where “typ” denotes which energy components the integrand represents. In the following sections we will investigate these integrands for the linear and error–function paths and make a comparison with the standard density functional BLYP.

5.3 The linear adiabatic connection

In the present section we discuss the linear adiabatic connection, where the electronic interaction is modified by a linear scaling of the two electron operator according to Eq. (5.1.2). The Figures 5.1, 5.2 and 5.3 present the adiabatic connection integrands, $\mathcal{W}_{\text{Jxc},\lambda}^{\text{int}}$, $\mathcal{W}_{\text{xc}}^{\text{int}}$ and $\mathcal{W}_{\text{c},\lambda}^{\text{int}}$ for the interaction at the three geometries. The curves for all the interactions were calculated using CCSD(T) relaxed densities as $\rho_{\text{inp}}(\mathbf{r})$ for the Lieb maximization in Eq. (3.3.12). As discussed in the theory, integrating these quantities recovers the Coulomb–exchange–correlation, exchange–correlation and the correlation energies for the interaction, respectively. However, as was discussed in Chapter 4, the relatively small magnitudes for these interactions make it necessary to establish the level of accuracy achieved in practice.

Furthermore it was discussed in Chapter 4 that the accuracy to which the Kohn–Sham densities reproduced the CCSD(T) densities was limited by numerical difficulties associated with performing the Lieb maximization. It was suggested that the discrepancies could be attributed to applying a Gaussian expansion in the representation of the effective potential $v_s(\mathbf{r})$. Whereas the analysis in Chapter 4 was performed for the non–interacting system, ($\lambda = 0$), we here obtain the values for the integrands at each interaction strength, λ . As for the non–interacting case the counterpoise correction of Boys and Bernardi [4] has been applied, but to each given value λ in order to account for the basis-set superposition error.

The Coulomb–exchange–correlation integrand $\mathcal{W}_{\text{xc}}^{\text{int}}$ shown in Figure 5.1 for the geometries $R = 8.0, 8.5$ and 9.0 a.u., is clearly dominated by the Coulomb contribution, which is constant for the linear AC. The three integrands appear as horizontal lines on the scale presented in the figure. We note that the decay which was observed for the Coulomb interaction energy in Table 4.2 for an increasing R is consistent with the curves in Figure 5.1, which are separated by between 0.025–0.03 a.u.

The exchange–correlation integrands are presented in Figure 5.2, and correspond to subtracting the dominant Coulomb contribution from $\mathcal{W}_{\text{xc},\lambda}^{\text{int}}$. All three curves demonstrate a subtle curvature as the interaction strength increases from $\lambda = 0$ to $\lambda = 1$. From the energy components studied in Chapter 4, it is clear that the exchange component of the interaction energy dominates the exchange–correlation contribution.

This contribution is constant for the linear AC and therefore implies that the curvature displayed in Figure 5.2 is a result of the correlation contribution. The correlation only integrands are presented in Figure 5.3. Their curvature reflects the suggestion that the correlation contribution to the interaction energy arising from long ranged dispersion effects is mainly of a dynamical nature. Another argument for the correlation contribution being dynamical is found in Görling–Levy perturbation theory [76, 77], where the correlation integrand can be presented by a Taylor expansion around $\lambda = 0$,

$$\mathcal{W}_{\text{c},\lambda} = \sum_{n=1}^{\infty} \lambda^n (n+1) E_{\text{c,GL}}^{(n+1)}[\rho] \quad (5.3.1)$$

where $E_{\text{c,GL}}^{(n+1)}[\rho]$ are the Görling–Levy correlation energies to order n . In the case of dynamical correlation energies, the expansion of Eq. (5.3.1) can be truncated at low order to yield an accurate approximation. Truncating at second order would result in a linear AC with a correct initial slope. Since the curves bend upwards this would represent an overestimate, but the subtle curvature suggests a low order approximation is reasonable.

The $\mathcal{W}_{\text{xc}}^{\text{int}}$ and $\mathcal{W}_{\text{c}}^{\text{int}}$ curves in Figure 5.2 and Figure 5.3 display small irregularities around $\lambda = 1$. We investigated the possible causes of these features, and stress that the convergence of the Lieb optimization was found to be adequate for all values of λ . In order to rule out the possibility of the BSSE introducing these errors, the uncorrected curves for the $\mathcal{W}_{\text{c}}^{\text{int}}$ were presented along with the corrected curves for the two geometries $R = 8.0$ and $R = 8.5$ a.u. in Figure 5.4, where the solid lines represent the corrected curves, and the dotted lines are the uncorrected. It is evident from the curves that even without the BSSE-correction irregularities still arise around $\lambda = 1$. The errors are consistent with the discrepancies between the CCSD(T) and Kohn–Sham densities found in Chapter 4.

5.3.1 Comparison with BLYP

We now proceed to examine the standard density functional BLYP. Consistent with the previous calculations presented in this work, floating basis functions and the BSSE counterpoise correction are employed for all values of λ . The energies for the dimer, the atom and the interactions are all presented in Table 5.1. The short sighted nature of standard density functionals, due to depending on the local density, or the density and

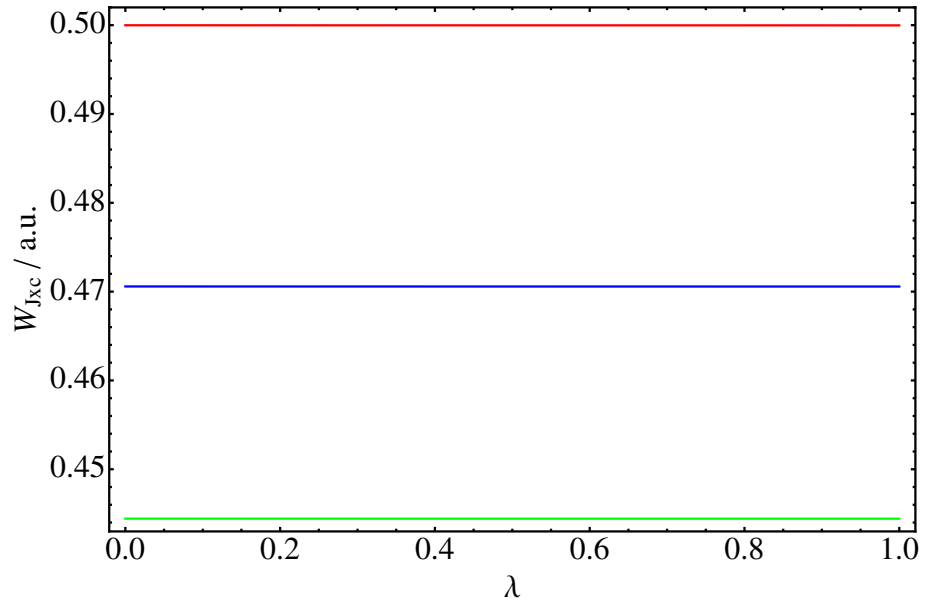


Figure 5.1: The W_{Jxc} integrand for the interaction at $R=8.0-9.0$ a.u. The red curve is $R = 8.0$ a.u., the blue is $R = 8.5$ a.u. and the green is $R = 9.0$ a.u.

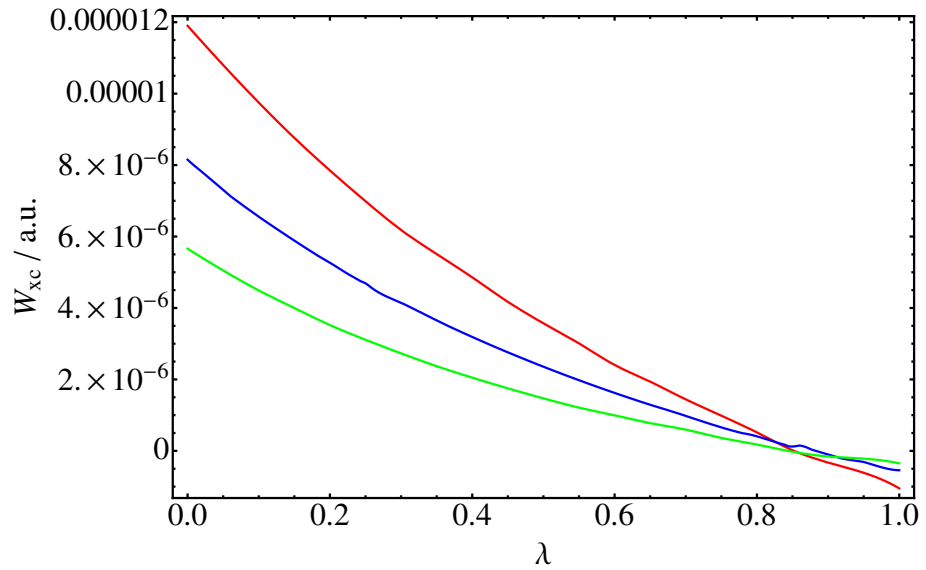


Figure 5.2: The W_{xc} integrand for the interaction at $R=8.0-9.0$ a.u. The red curve is $R = 8.0$ a.u., the blue is $R = 8.5$ a.u. and the green is $R = 9.0$ a.u.

its gradient, such as for GGAs, leads to an inability to recover the long-ranged dispersion energy. Comparing Tables 4.2 and 5.1 the total interaction energies whilst negative for CCSD(T) are positive for BLYP. Hence, whereas CCSD(T) yields an attractive dispersion interaction energy, BLYP returns a repulsive energy. The interaction energies for the exchange component, E_x^{int} that are approximated by BLYP have an incorrect sign in comparison to the CCSD(T) values obtained in Table 4.2, and therefore demonstrate a high degree of error. The interaction correlation energies, E_c^{int} recovered by BLYP show a similar trend to the ones obtained by CCSD(T) having the correct sign and the

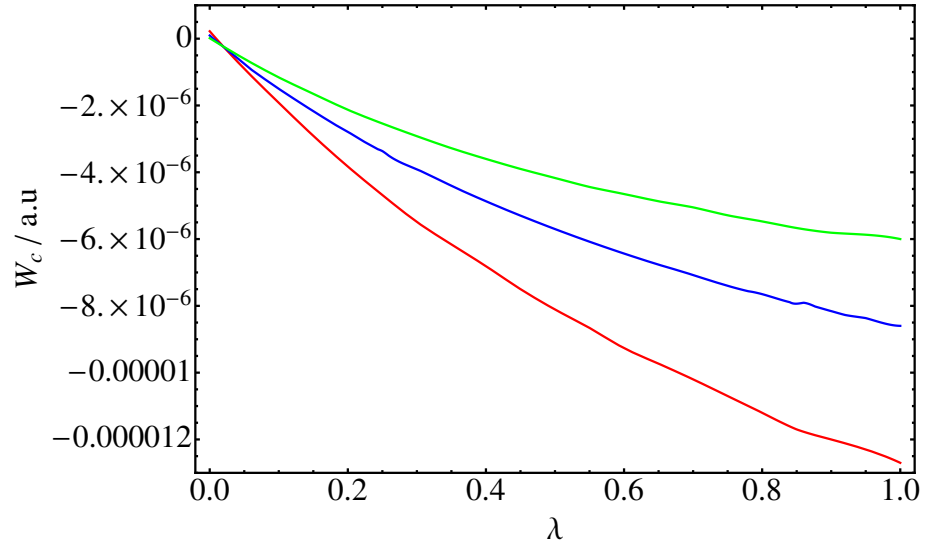


Figure 5.3: The \mathcal{W}_c integrand for the interaction at $R=8.0-9.0$ a.u. The red curve is $R = 8.0$ a.u., the blue is $R = 8.5$ a.u. and the green is $R = 9.0$ a.u.

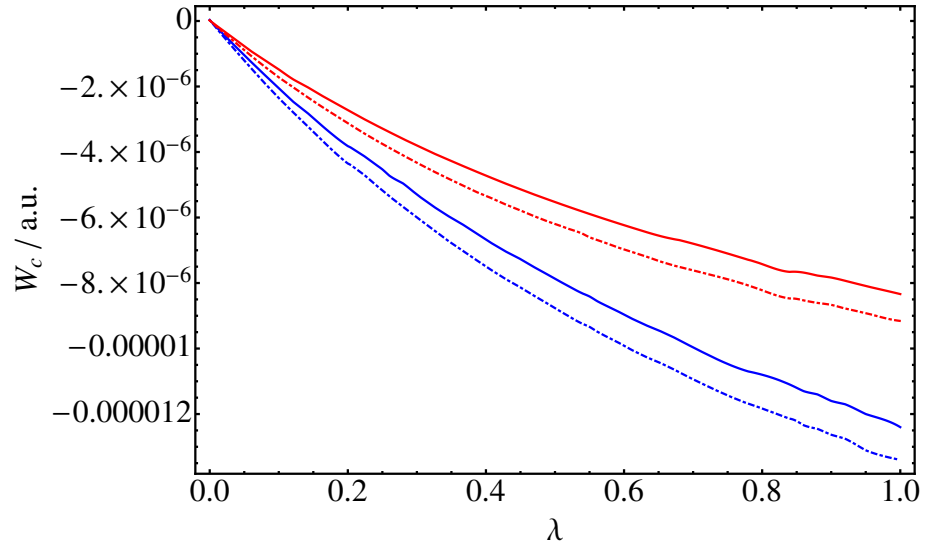


Figure 5.4: Comparison of BSSE corrected and uncorrected \mathcal{W}_c integrands at $R=8.0$ and 8.5 a.u. The red curve is $R = 8.0$ a.u., the blue is $R = 8.5$ a.u. The dashed lines are the uncorrected curves which have the same colour scheme.

same order of magnitude, but are significantly smaller.

Since the exchange contribution to the interaction AC, $\mathcal{W}_x^{\text{int}}$ is constant for the BLYP functional, we will consider the contributions from the correlation component, which changes in a non-trivial manner with λ . In the case of standard density functionals, the correlation integrand can be constructed from uniform coordinate scaled density relations, employing the general formula

$$\mathcal{W}_{c,\lambda}[\rho_{1/\lambda}] = 2\lambda E_c[\rho_{1/\lambda}] + \lambda^2 \frac{\partial E_c[\rho_{1/\lambda}]}{\partial \lambda} \quad (5.3.2)$$

Table 5.1: Kohn–Sham total and interaction energies (and their components) in a.u. calculated for the BLYP density functional approximation.

R	E_{tot}	E_{nn}	T_{s}	E_{ne}	E_{J}	E_{x}	E_{c}
<i>Dimer Total Energies</i>							
8.0	-5.813802281	0.500000000	5.746874997	-14.494935890	4.558197620	-2.036537982	-0.087401026
8.5	-5.813808651	0.470588235	5.746835150	-14.436057990	4.528758550	-2.036532668	-0.087399930
9.0	-5.813812214	0.444444444	5.746809026	-14.383733680	4.502595613	-2.036528192	-0.087399426
<i>Atom Energies in the Dimer Optimized Basis Set</i>							
8.0	-2.906908404	0.000000000	2.873382836	-6.747391171	2.029058560	-1.018259261	-0.043699368
8.5	-2.906907768	0.000000000	2.873381093	-6.747388877	2.029058585	-1.018259190	-0.043699379
9.0	-2.906907722	0.000000000	2.873381199	-6.747388862	2.029058509	-1.018259187	-0.043699381
<i>BSSE Corrected Interaction Energies</i>							
8.0	0.000014527	0.500000000	0.000109324	-1.000153549	0.500080500	-0.000019460	-0.000002289
8.5	0.000006885	0.470588235	0.000072963	-0.941280235	0.470641380	-0.000014288	-0.000001171
9.0	0.000003230	0.444444444	0.000046628	-0.888955955	0.444478594	-0.000009818	-0.000000663

where the integrand is dependent upon the coordinate scaled density $\rho_{1/\lambda}(\mathbf{r}) = \lambda^{-3}\rho(\mathbf{r}/\lambda)$ [78]. Applying this scaling relation to the LYP correlation functional was shown in Ref. [79] to yield

$$\begin{aligned}
E_c^{\text{LYP}}[\rho_{1/\lambda}] = & -a \int \frac{4\rho_\alpha\rho_\beta}{\rho(1+d\lambda\rho^{-1/3})} d\mathbf{r} \\
& - ab \int \omega_{1/\lambda} \left\{ \rho_\alpha\rho_\beta \left[2^{11/3}C_f(\rho_\alpha^{8/3} + \rho_\beta^{8/3}) + \left(\frac{47}{18} - \frac{7}{18}\delta_{1/\lambda} \right) |\nabla\rho|^2 \right. \right. \\
& - \left(\frac{5}{2} - \frac{1}{18}\delta_{1/\lambda} \right) (|\nabla\rho_\alpha|^2 + |\nabla\rho_\beta|^2) - \frac{\delta_{1/\lambda} - 11}{9} \left(\frac{\rho_\alpha}{\rho} |\nabla\rho_\alpha|^2 + \frac{\rho_\beta}{\rho} |\nabla\rho_\beta|^2 \right) \left. \right] \\
& - \left. \frac{2}{3}\rho^2|\nabla|^2 + \left(\frac{2}{3}\rho^2 - \rho_\alpha^2 \right) |\nabla\rho_\beta|^2 + \left(\frac{2}{3}\rho^2 - \rho_\beta^2 \right) |\nabla\rho_\alpha|^2 \right\} d\mathbf{r} \quad (5.3.3)
\end{aligned}$$

with ω and δ now being

$$\omega_{1/\lambda} = \frac{\exp(-c\lambda\rho^{-1/3})}{1+d\lambda\rho^{-1/3}} \rho^{-11/3} \quad (5.3.4)$$

$$\delta_{1/\lambda} = c\lambda\rho^{-1/3} + d\frac{\rho^{-1/3}}{1+d\lambda\rho^{-1/3}} \quad (5.3.5)$$

The resulting correlation integrands derived for LYP from Eq. (5.3.2) are presented in Figure 5.5 for the three geometries.

They display an erratic behaviour in comparison to the accurate curves of Figure 5.3, which could be due to the discrepancy between describing the atoms and the dimer using the BLYP functional, having a larger accuracy for the atoms, and failing to describe the dimer to similar accuracy. This can be attributed to the short-sighted nature of the standard density functionals. BLYP fails to describe long-range interactions, but in the case of atoms, these are much less significant. Hence BLYP has good accuracy for the atoms, however, the accuracy of the dimer is much more greatly compromised by missing the long-range interactions. It should be noted that all the AC-curves for BLYP were calculated using a self-consistent BLYP density. However, evaluating the curves with a CCSD(T) input density lead to nearly indistinguishable results.

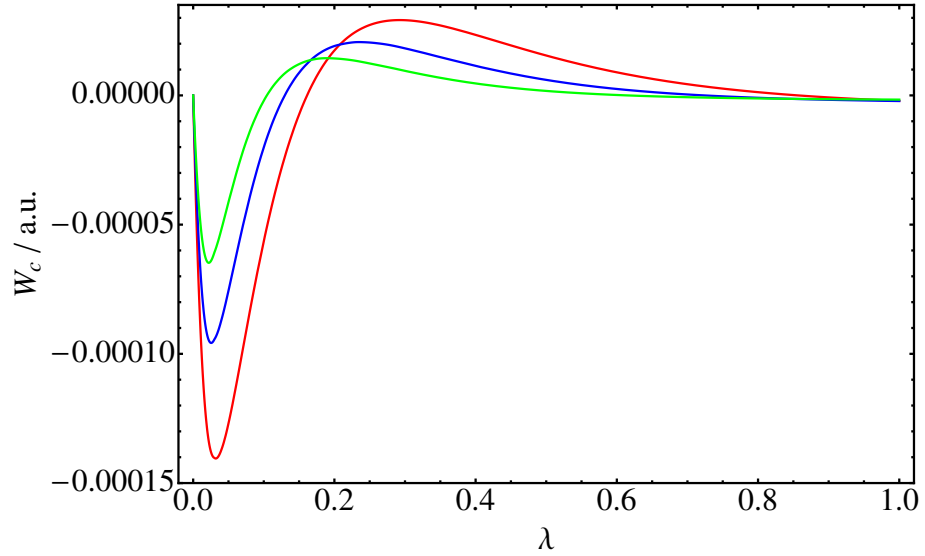


Figure 5.5: The \mathcal{W}_c integrand for the interaction at $R=8.0-9.0$ a.u. with BLYP. The red is 8.0, the blue 8.5 and the green is 9.0 a.u.

5.4 Range dependent contributions

The linear adiabatic connection plots discussed in the previous section demonstrated that the correlation contribution to the dispersion energy in the helium dimer was of a dynamic nature. In the present section we proceed to investigate the range (inter-electronic separations) for which the interactions important to dispersion occur. To this end the adiabatic connections for the interaction, $\mathcal{W}_{\text{Jxc}}^{\text{int}}$, $\mathcal{W}_{\text{xc}}^{\text{int}}$ and $\mathcal{W}_{\text{c}}^{\text{int}}$ are constructed for the error-function path [80] according to Eq. (5.1.3). The electronic interactions are modified with the coupling strength parameter λ , and the error-function results in all ranges initially being treated simultaneously, but for higher values of λ only the short-ranged interactions contribute. The choice of emphasizing the range is highly relevant to range-separated approaches [81, 82], where the division between short-range and long-range interactions is controlled by the parameter $\mu = \frac{\lambda}{1-\lambda}$. Density functionals are then employed in the description of the short-range interactions, and wave function methods applied for the long-range interactions.

The integrands for the Coulomb–exchange–correlation energy for the dimer are presented in Figure 5.6. The curves for the three geometries, $R = 8.0, 8.5$ and 9.0 a.u., become indistinguishable after $\lambda \approx 0.35$, such that the differences between the internuclear separations only arise for the long-range part. The direct Coulomb interaction is the dominant contribution to $\mathcal{W}_{\text{Jxc}}^{\text{dimer}}$ and the splitting of the curves below $\lambda \approx 0.35$ can be attributed to the long-ranged part of this interaction.

The curves for the error-function based integrands $\mathcal{W}_{\text{Jxc}}^{\text{int,erf}}$, $\mathcal{W}_{\text{xc}}^{\text{int,erf}}$, $\mathcal{W}_{\text{x}}^{\text{int,erf}}$, and $\mathcal{W}_{\text{c}}^{\text{int,erf}}$ are presented in Figures 5.7–5.10, respectively. Turning our attention first to Figure 5.7, where the scale reflects the dominant Coulomb contribution, we note that the contributions approach zero between $\lambda \approx 0.25$ and $\lambda \approx 0.35$. The interactions below this point appear to decay for an increasing internuclear separation, the repulsive Coulomb contribution being largest for $R = 8.0$ a.u. and smallest for $R = 9.0$ a.u. The

curves approach zero in the approximate area where we observed that the curves for $\mathcal{W}_{\text{Jxc}}^{\text{dimer}}$ became indistinguishable. The values for λ where the interactions approach zero correspond to a range of approximately $\mu = 0.33 - 0.5a_0^{-1}$. We note that this range includes the inverse of the van der Waals radius of the helium atom, $0.37a_0^{-1}$. Goll [16, 83, 84] suggested the use of this criteria to determine a useful value for μ in range-separated calculations.

The exchange–correlation integrand for the error–function curves, $\mathcal{W}_{\text{xc}}^{\text{int,erf}}$, is obtained by removing the classical Coulomb contribution from $\mathcal{W}_{\text{Jxc}}^{\text{int,erf}}$. In the case of range–separated methods, these exchange–correlation integrands are to be approximated, in part, by short–range density functionals. In comparison to the curves for $\mathcal{W}_{\text{Jxc}}^{\text{int,erf}}$, the shape is not completely localized to the short or long–range, displaying a large negative contribution for approximately $\lambda = 0.15$ to $\lambda = 0.25$ and a positive contribution which dominates the curve from $\lambda \approx 0.3$. In the interest of gaining more understanding of this behaviour we present the exchange integrand separately in Figure 5.9 by removing the correlation contribution, thus obtaining $\mathcal{W}_{\text{x}}^{\text{int,erf}}$. This plot reflects the E_{x} values from Table 4.2 which were found to be positive for all the internuclear separations. Furthermore, the shape of the plot indicates that the positive area of Figure 5.8 is the exchange contribution, which is dominant after $\lambda = 0.3$, and hence for the short–range interactions.

The correlation integrands for the error–function curves, $\mathcal{W}_{\text{c}}^{\text{int,erf}}$, are presented in Figure 5.10. The shape of the curves makes it evident that the correlation contribution is purely long–ranged, and clearly dominates the $\mathcal{W}_{\text{c}}^{\text{int,erf}}$ curve for low values of λ . Taking the values for which the correlation contribution is dominant into consideration, a higher range of $\mu = 0.5 - 0.65a_0^{-1}$ could be suggested as optimal values for a range–separated method. This coincides with the chosen value of $\mu = 0.5a_0^{-1}$ employed in studies of non–covalent interactions [80]. However, the choice of the optimal value of μ is system and geometry dependent, and will in addition be influenced by the choice of density functional to describe the short–range effects. The latter has not been taken into consideration in this work.

The results so far have highlighted many of the features of the dispersion interaction and the manner in which it can be treated in KS–DFT. The dispersion interaction was found to be long–ranged and with the dominant contribution being dynamical correlation, but being dependent upon several subtle cancellations between the energy terms. As an example, a poor approximation of the exchange term in BLYP led to the total interaction energy becoming repulsive rather than attractive. The findings of this chapter reflect the results in Chapter 4 as well as those of Allen and Tozer in Ref. [59]; the dispersion force arising from the long–ranged Coulomb interaction of a distant atom which induces a charge–rearrangement, resulting in an attraction between the nucleus and its own distorted density distribution.

5.5 The accuracy of the adiabatic connection for the interaction

It was briefly mentioned in the beginning of this chapter that the level of accuracy achieved in recovering the integrands had to be assessed. We therefore present some

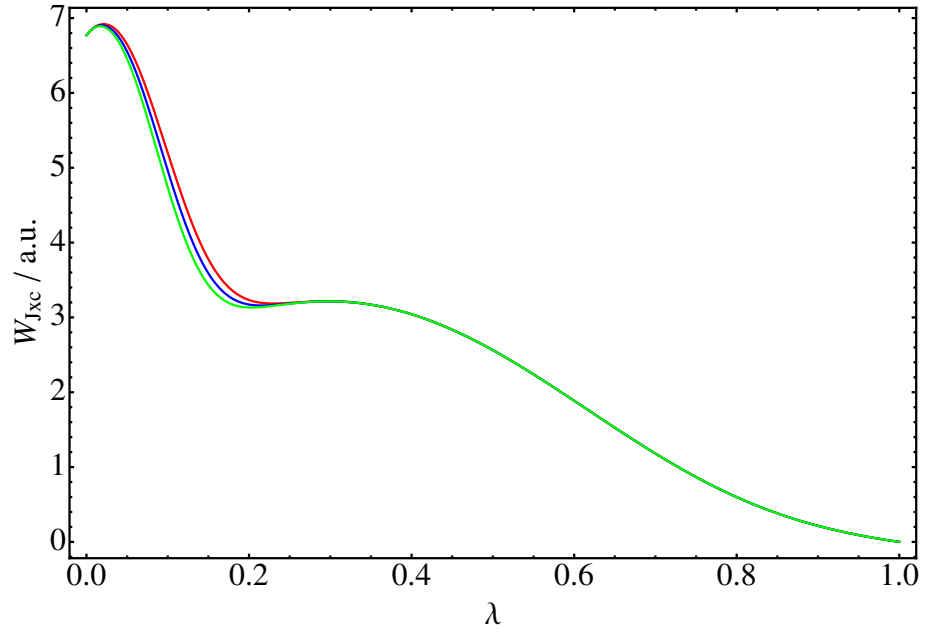


Figure 5.6: The \mathcal{W}_{JXC} integrand for the dimer at $R=8.0-9.0$ a.u. The red curve is $R = 8.0$ a.u., the blue is $R = 8.5$ a.u. and the green is $R = 9.0$ a.u.

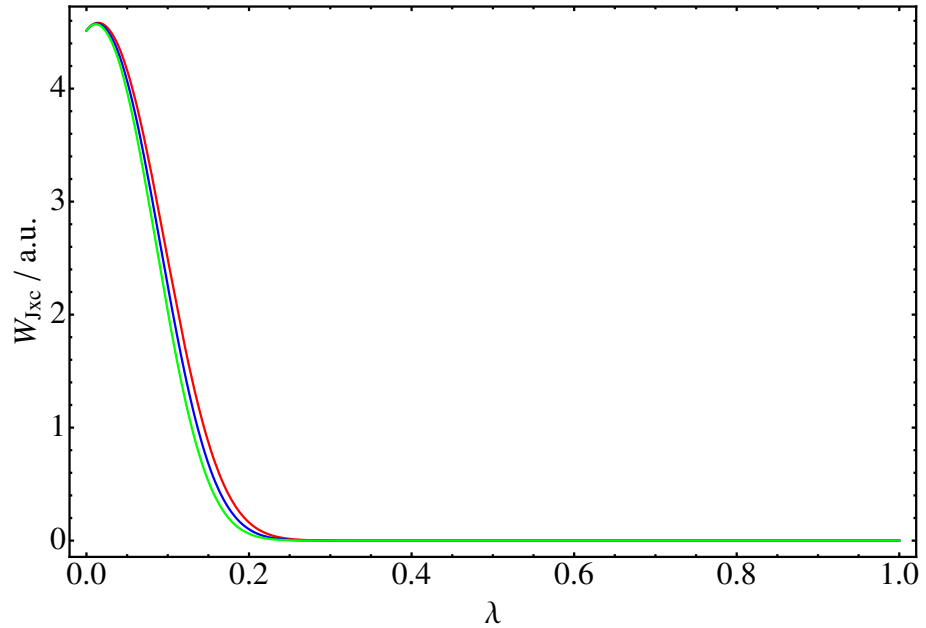


Figure 5.7: The \mathcal{W}_{JXC} integrand for the interaction energies at $R=8.0-9.0$ a.u. The red curve is $R = 8.0$ a.u., the blue is $R = 8.5$ a.u. and the green is $R = 9.0$ a.u.

comments regarding this topic. In connection with the linear connections it was mentioned that numerical difficulties associated with the Lieb maximization could have been a factor in the resulting discrepancies of the curves as well as the discrepancies found for the density differences in Chapter 4. We will make a comparison between the energy components obtained in Chapter 4, and listed in Table 4.2, to the integrated

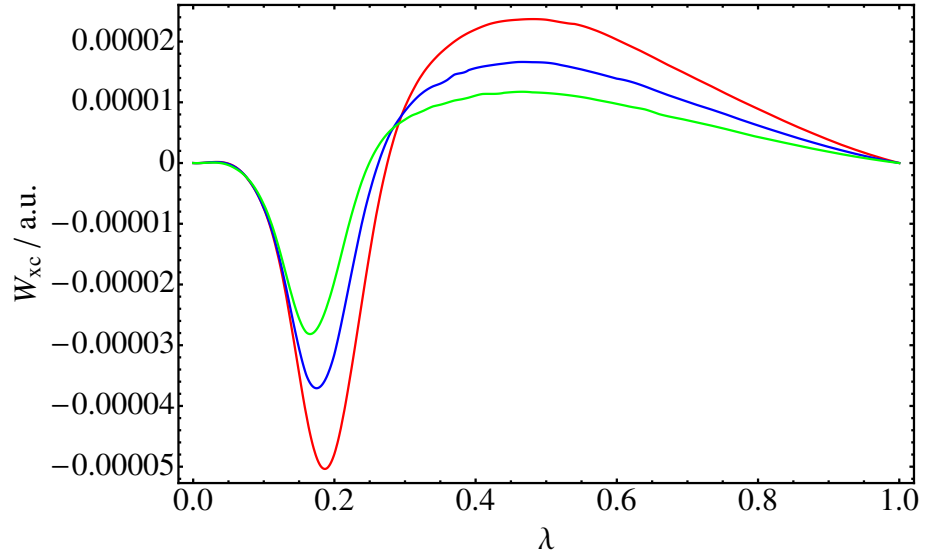


Figure 5.8: The \mathcal{W}_{xc} integrand for the interaction energies at $R=8.0-9.0$ a.u. The red curve is $R = 8.0$ a.u., the blue is $R = 8.5$ a.u. and the green is $R = 9.0$ a.u.

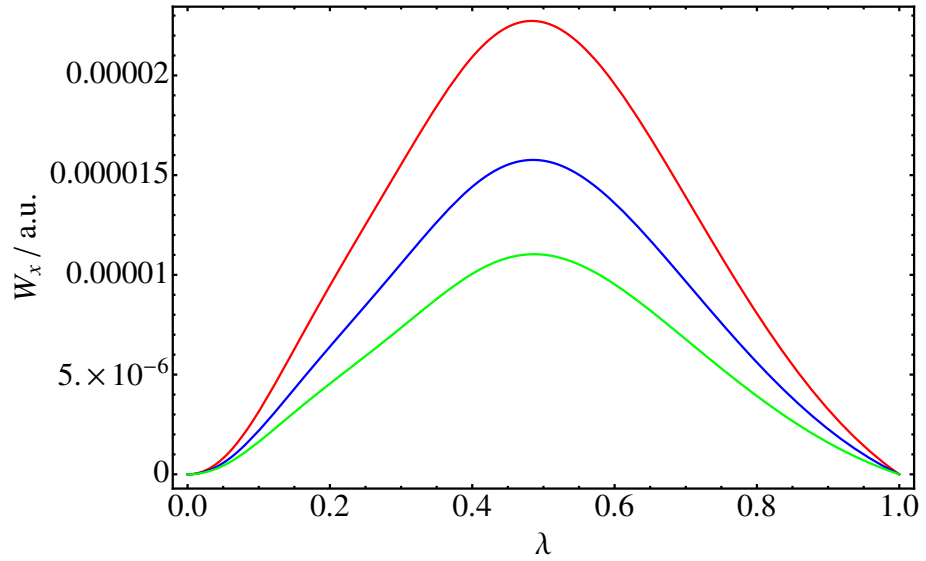


Figure 5.9: The \mathcal{W}_x integrand for the interaction energies at $R=8.0-9.0$ a.u. The red curve is $R = 8.0$ a.u., the blue is $R = 8.5$ a.u. and the green is $R = 9.0$ a.u.

quantities from both the linear and range-dependent adiabatic connection curves.

Tables 5.2 and 5.3 present the integrated values of \mathcal{W}_{Jxc}^{int} , \mathcal{W}_{xc}^{int} and \mathcal{W}_c^{int} for the linear and range-dependent curves, yielding E_{Jxc}^{int} , E_{xc}^{int} and E_c^{int} respectively, along with the same components from Table 4.2. For the linear connections, we observe discrepancies of approximately 5×10^{-7} a.u. for the E_{xc}^{int} and E_c^{int} components, the components derived in Chapter 4 being more positive in both cases. The range-dependent integrated exchange-correlation components lie above the corresponding components from Chapter 4, and the integrated values for the correlation display a smaller discrepancy. It is interesting to note that for the interaction connections the BSSE varies with the interaction strength

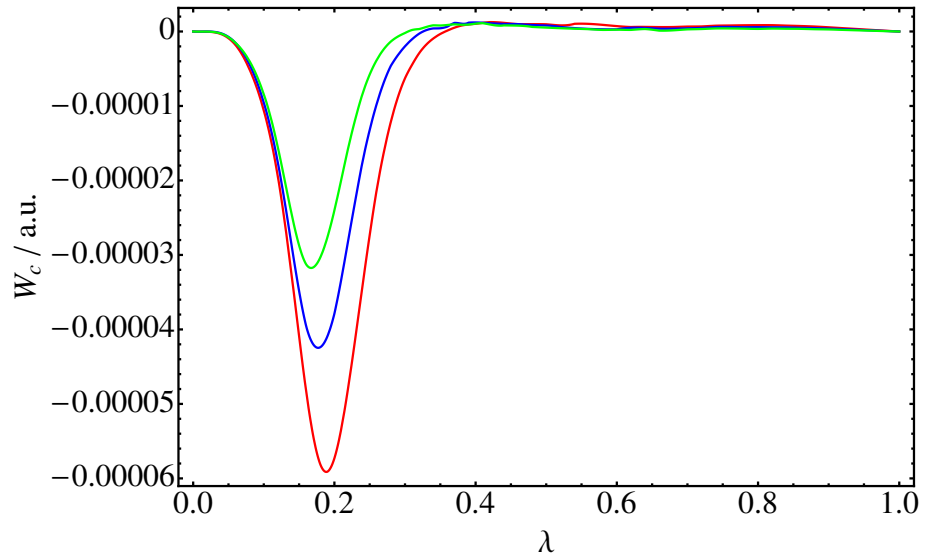


Figure 5.10: The \mathcal{W}_c integrand for the interaction energies at $R=8.0-9.0$ a.u. The red curve is $R = 8.0$ a.u., the blue is $R = 8.5$ a.u. and the green is $R = 9.0$ a.u.

λ . We note from Figure 5.4 that the difference between the corrected and un-corrected curves for the linear ACs increases with an increasing λ . The consequence of this is that the definition for the counterpoise correction applied in Chapter 4 for $\lambda = 0$ and $\lambda = 1$ is different from taking the counterpoise correction at each value of λ for the integrands, e.g $\mathcal{W}_c^{\text{int,lin}}$. This becomes evident when the BSSE for E_c^{int} in Chapter 4 is compared to the corresponding correction for the integrated values. Looking at the internuclear separation of $R = 8.5$ a.u. for the correlation energy we find that in Chapter 4 the BSSE accounts for an energy increase of 3.12×10^{-7} a.u., whereas for the adiabatic connections it accounts for 6.06×10^{-7} and 6.23×10^{-7} a.u for the linear and range-dependent ACs respectively. Here as previously discussed, we have applied the counterpoise correction to each value of λ for both the linear and range-dependent path. The discrepancy between the integrated results and those in Table 4.2 is of the order 5×10^{-7} a.u and we regard this as a measure of the accuracy achieved. This level of accuracy is sufficient for the qualitative discussion presented here and investigations are ongoing to improve the accuracy further.

Table 5.2: The energy integrands of the linear interaction calculated for the three geometries at uncontracted d-aug-cc-pVQZ/d-aug-cc-pV6Z level. All the energies are in a.u., and E_{xc} and E_c are of the order 10^{-6} a.u.

	R=8.0		R=8.5		R=9.0	
Energy	Components	$\int \mathcal{W}$	Components	$\int \mathcal{W}$	Components	$\int \mathcal{W}$
E_{Jxc}	0.49998	0.49998	0.47058	0.47058	0.44444	0.444436
E_{xc}	4.72	4.34	3.37	2.97	2.40	1.84
E_c	-6.95	-7.33	-4.69	-5.08	-3.25	-3.80*

Table 5.3: The energy integrands of the range-dependent interaction calculated for the three geometries at uncontracted d-aug-cc-pVQZ/d-aug-cc-pV6Z level. All the energies are in a.u., and E_{xc} and E_c are of the order 10^{-6} a.u.

Energy	R=8.0		R=8.5		R=9.0	
	Components	$\int \mathcal{W}$	Components	$\int \mathcal{W}$	Components	$\int \mathcal{W}$
E_{Jxc}	0.49998	0.49991	0.47058	0.47051	0.44444	0.44438
E_{xc}	4.72	4.95	3.37	3.54	2.40	2.55
E_c	-6.95	-6.72	-4.69	-4.52	-3.25	-3.10

Chapter 6

Orbital dependent functionals

Chapters 4 and 5 presented a detailed analysis of the dispersion interaction for the helium dimer. The problems displayed by standard density functionals to describe the dispersion interaction were highlighted by the failure of BLYP to recover the correlation energy. One possible solution to deal with the “short-sighted” nature of density functional approximations, is to introduce non-locality by incorporating contributions from orbital dependent correlation terms in the exchange–correlation functional. The double hybrid functionals of Grimme et al. [23, 24] serve as typical examples. These functionals include contributions from post-SCF perturbation theory. Here we consider the double hybrid B2PLYP functional and a new form denoted B2-DC-PLYP, based on the degeneracy corrected perturbation theory (DCPT2) of Ref. [27]. A family of functionals based on random phase approximation (RPA) correlation energies are also investigated. The focus of this chapter will be to investigate these forms to determine their stability when evaluated in a self-consistent manner. This will be performed with the use of the numerical procedures outlined in Chapter 3.

6.1 The B2PLYP double hybrid functional

One of the most notable examples of a double hybrid functional is the B2PLYP functional of Grimme et al. [23]. This exchange–correlation functional has the form

$$E_{xc}^{\text{B2PLYP}} = (1 - a)E_x^{\text{HF}} + aE_x^{\text{Becke88}} + bE_c^{\text{LYP}} + (1 - b)E_c^{\text{MP2}} \quad (6.1.1)$$

where the first term is the Hartree–Fock exchange energy, the second is the exchange functional devised by Becke [40], the third term is the correlation functional of Lee, Yang and Parr [39], and the last term is the MP2 correlation energy. Grimme determined the two parameters a and b by fitting over the G2/97 set of experimental data [23], the resulting values being $a = 0.47$ and $b = 0.73$. The calculations are performed by first running a self-consistent Kohn–Sham calculation applying the GGA functional defined by the first three terms of Eq. (6.1.1) and then using the resulting set of orbitals to evaluate the MP2 correlation energy,

$$E_c^{\text{MP2}} = \frac{1}{4} \sum_{ia} \sum_{jb} \frac{[(ia|jb) - (ib|ja)]^2}{\varepsilon_i + \varepsilon_j - \varepsilon_a - \varepsilon_b} \quad (6.1.2)$$

here given in spin orbital notation. It should be noted that the application of many-body perturbation techniques to the Kohn–Sham system results in a single excitation contribution to the second-order energy. This term is neglected in the application of B2PLYP since the doubles term typically represents the dominant contribution to the correlation energy.

As a part of the work presented in this thesis, the B2PLYP functional was implemented in the DALTON program [49]. The performance of this functional for calculating the energy of the diatomic molecules H_2 , Li_2 , F_2 and N_2 as a function of an increasing internuclear separation R was investigated, and the results are presented in Figure 6.1. All of the calculations were performed using the correlation consistent cc-pCVTZ basis set of Dunning [70, 71]. We included core-correlated functions since the MP2 contribution correlates all the orbitals in our B2PLYP calculations. The resulting

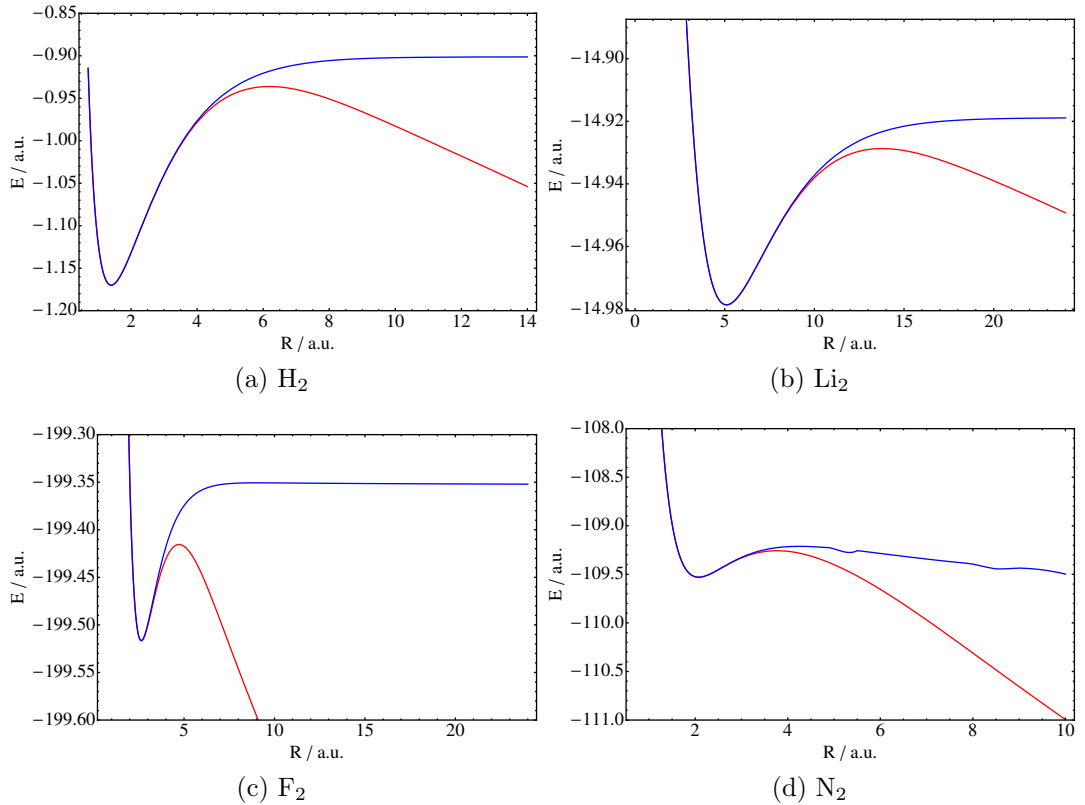


Figure 6.1: The B2PLYP (red) and B2-DC-PLYP (blue) energies as a function of internuclear separation, R , for the diatomic molecules (a) H_2 (b) Li_2 (c) F_2 and (d) N_2 . All calculations were performed in the cc-pCVTZ basis set. All quantities are in a.u.

potential energy curves obtained with B2PLYP display the problems associated with MP2 to describe quasi-degenerate systems, as the internuclear separation is increased. As the occupied and virtual orbital energies approach each other, the correlation energy for all of the systems in Figure 6.1 becomes much too negative, resulting in a too negative total energy. This causes divergence for large R , such that the functional can only describe the systems reliably near the equilibrium geometry. The most rapid divergence is observed for the triply bonded N_2 .

The failure of B2PLYP at large internuclear separations, R , is due to the orbital eigenvalue differences in the denominator of Eq. (6.1.2). As R increases, the HOMO and LUMO orbital energies become increasingly similar, resulting in near degeneracies. Therefore we are motivated to consider other alternatives for the orbital dependent correlation functional such that this problem is circumvented, as discussed in the following subsection.

6.2 Double-hybrid functionals based on DCPT2

The DCPT2 method devised by Assfeld, Almlöf and Truhlar [27] built upon the approach of Kuhler et al. [85] to deal with quasi-degeneracies occurring in the quantum theory of molecular vibrations. We will here give a brief outline the method. Because of Brillouin's theorem, only doubly excited states couple to the ground state in MP2 theory. We denote the ground state as Ψ_0 , and the doubly excited configurations as Ψ_{ij}^{ab} (where i and j are the occupied and a, b are unoccupied orbitals) as s . Each contribution to the second order correlation energy may then be expressed in spin orbital notation as,

$$E_{0 \rightarrow s}^{(2)} = -\frac{V_{s0}^2}{E_{s0}} \quad (6.2.1)$$

where V_{s0}^2 is

$$V_{s0}^2 = [(ia|jb) - (ib|ja)] \quad (6.2.2)$$

and

$$E_{s0} = D_{abij} = \varepsilon_a + \varepsilon_b - \varepsilon_i - \varepsilon_j \quad (6.2.3)$$

The effective Hamiltonian is given as

$$\mathbf{H} = \begin{pmatrix} E_0 & 0 \\ 0 & E_0 + E_{s0} \end{pmatrix} + \lambda \begin{pmatrix} 0 & V_{s0} \\ V_{s0} & 0 \end{pmatrix} \quad (6.2.4)$$

where E_0 is the unperturbed ground state energy, and λ is the perturbation parameter. The application of second-order perturbation theory to this Hamiltonian gives the result of Eq. (6.2.1) for each contribution to the correlation energy. Assfeld, Almlöf and Truhlar [27] proposed to treat them in an exact manner by diagonalizing the Hamiltonian in Eq. (6.2.4) for each double excitation contribution, which may be written as

$$E_{0 \rightarrow s}^{(2)} = \frac{1}{2} \sum_s \left(E_{s0} - \sqrt{E_{s0}^2 + 4V_{s0}^2} \right). \quad (6.2.5)$$

We recover the total DCPT2 correlation energy by summing over all possible contributions, switching to spatial orbital notation gives

$$\begin{aligned} E_c^{\text{DCPT2}} &= \frac{1}{2} \sum_{ijab} \left(D_{abij} - \sqrt{D_{abij}^2 + 4(ia|jb)} \right) \\ &+ \frac{1}{4} \sum_{ijab} \left(D_{abij} - \sqrt{D_{abij}^2 + 4[(ia|jb) - (ib|ja)]^2} \right) \end{aligned} \quad (6.2.6)$$

The above expression is easy to implement in any code which can perform calculations using MP2, and has been implemented in the DALTON program as part of this work. The lack of an orbital energy difference denominator means that the expression should be more applicable in the case of quasi-degeneracy.

Considering the failure of the B2PLYP double hybrid for obtaining potential energy curves for stretching even simple bonds as is observed in Figure 6.1, we now investigate whether a new double hybrid with DCPT2 correlation energy offers any improvement. In Figure 6.1 we note how DCPT2 and MP2 have similar correlation energies far from any degeneracies which implies that DCPT2 is a convenient choice as a replacement for the MP2 correlation component in B2PLYP. The parameters for B2PLYP were obtained through optimization over the G2/97 set which contains molecules close to their equilibrium geometries, such that there is a low probability of any degeneracies occurring. We therefore make the assumption that the same parameters a and b in Eq. (6.1.1) may be employed as for B2PLYP, and the correlation contribution using MP2 theory may be replaced by the DCPT2 correlation energy from Eq. (6.2.6).

The potential energy curves obtained employing this new functional, which we will refer to as B2-DC-PLYP, are presented in Figure 6.1 along with the curves obtained with standard B2PLYP for the diatomic molecules, H_2 , Li_2 , F_2 and N_2 . The results show that for short to intermediate values of R , there is close agreement between the two methods. As the internuclear separation is increased, the Kohn–Sham orbital energies used in the perturbation expression of Eq. (6.1.2) start to become degenerate. When this occurs the potential energy curves obtained with the two methods begin to display significant differences. In the case of the only triple bond included in the molecular set, N_2 , B2-DC-PLYP does not result in a complete divergence, but still displays an unphysical maximum around 6.0 a.u. and an asymptote which is much too low. The single bonds on the other hand appear reasonable, having no divergence for a large internuclear separation, and displaying a qualitatively correct behaviour with regard to having a flat, plateau as the dissociation limit is approached. However, it should be noted that the dissociation limits approached are not accurate. For example, in the case of H_2 this limit is too high, being -0.9 a.u instead of -1.0 a.u.

Having found promising results for the B2-DC-PLYP functional stretching single bonds, we now consider the limiting case of $a = 0$ and $b = 0$ in Eq. (6.1.1) for the standard B2PLYP and B2-DC-PLYP functionals. This choice of parameters represents pure MP2 and DCPT2 calculations respectively. These parameters were applied to F_2 and the results are shown in Figure 6.2. In comparison with Figure 6.1 MP2 diverges at a quicker rate as R increases than B2PLYP. This reflects the fact that only 27% of MP2 is included in B2PLYP. However, B2PLYP does not offer a substantial improvement, since the MP2 correlation component included is evaluated using Kohn–Sham orbitals, which have a smaller HOMO–LUMO gap than Hartree–Fock. Hence, as the bond is stretched, degeneracies are approached at a faster rate than if Hartree–Fock orbitals had been employed. The potential energy curves for F_2 evaluated using pure DCPT2 do not reflect the qualitatively correct behaviour of B2-DC-PLYP, but instead gives an unphysical maximum and finite but too low asymptote. The relative success of B2-DC-PLYP can be attributed to the small fraction of DCPT2 correlation (27%) included as well as the relatively high amount of Hartree–Fock exchange (53%). Still, the qualitatively reasonable results obtained for B2-DC-PLYP for the dissociation of

single bonded species are remarkable considering the sensitivity of the results to the parameters of Eq. (6.1.1).

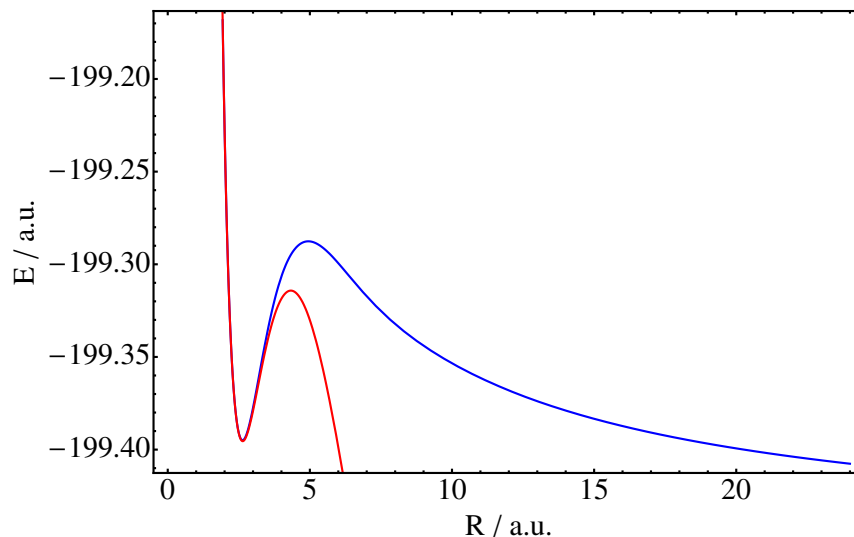


Figure 6.2: Dissociation of F_2 with full Hartree–Fock exchange and MP2/DCPT2 correlation contributions. The red curve is MP2 and the blue is DCPT2. The calculations were performed in the the cc-pCVTZ basis.

6.3 A self-consistent DCPT2 double hybrid

Despite the B2-DC-PLYP functional of the previous section only demonstrating limited success for obtaining the potential energy curves of single bonded molecules, it is important to note that a finite value is obtained for E_c^{DCPT2} in the case of degenerate orbital energies. In order to have a fully rigorous treatment of B2PLYP and B2-DC-PLYP within the Kohn–Sham framework, the OEP method has to be employed. Several authors have reported difficulties associated with evaluating functionals derived from perturbation theory when applying the OEP approach [86–88]. As described in Chapter 2, these methods minimize the energy functional with respect to variations in the Kohn–Sham potential, $v_s(\mathbf{r})$. Therefore, if a potential is constructed which forces the orbital eigenvalues to become degenerate, then this will lead to unphysical correlation energies in the case of MP2 in Eq. (6.1.2). Solutions to avoid this have been proposed, notably by Bartlett et al. [86, 87, 89] who introduced a series of alternative perturbation theories especially designed to avoid this problem. These theories employ a re-summation of the perturbation series which results in a denominator shift in Eq. (6.1.2), and hence avoid the issue of divergence. The DCPT2 correlation energy expression would appear to be an alternative solution which removes the problem of degeneracies from the OEP calculations. We therefore proceed to investigate the possibility of a self-consistent DCPT2 double hybrid, starting with the case of $a = 0$ and $b = 0$, and employing the numerical optimization techniques described in Chapter 3.

Initially, we chose to consider the simple example of the helium atom in Pople's [90] 3-21G basis set. The direct optimization techniques which were discussed in Chapter 3 were used with the basis set in the potential expansion in Eq. (3.1.1) set equal to the 3-21G orbital basis such that the OEP(DCPT2) energy is a function of only the two expansion parameters b_1 and b_2 . The OEP optimization was carried out using the Nelder–Mead algorithm outlined in Chapter 3. The energy may therefore be plotted as a surface in these two parameters, and this has been carried out over the range -50 to +50.

The resulting surfaces are presented in Figure 6.3. The effect of a smoothing norm regularization procedure on these surfaces has also been considered. The technique of Heaton–Burgess et al. [69] was chosen, where the term,

$$\|\Delta v_b(\mathbf{r})\|^2 = \sum_t \sum_u b_t b_u \langle g_t(\mathbf{r}) | -\nabla^2 | g_u(\mathbf{r}) \rangle \quad (6.3.1)$$

weighted by a parameter, λ , modifies the energy functional which is to be minimized. This term measures the smoothness of the potential in Eq. (3.1.1) and raises the energy in the regions where the potential is oscillatory. The size of the parameter λ determines how smooth the potential will be in the evaluation of the energy, the larger this parameter is, the larger the extent to which a smooth behaviour is enforced. The subsequent values of λ considered in Figure 6.3 are $10^{-5}, 10^{-4}, 10^{-3}, 10^{-2}$. The smallest smoothing norm of 10^{-5} results in a surface similar to the unregularized case which resembles a long narrow valley, presenting a difficult optimization problem. However, given sufficient iterations the Nelder–Mead approach does find a minimum. By increasing the parameter, we note how the surface smoothens, making it easier for the optimizer to locate a proper minimum, until at 10^{-2} the surface displays a clear minimum. Table 6.1 lists the behaviour of the DCPT2 correlation energy as a function of the smoothing norm parameter, λ , at the optimal values of the expansion parameters b_1^* and b_2^* . A large number of iterations, typically between 5000-10000, are required to reach convergence.

Table 6.1: The self-consistent DCPT2 correlation energy contributions for several values of the parameter λ used in the smoothing-norm method. The values of the optimal expansion parameters b_1^* and b_2^* are given, along with the HOMO-LUMO gap. All calculations use the 3-21G basis set and all quantities are in a.u.

λ	E_c	HOMO-LUMO gap	b_1^*	b_2^*
10^{-5}	-0.26216	1.3×10^{-9}	-10.081	50.160
10^{-4}	-0.01559	2.19	0.334	1.591
10^{-3}	-0.01515	2.26	0.035	0.140
10^{-2}	-0.01511	2.26	0.035	0.013

The results demonstrate how the optimal expansion parameters in the case of a norm of 10^{-5} are located in the top left of the valley in Figure 6.3. The minimum value of -0.26216 a.u is much too negative when compared to the FCI for helium of -0.01490 a.u for the correlation energy. The associated value for the HOMO-LUMO gap is essentially zero. The correlation energies and associated gaps for the larger values

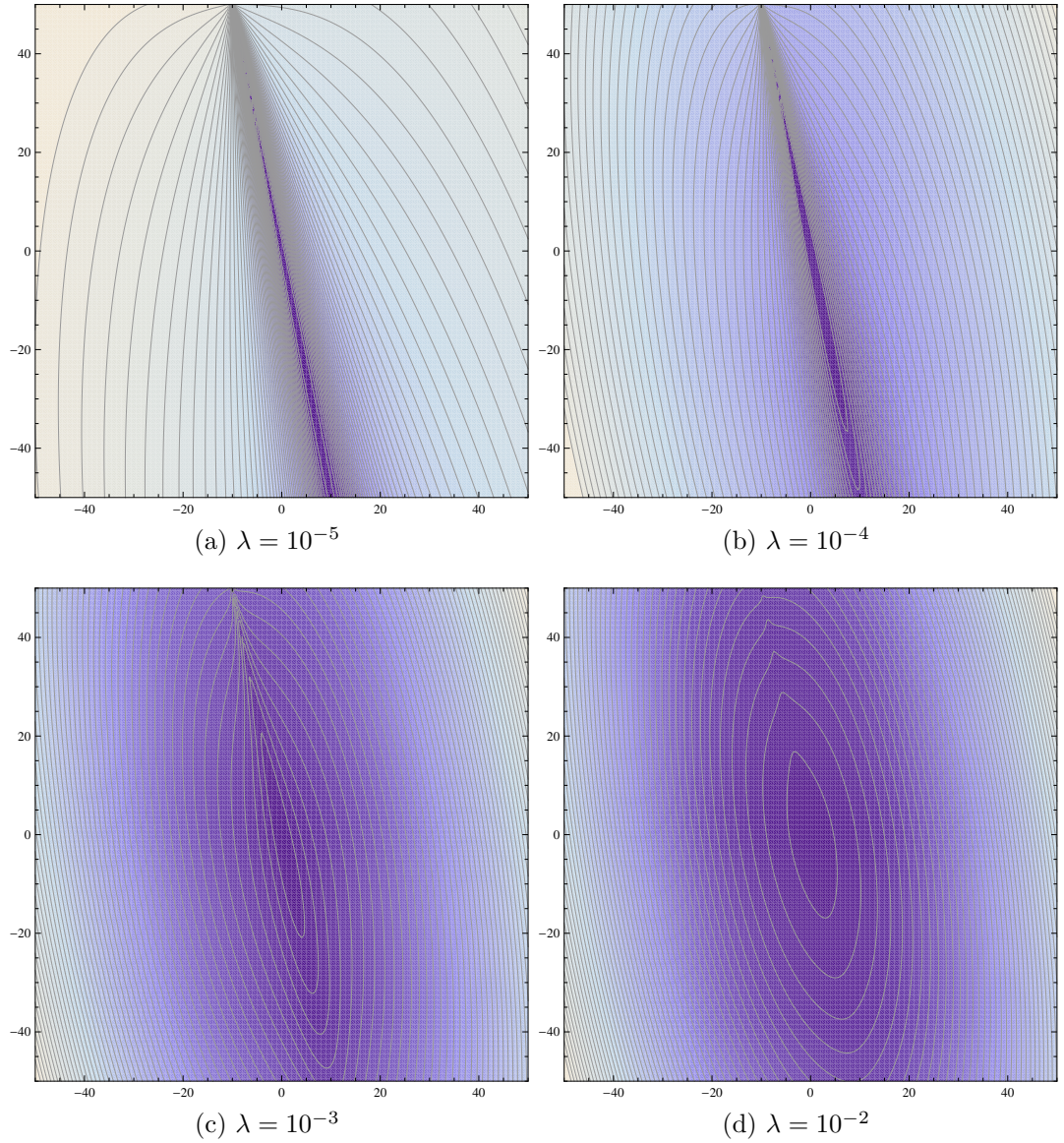


Figure 6.3: The energy of the helium atom in the 3-21G basis set as a function of the potential expansion parameters b_1 and b_2 for a range of a smoothing-norm parameter, λ , values from 10^{-5} to 10^{-2} , calculated using the Nelder–Mead algorithm.

of λ reflect how the use of the smoothing norm regularization avoids these degeneracies, resulting in more reasonable correlation energies and HOMO-LUMO gaps. The optimal point on the surface, given by (b_1^*, b_2^*) , moves down the valley and into the centre of the surface, which is fully consistent with the behaviour of a smooth potential for which b_1 and b_2 have reasonable values, as opposed to the large values at $\lambda = 10^{-5}$. However, without the use of a smoothing norm, the resulting correlation energies will be below the correct value.

In order to highlight the difficulties associated with using either DCPT2 or MP2 to account for the correlation energy, the respective energies for the helium atom were examined as a function of the HOMO-LUMO gap. For a two electron system, the

DCPT2 energy expression in Eq. (6.2.6) reduces to

$$E_c^{\text{DCPT2}} = \frac{1}{2} \left(D_{abij} - \sqrt{D_{abij}^2 + 4(ia|jb)^2} \right). \quad (6.3.2)$$

Because of the existence of only one occupied and one virtual orbital in the case of helium, the second term in Eq. (6.2.6) is cancelled since $(ia|jb) = (ib|ja)$. It becomes evident from Eq. (6.3.2) that when the occupied and virtual orbitals become degenerate, the expression simply becomes

$$E_c^{\text{DCPT2}} = -(ia|jb). \quad (6.3.3)$$

the corresponding divergent MP2 term is given by

$$E_c^{\text{MP2}} = \frac{-(ia|jb)^2}{D_{abij}} \quad (6.3.4)$$

The behaviour for both these energy expressions is shown in Figure 6.4, where the DCPT2 and MP2 are evaluated for a fixed set of orbitals.

The two energies remain similar in the area where there are no degeneracies, having negative correlation energies when the HOMO-LUMO gap is positive. Both energies decay as the gap closes, but DCPT2 displays a slow decline towards the value of $-(ia|jb)$, as opposed to MP2 which diverges sharply towards $-\infty$. The MP2 correlation energies become positive for the negative HOMO-LUMO gaps, whereas the DCPT2 energies become increasingly negative. However, since we enforce occupations corresponding to the aufbau principle in our calculations we are restricted to the lower right quadrant in our DCPT2 calculations.

The results presented in this section concerning DCPT2 demonstrate that this energy expression does not solve the difficulties associated with the use of perturbation expressions as self-consistent orbital dependent functionals, even though bounded energies are obtained for degenerate HOMO-LUMO gaps. The simple removal of the energy denominator does not prevent the evaluation of the energy expression with the OEP method leading to unphysically negative values. However, the analysis presented does highlight the advantage of applying numerical techniques for prototyping new methods. The derivation of the analytical gradients needed to optimize E_c^{DCPT2} is straight-forward, but their efficient implementation may be time consuming and their energy expressions can prove cumbersome see Refs. [86, 88] for similar expressions.

6.4 Correlation functionals from the random-phase approximation

Correlation energy functionals based on the RPA have received a great deal of attention recently [28, 91, 92]. Many variants have been developed, for an overview of the different correlation energy expressions the reader is referred to Ref. [93]. We begin this section by outlining the RPA methods applied in this thesis, starting from the closed-shell RPA eigenvalue problem

$$\begin{pmatrix} \mathbf{A} & \mathbf{B} \\ -\mathbf{B} & -\mathbf{A} \end{pmatrix} \begin{pmatrix} \mathbf{X} \\ \mathbf{Y} \end{pmatrix} = \begin{pmatrix} \mathbf{X} \\ \mathbf{Y} \end{pmatrix} \Omega, \quad (6.4.1)$$

where $\mathbf{\Omega}$, \mathbf{A} , \mathbf{B} , \mathbf{X} and \mathbf{Y} are matrices with the dimension $ov \times ov$, o representing the total number of occupied orbitals and v being the number of virtual. The diagonal matrix $\mathbf{\Omega}$ contains the approximate excitation energies of the system, and the elements of the matrices \mathbf{A} and \mathbf{B} are given in spin-orbital notation as:

$$A_{ia,jb} = (\varepsilon_a - \varepsilon_i)\delta_{ij}\delta_{ab} + [(ia|bj) - (ij|ab)] \quad (6.4.2)$$

and

$$B_{ia,jb} = (ia|jb) - (ib|ja) \quad (6.4.3)$$

The Tamm–Dancoff approximation (TDA) sets $\mathbf{B} = \mathbf{0}$ reducing the problem to

$$\mathbf{Az} = \mathbf{z}\nu \quad (6.4.4)$$

where ν are the Tamm–Dancoff excitation energies. Since the RPA problem includes de-excitation operators in addition to the excitation operators in the TDA it may be considered to have a correlated ground state. To extract an RPA correlation energy we take the difference between the RPA and TDA excitation energies,

$$E_c^{\text{RPA}} = \frac{1}{2} \sum_i' (\omega_i - \nu_i) = \frac{1}{2} \text{Tr}(\omega - \mathbf{A}) \quad (6.4.5)$$

where the prime denotes that only the positive eigenvalues ω_i in $\mathbf{\Omega}$ are used.

It was noted by Sanderson [94] and Freeman [95], and more recently by Scuseria et al. [28] and Kresse and Grüneis [92] that the RPA correlation energy can be obtained through the ring-coupled-cluster-doubles approach (RCCD) by solving the Riccati equation

$$\mathbf{B} + \mathbf{AT} + \mathbf{TA} + \mathbf{TB}\mathbf{T} = \mathbf{0} \quad (6.4.6)$$

for \mathbf{T} , which are the coupled cluster amplitudes. This yields the correlation energy

$$E_c^{\text{RCCD}} = \frac{1}{2} \text{Tr}(\mathbf{BT}) = E_c^{\text{RPA}}. \quad (6.4.7)$$

This procedure has been implemented in the DALTON program by Coriani et al. [96] for closed shell systems. The full RPA/RCCD correlation energy in Eq. (6.4.7) can be viewed as a relatively inexpensive orbital dependent correlation functional, but is plagued by instabilities when the closed shell reference state contains triplet instabilities.

A much more robust variant of the RPA correlation energy is the direct RPA (dRPA), which coincides with the RPA correlation energy derived through the adiabatic fluctuation dissipation theorem by Furche [91] for pure density functionals. This form of RPA can also be expressed through a RCCD formulation with a modification to the matrices \mathbf{A} and \mathbf{B} , such that their matrix elements become

$$A_{ia,jb}^{\text{dR}} = (\varepsilon_a - \varepsilon_i)\delta_{ij}\delta_{ab} + (ia|bj) \quad (6.4.8)$$

$$B_{ia,jb}^{\text{dR}} = (ia|jb) \quad (6.4.9)$$

The difference between Eq. (6.4.8) and (6.4.9) and (6.4.2) and (6.4.3) is that the integrals are not antisymmetrized. Solving the Riccati Eq. (6.4.6) with the above integrals yields the direct-RCCD (dRCCD) correlation energy,

$$E_c^{\text{dRCCD}} = \frac{1}{2} \text{Tr}(\mathbf{B}_{\text{dR}}\mathbf{T}_{\text{dR}}) = E_c^{\text{dRPA}} \quad (6.4.10)$$

where the amplitudes \mathbf{T}_{dR} are the solution to Eq. (6.4.6) using \mathbf{A} and \mathbf{B} of Eq. (6.4.8) and (6.4.9). The advantage of the dRPA correlation energy over RPA is that it is not affected by the triplet instabilities in the ground state. A further advantage, which was observed by Furche [91] is that it should by construction be free of the problems pertaining to the use of the OEP to evaluate perturbation type correlation energies, which were discussed in Section (6.3).

The application of non-antisymmetrized integrals in the Eq. (6.4.10) can be viewed as a drastic step, however, the correlation energy is guaranteed to be real if the orbitals follow the aufbau principle. This is in contrast to the full RPA which may have complex solutions in the case of having an unstable reference. Still it is of interest to improve the accuracy of the dRPA correlation energy. Freeman proposed to add a term containing second-order screened exchange (SOSEX) contribution to the energy expression for the dRPA, and Grüneis et al. [92] investigated this proposed method. In the work presented here, the dRPA+SOSEX method, referred to from here as SOSEX, is evaluated within the framework of the dRCCD approach. The Eq. (6.4.6) is solved using \mathbf{A} and \mathbf{B} of Eq. (6.4.8) and (6.4.9) to obtain the amplitudes \mathbf{T}_{dR} , and the correlation energy is then

$$E_c^{\text{SOSEX}} = \frac{1}{2} \text{Tr}(\mathbf{B} \mathbf{T}_{\text{dR}}) \quad (6.4.11)$$

where \mathbf{B} is defined by Eq. (6.4.3).

Before investigating the suitability of the dRPA and SOSEX correlation energy functionals for use in a self-consistent manner through the application of the OEP method, it is first of interest to investigate how orbital dependent functionals influence the choice of suitable basis sets. We begin by considering the work of Jiang and Engel [97], who reported benchmark dRPA results for atoms using a basis set free numerical implementation. The manner in which these calculations were performed was by first minimizing the Hartree–Fock energy functional using the OEP method, which we will denote OEP(HF), and then using the resulting set of orbitals and orbital energies to evaluate the dRPA correlation energy. We carried out this procedure using the DALTON code, but with finite basis sets. The total energy expression for the dRPA method then becomes

$$E_{\text{tot}}^{\text{dRPA}} = E^{\text{HF}}[\varphi_p^{\text{OEP(HF)}}] + E_c^{\text{dRPA}}[\varphi_p^{\text{OEP(HF)}}, \varepsilon_p^{\text{OEP(HF)}}] \quad (6.4.12)$$

The correlation energy of the Ne atom was found by Jiang and Engel [97] to be -0.597 a.u for the term $E_c^{\text{dRPA}}[\varphi_p^{\text{OEP(HF)}}, \varepsilon_p^{\text{OEP(HF)}}]$. The corresponding value obtained through DALTON at the un-contracted aug-cc-pVQZ level was -0.5535 a.u, and for aug-cc-pV5Z this value was -0.5743 a.u. This demonstrates the problem of slow basis set convergence associated with the use of orbital dependent correlation energy functionals. We therefore apply the extrapolation formula of Helgaker et al. [98],

$$E_{XY}^* = \frac{X^3 E_X - Y^3 E_Y}{X^3 - Y^3} \quad (6.4.13)$$

where X and Y are the cardinal numbers, in this case 4 and 5 respectively. This results in the value of -0.596 a.u for the correlation energy of Ne, which is in close agreement with the number of Jiang and Engel [97]. The slow basis set convergence

towards the extrapolated value is emphasized in Figure 6.5, where it becomes evident that a much larger basis set than aug-cc-pV5Z must be employed to match Engel’s numbers. The focus of the work presented in this chapter is to investigate whether using the OEP methods to evaluate the dRPA and SOSEX correlation energies will lead to stable results, unlike those found for the case of DCPT2. Hellgren et al [99] evaluated the dRPA energies of a set of closed shell atoms using the OEP approach with a numerical method based on cubic splines. The reported results showed that dRPA consistently gives much too negative correlation energies, which is consistent with the values we found for the post-SCF evaluation of Ne. The post-SCF correlation energy we calculated was -0.596 a.u, the value of Jiang and Engel [97] was -0.597 a.u and the value reported by Hellgren et al. [99] was -0.598 a.u, all of which represent an overestimation of the accurate correlation value obtained by Chakravorty et al [100] of -0.390 a.u. We do not have corresponding values to compare with for SOSEX, as to our knowledge the OEP method has not been applied to evaluate the SOSEX energy functional. Furthermore, we have not discovered any studies of OEP(dRPA) or OEP(SOSEX) for molecules.

We applied the numerical optimization techniques outlined in Chapter 3 to evaluate the energy expression of dRPA and SOSEX with the OEP method for a small set of molecules. The numerical techniques employed allow us to perform these calculations without having to derive the analytic gradients. Preliminary investigations used the cc-pVTZ basis set. The calculations used the quasi-Newton approach with the approximate Hessian of Eq. (3.3.3) and the central finite difference formula of Eq. (3.2.6). The step length in the finite difference evaluation was chosen following preliminary calculations to be 10^{-3} and the geometries of all the molecules considered were optimized at the CCSD(T)/cc-pVTZ level.

Table 6.2 contains the results for the self-consistent OEP(dRPA) calculations, the dRPA calculations obtained using a post-SCF method based on a Hartree-Fock reference for the orbitals and orbital eigenvalues, and for comparison, coupled-cluster-doubles (CCD). The stability of the OEP(dRPA) results are in sharp contrast to the ones observed for DCPT2. Furthermore, the OEP(dRPA) results are in close agreement to the post-SCF dRPA values, with differences on the order of 10^{-4} a.u. This is an indication that performing a self-consistent calculation with dRPA will have a minimal effect on the resulting total energies. Both the energies obtained from self-consistent dRPA and post-SCF dRPA are too negative in comparison to the values calculated using the CCD method. This reflects the findings of Hellgren et al. [99] that dRPA correlation energies are much more negative than the corresponding accurate values. The HOMO-LUMO gaps are included in Table 6.2, and are compared with the results obtained by applying the WY method [55] to the relaxed CCD density. The resulting HOMO-LUMO gaps are here denoted as WY(CCD). The trend observed is that HOMO-LUMO gaps for OEP(dRPA) are relatively close to the ones of WY(CCD). Table 6.3 contains the similar values for the SOSEX energy functional, performed in post-SCF and self-consistent manners. As for the dRPA results, the two manners of evaluating the SOSEX energy functionals yields relatively similar energies, although they display larger differences than in the case of dRPA. The HOMO-LUMO gaps presented for OEP(SOSEX) remain close to the gaps for OEP(dRPA), but demonstrating a small but consistent increase in value, the largest difference being found for the case of F_2 . As

Table 6.2: Single-point energy calculations with OEP(dRPA) in the cc-pVTZ basis set in a.u. The geometries of all molecules were optimized with CCSD(T)/cc-pVTZ

Molecule	Convergence	$\epsilon_{\text{LUMO}}^{\text{OEP(dRPA)}} - \epsilon_{\text{HOMO}}^{\text{OEP(dRPA)}}$	OEP(dRPA)	dRPA	CCD	$\epsilon_{\text{LUMO}}^{\text{WY(CCD)}} - \epsilon_{\text{HOMO}}^{\text{WY(CCD)}}$
CO	1.42E-05	0.271	-113.2141	-113.2136	-113.1589	0.265
H ₂ O	2.29E-07	0.280	-76.3849	-76.3851	-76.3368	0.270
C ₂ H ₂	9.16E-08	0.266	-77.2550	-77.2557	-77.1984	0.260
HCN	1.02E-04	0.307	-93.3356	-93.3358	-93.2814	0.302
F ₂	3.64E-05	0.165	-199.3811	-199.3796	-199.2971	0.146
NH ₃	5.49E-07	0.244	-56.5287	-56.5297	-56.4795	0.239
N ₂	2.30E-04	0.323	-109.4289	-109.4288	-109.3771	0.314

expected from Eq. (6.4.10) and (6.4.11), the largest difference in the quantities reported for dRPA and SOSEX are the total energies. This matches the trend observed by Klopper et al [93] that dRPA yields too negative correlation energies, whereas SOSEX yields too positive values. This is consistent with the values presented in Tables 6.2 and 6.3, where dRPA results in too negative total energies compared to the CCD results, and the values of SOSEX lie above the corresponding CCD results. Taken

Table 6.3: Single-point energy calculations with OEP(SOSEX) in the cc-pVTZ basis set in a.u. The geometries of all molecules were optimized with CCSD(T)/cc-pVTZ

Molecule	Convergence	$\epsilon_{\text{LUMO}}^{\text{OEP(SOSEX)}} - \epsilon_{\text{HOMO}}^{\text{OEP(SOSEX)}}$	OEP(SOSEX)	SOSEX	CCD	$\epsilon_{\text{LUMO}}^{\text{WY(CCD)}} - \epsilon_{\text{HOMO}}^{\text{WY(CCD)}}$
CO	2.51E-06	0.274	-113.0573	-113.0588	-113.1589	0.265
H ₂ O	6.87E-07	0.282	-76.2658	-76.2667	-76.3368	0.270
C ₂ H ₂	5.06E-06	0.271	-77.1003	-77.1024	-77.1984	0.260
HCN	1.18E-04	0.309	-93.1769	-93.1791	-93.2814	0.302
F ₂	2.52E-06	0.178	-199.1580	-199.1598	-199.2971	0.146
NH ₃	3.04E-06	0.247	-56.4103	-56.4117	-56.4795	0.239
N ₂	3.60E-07	0.327	-109.2679	-109.2699	-109.3771	0.314

together, the results for dRPA and SOSEX demonstrate enough stability to be applied as correlation functionals in Kohn–Sham OEP calculations. However, this comes at the cost of slow basis set convergence. Further investigation is needed to determine their absolute accuracy and whether they may profitably be combined with density functional approximations within a self-consistent framework. However, as opposed to the results for DCPT2, implementation of the analytic gradients would in this case be a worthwhile endeavour.

6.5 An adiabatic connection analysis of dRPA and SOSEX

The final part of this chapter is dedicated to the investigation of the relevance of the adiabatic connection to the dRPA and SOSEX functionals discussed in the previous section. The adiabatic connection was previously employed in Chapter 5 for the study of the dispersion interaction in the helium dimer. The relevance of the dRPA correlation energy to density functional calculations has previously been demonstrated by Furche [91], who derived the dRPA correlation energy via a consideration of the adiabatic connection. It was shown in Ref. [91] that the correlation integrand $\mathcal{W}_c^{\text{dRPA}}[\rho]$

can be expressed through the eigenvectors of Eq. (6.4.1) as

$$\mathcal{W}_c^{dRPA}[\rho] = \text{Tr}(\mathbf{B}\mathbf{P}_\lambda)d\lambda \quad (6.5.1)$$

where

$$\mathbf{P}_\lambda = (\mathbf{X}_\lambda + \mathbf{Y}_\lambda)(\mathbf{X}_\lambda + \mathbf{Y}_\lambda)^T - \mathbf{I} \quad (6.5.2)$$

where \mathbf{I} is the identity matrix. There exists no such corresponding explicit expression for SOSEX integrand. However, we may apply the techniques used to carry out the Lieb maximization approach to calculate the SOSEX AC consistent with the OEP(SOSEX) energy.

As a simple example we consider the helium atom and write the Lieb functional for the model energy as

$$F_\lambda^{\text{mod}}[\rho] = \sup_v (F_\lambda^{\text{mod}}[v] - (v|\rho)) \quad (6.5.3)$$

where mod will denote either dRPA or SOSEX. The density is determined by performing an OEP(dRPA) or OEP(SOSEX) calculation and is constructed from the resulting Kohn–Sham orbitals. It is then used as an input density into Eq. (6.5.3) for all interaction strengths, λ . By performing the Lieb maximization for *lambda* values in the interval $0 \leq \lambda \leq 1$ we can determine the correlation integrand through

$$\mathcal{W}_{c,\lambda}^{\text{mod}}[\rho] = \frac{dF_\lambda^{\text{mod}}[\rho]}{d\lambda} - E_x[\rho] - E_J[\rho] \quad (6.5.4)$$

where the E_x and E_J are the exchange and Coulomb energies respectively. By applying the OEP(dRPA) and OEP(SOSEX) methods to calculate the input density, integration of the resulting AC curves between $\lambda = 0$ and $\lambda = 1$ returns the exact correlation energies of the OEP calculations.

The correlation energies as a function of the interaction strength, λ , for the dRPA and SOSEX model energies are presented in Figure 6.6. The curves demonstrate how the correlation energy is switched on in a smooth manner for an increasing interaction strength, and are consistent with the dynamical correlation in this simple system. All calculations were performed in the aug-cc-pVTZ basis set. The corresponding adiabatic connection curves are presented in Figure 6.7, and have the shape one would expect for dynamical correlation. Furthermore, the curves for both methods integrate to recover the correlation energy for the full interaction strength consistent with the results of self-consistent evaluations. The analysis presented here could, when refined, provide a valuable tool for the construction of new functional forms incorporating both density-functional and dRPA/SOSEX components, giving valuable insight into the practical performance of these functionals and providing guidance as to how best to combine them with standard density-functional approximations.

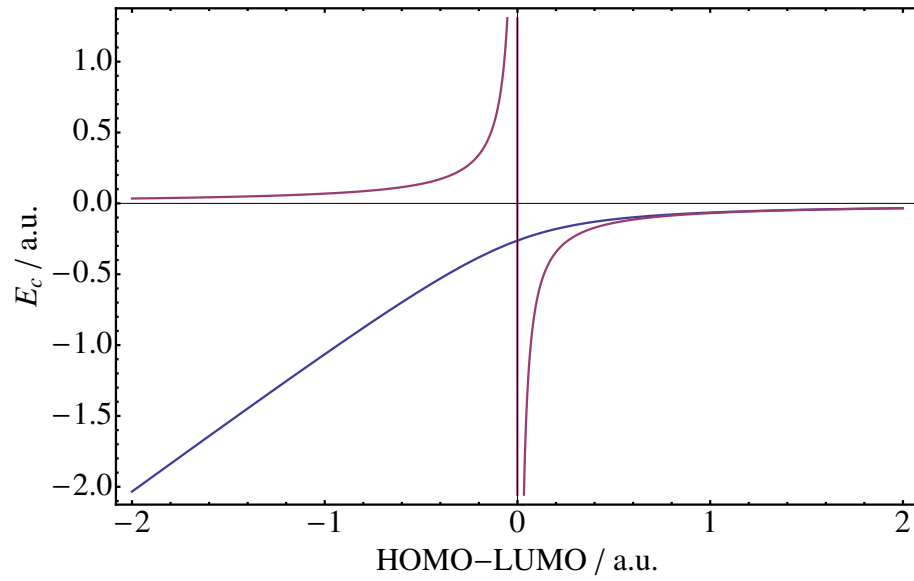


Figure 6.4: The DCPT2 and MP2 correlation energies of the helium atom in the 3-21G basis set as a function of the HOMO-LUMO gap. All quantities are in a.u.

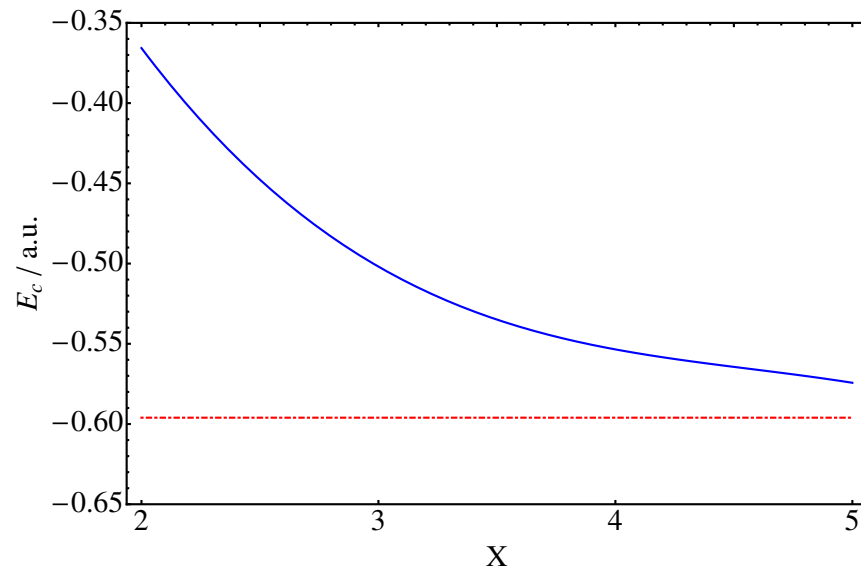


Figure 6.5: The correlation energy (in a.u.) of the neon atom calculated with the dRPA method using the uncontracted aug-cc-pCVXZ family of basis sets, with cardinal number $X = 2, 3, 4$ and 5 . The extrapolated value is shown by the red line.

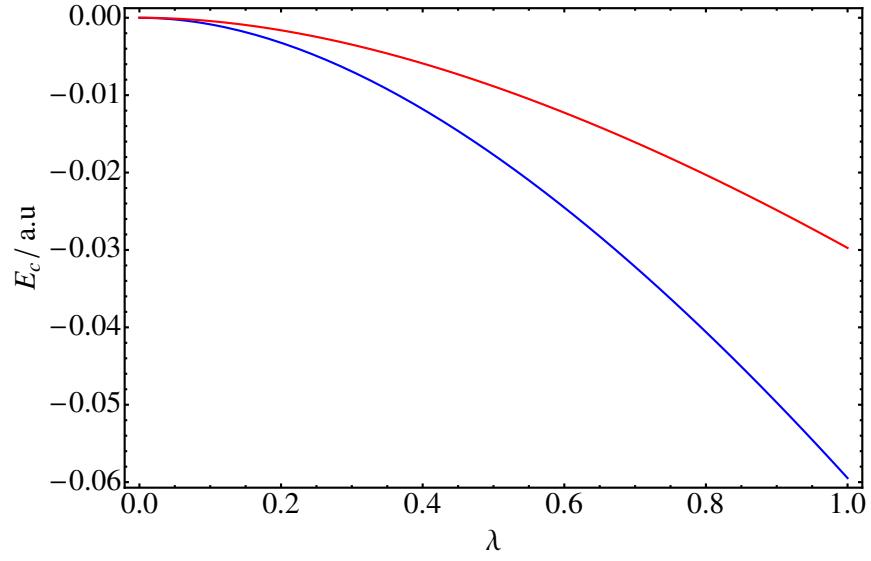


Figure 6.6: The correlation energy (in a.u.) as a function of the interaction strength λ for the helium atom calculated using the SOSEX and dRPA methods in the uncontracted aug-cc-pCVTZ basis set. SOSEX is in red and dRPA in blue.

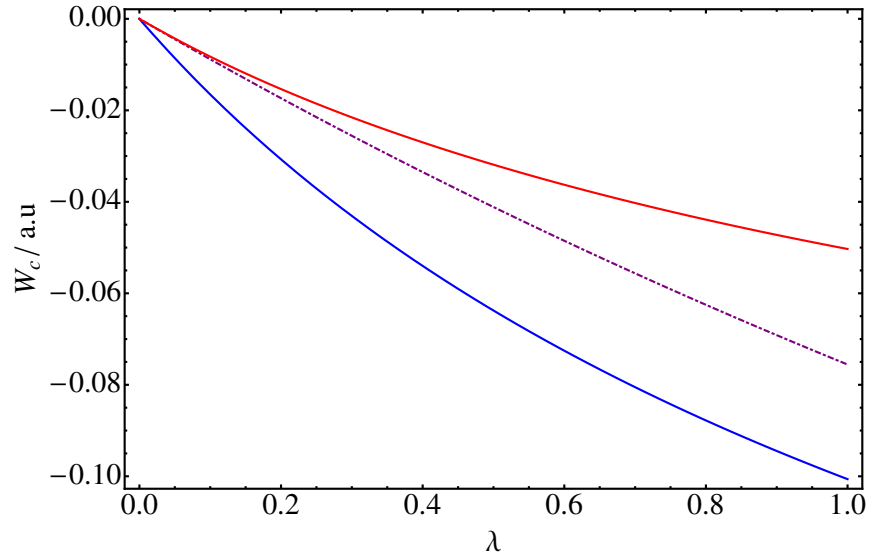


Figure 6.7: The correlation integrand, $\mathcal{W}_{c,\lambda}[\rho]$, for the helium atom (in a.u.) calculated with the SOSEX and dRPA methods using the uncontracted aug-cc-pVTZ basis set. SOSEX is in red and dRPA in blue.

Chapter 7

Conclusions and Future Work

The central theme of this thesis has been the understanding of how dispersion interactions should be treated in Kohn–Sham theory. We have shown how long-ranged Coulombic interactions between the helium atoms in the helium dimer induce subtle density distortions, which give rise to the dispersion forces. The work here brings the observations of Tozer and Allen [59], made in the context of Hartree–Fock–Kohn–Sham theory, into the full Kohn–Sham framework where most practical DFT calculations are performed. These calculations provide support for Feynman’s conjecture that the dispersion force arises as a result of the attraction of each nucleus towards its own distorted density.

The calculations also provided a stern test of the WY optimization technique [55] employed throughout this thesis. Overall, the accuracy was found to be sufficient for a qualitative analysis of the dispersion interaction. Further improvement of the accuracy of the technique is one area in which future work is required, in particular, with respect to the balance between the basis sets used to represent the molecular orbitals and the Kohn–Sham potential. Very recent calculations as part of this work have demonstrated that substantial improvements are possible using alternative basis sets.

Whilst the perspective offered by the dispersion forces is informative, it does not offer insight into how the dispersion interaction energy behaves and how it should be approximated in the Kohn–Sham approach. The central work in this project was therefore to consider the link between the Kohn–Sham non-interacting system and the physical system via the adiabatic connection. Considering this connection for the helium dimer and the individual atoms from which it is composed, it was possible to construct a function of the electronic interaction strength, which upon integration yields the exchange and correlation contributions to the interaction energies. These components are the central quantities for which approximations must be derived to allow a practical treatment of dispersion interactions in the Kohn–Sham approach.

The Lieb formulation of DFT [33] allowed us to study the evolution from the Kohn–Sham system to the physical system as a function of the electronic interaction strength in some detail. From these calculations it was possible to gain a great deal of insight into the dispersion interaction energy. In the first instance, we considered switching on the interactions in a simple linear fashion. The shape of the resulting adiabatic connection curve clearly revealed that the dispersion interaction energy is dominated by a dynamical correlation contribution. To gain further insight the electronic interactions were also

introduced in a range-dependent fashion. In this case the electronic interactions were weighted by an error-function contribution such that as the interaction parameter was increased the contributions considered arise from shorter and shorter inter-electronic distances. In this manner the long-ranged nature of the correlation contribution to the dispersion interaction energy was emphasized.

Whilst the failures of standard density functionals are well documented for dispersion interactions, a similar analysis of the linear adiabatic connection for the BLYP functional showed that failures due to the “short-sighted” nature of the approximations involved are also manifested in the interaction adiabatic connections. Taken together these results illustrate the long-ranged dynamically correlated nature of the dispersion interaction energies. The error-function based range-dependent adiabatic connections provide support for the use of range-separated approaches, which mix short-ranged density-functional and long-ranged wave-function based contributions, as a way to perform calculations with a reasonable treatment of dispersion interactions. However, they also highlight the point that some care must be taken in choosing the parameter used to define the separation in these methods and that this quantity may be strongly system and functional dependent. A draft manuscript based on the study of the helium dimer carried out in this thesis is included as an appendix.

In future work we hope to improve the accuracy of the calculations further and apply the same technique to a range of larger systems. The resulting interaction adiabatic connection curves should provide valuable data for the calibration of existing dispersion corrections and range-separated treatments, as well as being useful to guide the development of new approximations.

The hybridization of Kohn–Sham and wave function theories, as is done in range-separated approaches, represents one route towards a reliable treatment of dispersion interactions. A more fundamental solution, however, which remains within the framework of Kohn–Sham theory, is to introduce greater non-locality into the exchange–correlation approximations that are used. This can be achieved by the use of explicitly orbital dependent correlation functionals. The final part of this thesis was dedicated to the investigation of functionals of this type. Whilst in future these functionals may be applied to the dispersion interactions, here the emphasis was on prototypical implementations to determine their stability and suitability for use in self-consistent Kohn–Sham calculations.

We first analyzed a typical example of a functional including an orbital dependent correlation component, named B2PLYP. The MP2 contribution in this functional was found to cause the energy to become un-physically negative as orbital energy degeneracies are approached. This was illustrated by studying the potential energy curves for a variety of simple diatomic molecules. To improve the behaviour of this functional form the replacement of the MP2 contribution by the DCPT2 energy of Assfeld, Almlöf and Truhlar [27] was investigated. This new form, named B2-DC-PLYP gave qualitatively better potential energy curves, particularly for the dissociation of single bonds. Further investigation revealed however, that this behaviour is a result of a fortuitous and delicate balance between the density functional, Hartree–Fock and perturbation theory based contributions to this functional.

It has been widely reported that orbital dependent correlation functionals based on perturbation theory expressions are particularly unsuitable for self-consistent use in

the Kohn–Sham scheme, owing to denominators that contain orbital energy differences which cause the correlation energy to diverge as orbitals become degenerate in energy. However, the DCPT2 contribution contains no such denominators and as such its self-consistent evaluation was investigated. Unfortunately, despite the lack of orbital energy denominators, it was found that this contribution gives un-physically low, although bounded, correlation energies in the case of orbital degeneracies. It was demonstrated that self-consistent calculations converge to solutions with orbital degeneracies in practice and so the DCPT2 approach does not represent a useful correlation functional for use in Kohn–Sham calculations.

Recently, a great deal of attention has been paid to functionals based on the random-phase approximation. In the final part of the thesis we examined the self-consistent use of the most popular and robust dRPA and SOSEX variants of these methodologies. Calculations were performed in a fully self-consistent fashion for a variety of small molecular systems. To our knowledge these calculations represent the first self-consistent evaluation of these functionals for molecular systems. The results demonstrate that these orbital dependent correlation functionals do not suffer from instabilities, which plague perturbation-theory based forms and represent good candidates for further development. It was also demonstrated that both of these forms may be analyzed in terms of their associated adiabatic connections. In future work we hope to develop these prototype calculations to enable us to use this adiabatic connection analysis to guide the development of new density-functional approximations containing dRPA and SOSEX contributions. The aim for these functionals is to simultaneously deliver a reliable treatment of dispersion interactions and a good description of thermo-chemical properties, on which the performance of density functional approximations are usually evaluated.

Bibliography

- [1] W. Kohn and L. J. Sham, Phys. Rev. **140**, A1133 (1965).
- [2] S. Kristyn and P. Pulay, Chem. Phys. Lett. **229**, 175 (1994).
- [3] E. J. Meijer and M. Sprik, J. Chem. Phys. **105**, 8684 (1996).
- [4] P. Hobza, J. Šponer and T. Reschel, J. Comput. Chem. **16**, 1315 (1995).
- [5] A. K. Rappé and E. R. Bernstein, J. Phys. Chem. A. **104**, 6117 (2000).
- [6] N. Kurita and H. Sekino, Chem. Phys. Lett. **348**, 139 (2001).
- [7] T. van Mourik and R. J. Gdanitz, J. Chem. Phys. **116**, 9620 (2002).
- [8] J. Harris and R. O. Jones, J. Phys. F. Met. Phys. **4**, 1170 (1974).
- [9] D. C. Langreth and J. P. Perdew, Solid State Commun. **17**, 1425 (1975).
- [10] O. Gunnarsson and B. I. Lundqvist, Phys. Rev. B. **13**, 4274 (1976).
- [11] D. C. Langreth and J. P. Perdew, Phys. Rev. B. **15**, 2884 (1977).
- [12] D. C. Langreth, M. Dion, H. Rydberg, E. Schröder, P. Hyldgaard and B. I. Lundqvist, Int. J. Quant. Chem. **101**, 599 (2005).
- [13] J. F. Dobson, J. Wang, B. P. Dinte, K. McLennan and H. M. Le, Int. J. Quant. Chem. **101**, 579 (2005).
- [14] J. F. Dobson and J. Wang, Phys. Rev. B. **62**, 10038 (2000).
- [15] J. F. Dobson and J. Wang, Phys. Rev. Lett. **82**, 2123 (1999).
- [16] E. Goll, H. J. Werner, H. Stoll, T. Leininger, P. Gori-Giorgi and A. Savin, Chem. Phys. **329**, 276 (2006).
- [17] T. Leininger, H. Stoll, H. J. Werner and A. Savin, Chem. Phys. Lett. **275**, 151 (1997).
- [18] R. Pollet, A. Savin, T. Leininger and H. Stoll, J. Chem. Phys. **116**, 1250 (2002).
- [19] A. D. Becke and M. R. Roussel, Phys. Rev. A. **39**, 3761 (1989).
- [20] A. D. Becke and E. R. Johnson, J. Chem. Phys. **122**, 154104 (2005).

- [21] A. D. Becke and E. R. Johnson, J. Chem. Phys. **123**, 154101 (2005).
- [22] A. D. Becke, J. Chem. Phys. **88**, 1053 (1988).
- [23] S. Grimme, J. Comput. Chem. **27**, 1787 (2006).
- [24] S. Grimme, J. Comput. Chem. **25**, 1463 (2004).
- [25] S. N. Steinmann, G. Csonka and C. Corminboeuf, J. Chem. Theory Comput. **5**, 2950 (2009).
- [26] R. P. Feynman, Phys. Rev. **56**, 340 (1939).
- [27] X. Assfeld, J. E. Almlöf and D. G. Truhlar, Chem. Phys. Lett. **241**, 438 (1995).
- [28] B. G. Janesko, T. M. Henderson and G. E. Scuseria, J. Chem. Phys. **131**, 034110 (2009).
- [29] T. Helgaker, P. Jørgensen and J. Olsen. *Molecular Electronic-Structure Theory*. John Wiley and Sons, Ltd., 2000.
- [30] R. G. Parr and W. Yang. *Density-Functional Theory of Atoms and Molecules*. Oxford University Press, 1989.
- [31] P. Hohenberg and W. Kohn, Phys. Rev. **136**, B 864 (1964).
- [32] M. Levy, Proceedings of the National Academy of Sciences. **76**, 6062 (1979).
- [33] E. H. Lieb, Int. J. Quantum Chem. **24**, 243 (1983).
- [34] T. Helgaker, P. Jørgensen and J. Olsen. *Density-functional theory*. To be published.
- [35] S. Kümmel and L. Kronik, Rev. Mod. Phys. **80**, 3 (2008).
- [36] F. Bloch, Z. Physik. **57**, 545 (1929).
- [37] P. A. M. Dirac, Proc. Camb. Phil. Soc. **26**, 376 (1930).
- [38] A. D. Becke, Phys. Rev. A. **38**, 3098 (1988).
- [39] C. Lee, W. Yang and R. G. Parr, Phys. Rev. B. **37**, 785 (1988).
- [40] A. D. Becke, J. Chem. Phys. **98**, 5648 (1993).
- [41] P. J. Stephens, F. J. Devlin, C. F. Chabalowski and M. J. Frisch, J. Chem. Phys. **98**, 11623 (1994).
- [42] W. Koch and M. C. Holthausen. *A Chemist's Guide to Density Functional Theory*. Wiley-VCH Verlag GmbH, 2 edition, 2000.
- [43] R. T. Sharp and G. K. Horton, Phys. Rev. **90**, 317 (1953).
- [44] J. D. Talman and W. F. Shadwick, Phys. Rev. A. **14**, 36 (1976).

- [45] V. Sahni, J. Gruenebaum and J. P. Perdew, Phys. Rev. B. **26**, 4371 (1982).
- [46] A. Görling and M. Levy, Phys. Rev. A. **50**, 196 (1994).
- [47] W. Yang and Q. Wu, Phys. Rev. Lett. **89**, 143002 (2002).
- [48] Q. Zhao, R. C. Morrison and R. G. Parr, Phys. Rev. A. **50**, 2138 (1994).
- [49] DALTON, a molecular electronic structure program, release 2.0 (2005), see <http://daltonprogram.org/>.
- [50] J. A. Nelder and R. Mead, Comp. J. **7**, 308 (1965).
- [51] F. Colonna and A. Savin, J. Chem. Phys. **110**, 2828 (1999).
- [52] A. Savin, F. Colonna and R. Pollet, Int. J. Quant. Chem. **93**, 166 (2003).
- [53] W. H. Press, S. A. Teukolsky, W. T. Vetterling and B. P. Flannery. *Numerical Recipes in Fortran*. Cambridge University Press, 2nd edition, 1992.
- [54] E. Engel, Orbital-dependent functionals for the exchange–correlation energy: A third generation of density functionals, in *A Primer in Density Functional Theory*, edited by C. Fiolhais, F. Noqueira and M. A. L. Marques, pp. 56–117. Springer-Verlag, Berlin Heidelberg, 2003.
- [55] Q. Wu and W. Yang, J. Chem. Phys. **118**, 2498 (2003).
- [56] A. D. Becke, J. Chem. Phys. **107**, 8554 (1997).
- [57] S. Grimme, J. Chem. Phys. **124**, 034108 (2006).
- [58] T. Korona, H. L. Williams, R. Bukowski, B. Jeziorski and K. Szalewicz, J. Chem. Phys. **106**, 5109 (1997).
- [59] M. J. Allen and D. J. Tozer, J. Chem. Phys. **117**, 11113 (2002).
- [60] K. L. C. Hunt, J. Chem. Phys. **78**, 6149 (1983).
- [61] A. C. Hurley, Proc. R. Soc. London Ser. A. **226**, 170 (1954).
- [62] A. C. Hurley, J. Comput Chem. **9**, 75 (1988).
- [63] T. Helgaker and J. Almlöf, J. Chem. Phys. **89**, 4889 (1988).
- [64] P. Jørgensen and T. Helgaker, J. Chem. Phys. **89**, 1560 (1988).
- [65] T. Helgaker and P. Jørgensen, Theo. Chim. Acta. **75**, 111 (1989).
- [66] T. Helgaker. in *The Encyclopaedia of Computational Chemistry*, edited by P. v R Schleyer, N. L. Allinger, T. Clark, J. Gasteiger, P. A. Kollman, H. F. Schaefer III and P. R. Schreinerp. 1157. Wiley, Chichester, 1998.

- [67] H. Koch, H. J. A. Jensen, P. Jørgensen, T. Helgaker, G. E. Scuseria and H. F. Schaefer III, *J. Chem. Phys.* **92**, 4924 (1990).
- [68] S. F. Boys and F. Bernardi, *Molecular Physics*. **19**, 553 (1970).
- [69] F. A. Bulat, T. Heaton-Burgess, A. J. Cohen and W. Yang, *J. Chem. Phys.* **127**, 174101 (2007).
- [70] J. Thom H. Dunning, *J. Chem. Phys.* **90**, 1007 (1989).
- [71] T. V. Mourik, A. K. Wilson and J. Thom H. Dunning, *Mol. Phys.* **96**, 529 (1999).
- [72] T. H. Dunning, *J. Phys. Chem. A*. **104**, 9062 (2000).
- [73] C. J. Umrigar and X. Gonze, *Phys. Rev. A*. **50**, 3827 (1994).
- [74] A. M. Teale, S. Coriani and T. Helgaker, *J. Chem. Phys.* **130**, 104111 (2009).
- [75] A. M. Teale, S. Coriani and T. Helgaker, *J. Chem. Phys.* **133**, 164112 (2010).
- [76] A. Görling and M. Levy, *Phys. Rev. B*. **47**, 13105 (1993).
- [77] A. Görling and M. Levy, *Phys. Rev. A*. **52**, 4493 (1995).
- [78] M. Levy and J. P. Perdew, *Phys. Rev. A*. **32**, 2010 (1985).
- [79] A. J. Cohen, P. Mori-Sanchez and W. Yang, *J. Chem. Phys.* **127**, 034101 (2007).
- [80] R. Pollet, F. Colonna, T. Leininger, H. Stoll, H.-J. Werner and A. Savin, *Int. J. Quant. Chem.* **91**, 84 (2003).
- [81] E. Fromager, J. Toulouse and H. J. A. Jensen, *J. Chem. Phys.* **126**, 074111 (2007).
- [82] E. Fromager, F. Real, P. Wahlin, U. Wahlgren and H. J. A. Jensen, *J. Chem. Phys.* **131**, 054107 (2009).
- [83] E. Goll, H.-J. Werner and H. Stoll, *Phys. Chem. Chem. Phys.* **7**, 3917 (2005).
- [84] E. Goll, M. Ernst, F. Moegle-Hofacker and H. Stoll, *J. Chem. Phys.* **130**, 234112 (2009).
- [85] K. M. Kuhler, D. G. Truhlar and A. D. Isaacson, *J. Chem. Phys.* **104**, 4664 (1996).
- [86] I. Grabowski, S. Hirata, S. Ivanov and R. J. Bartlett, *J. Chem. Phys.* **116**, 4415 (2002).
- [87] R. J. Bartlett, V. F. Lotrich and I. V. Schweigert, *J. Chem. Phys.* **123**, 062205 (2005).
- [88] P. Mori-Sanchez, Q. Wu and W. Yang, *J. Chem. Phys.* **123**, 062204 (2005).

- [89] R. J. Bartlett, I. V. Schweigert and V. F. Lotrich, *J. Mol. Struc. (THEOCHEM)*. **771**, 1 (2006).
- [90] J. S. Binkley, J. A. Pople and W. J. Hehre, *J. Am. Chem. Soc.* **102**(3), 939 (1980).
- [91] F. Furche, *Phys. Rev. B.* **64**, 195120 (2001).
- [92] J. Paier, B. G. Janesko, T. M. Henderson, G. E. Scuseria, A. Grüneis and G. Kresse, *J. Chem. Phys.* **132**, 094103 (2010).
- [93] W. Klopper, A. M. Teale, S. Coriani, T. B. Pedersen and T. Helgaker, *Chem. Phys. Lett.* (in press) (2011).
- [94] E. A. Sanderson, *Phys. Lett.* **19**, 141 (1965).
- [95] D. L. Freeman, *Phys. Rev. B.* **15**, 5512 (1977).
- [96] An implementation of the various RPA correlation energies has been carried out in the DALTON program by S. Coriani, M. F. Iozzi and T. B. Pedersen and has been used with their kind permission in this work.
- [97] H. Jiang and E. Engel, *J. Chem. Phys.* **127**, 184108 (2007).
- [98] T. Helgaker, T. A. Ruden, P. Jørgensen, J. Olsen and W. Klopper, *J. Phys. Org. Chem.* **17**, 913 (2004).
- [99] M. Hellgren and U. von Barth, *Phys. Rev. B.* **76**, 075107 (2007).
- [100] S. J. Chakravorty, S. R. Gwaltney, E. R. Davidson, F. A. Parpia and C. F. Fischer, *Phys. Rev. A.* **47**, 3649 (1993).

Appendix A

Appendix: Draft Manuscript

A draft manuscript entitled “Dispersion interactions in Density-Functional Theory: An Adiabatic Connection Analysis” prepared using the results contained in this thesis is attached in the following pages.